Solent University

School of Maritime Science and Engineering

MSc Superyacht Design

Inigo Fuertes Ballesteros

PERFORMANCE COMPARISON BETWEEN A FLETTNER ROTOR AND A WING SAIL FOR SUPERYACHT APPLICATIONS

This project is submitted in part fulfilment of the Degree of

Master of science in Superyacht Design

Solent University

September 2020

ABSTRACT

This document presents the numerical investigation completed for the comparison between a Flettner rotor and a wing-sail for superyacht applications. The performance of full scale Flettner rotor and wing-sail are investigated using computational fluid dynamics for a variety of wind conditions and geometries with the intention of demonstrating factors that may affect the performance in real-world applications. In addition, two airfoil profiles were investigated; the NACA0012H and EPPLER 473. Results from the computational fluid dynamics analysis were then incorporated into a performance prediction model to assess potential power savings, taking into account factors such as the aero/hydrodynamic resistance of a vessel and the expected wind conditions. In contrast to previous studies, in this project, the utilization of the Flettner rotor and the wing sail were focus on superyacht applications, where reduced deck spaces and lower vessel sizes must be considered.

The candidate type of superyacht was a 3000GT 70 metre explorer with an open deck area fore and aft of the superstructure. The Holtrop and Mennen powering method established an effective power of 1817 kW to reach the maximum speed of 18 knots, and 662kW to reach the cruising speed of 14 knots. Power savings of up to 17.7% were reported from the study; the Flettner rotor showed the largest power savings. However, it is shown that the ship angle relative to the wind and the wind speed is a crucial aspect for the effectiveness of the device. Moreover, the polar plot shows that at angles close to 0° and 180° the device does not produce usable thrust, which increases the effective power due to aerodynamic windage.

ACKNOWLEDGEMENTS

The author would like to express a special thank you to the following people for their contributions towards this project. Without their help this project would not have been possible.

- To my supervisor Jonathan Ridley for continuous support and feedback on my work.
- To Giles Barkley for assisting on the project.
- To my family Javier & Yolanda

TABLE OF CONTENTS

TABLE OF FIGURES

NOMENCLATURE

Item	Description
α	Angle of attack
AR	Aspect ratio
D	Diameter [m]
CD	Drag coefficient
FD	Drag force [N]
GT	Gross tonnage
CL	Lift coefficient
FL	Lift force [N]
PR	Required power required to rotate a rotor [W]
Re	Reynolds number
ε	Rotor efficiency
PT	Thrust power produced by the rotor [W]
VPP	Velocity prediction program
λ	Velocity ratio

1 INTRODUCTION

1.1 BACKGROUND OF WIND-ASSISTED PROPULSION

During the oil crisis of the 1970s the possibility of using wind energy as an auxiliary propulsion for commercial ships gained interest, as the price of oil increased due to the oil embargo proclaimed by the Organization of Arab Petroleum Exporting Countries against the states suspected to support Israel during the Arab-Israeli War. As a consequence of this action, the price of oil increased fourfold, causing a shock to the worldwide economy. In this political and economical frame, the shipping industry was strongly hit. With the intention of reducing fuel expenses, the academic and maritime sector turned their attention towards the wind energy.

With the aim of using wind energy in the shipping sector, it was evident that a return to pure sailing ships was unfeasible. In order to ensure the same trade schedule and the same number of crew as standard mechanical ships did, hybrid ships were considered instead. However, the relatively short duration of the crisis and the subsequent fall in fossil fuel prices caused further research curtailed. During this time, several wind-assisted ships began to appear. An example of this is the retrofit project of the *Na Mata-i-sau*, a 27-metre passenger/cargo ship (≈300 GT) with auxiliary sail rigs (Figure 1.2). This performed above expectation, resulting in fuel savings of 23%-30%, compared to an analogous ship (Satchwell, 1986).

Figure 1.2: Na Mata-i-sau, Fiji, 1984 (Source: ADB, 1985)

Figure 1.2: Shin Aitoku Maru, Japan (Source: http://entsyklopeedia.ee/galerii/purjelaev1)

In Japan, the NKK classification society and the Japanese Marine Machinery Development Association (JAMDA) successfully trialled modern square sails, initially on the 900 t oil tanker *Shin Aitoku Maru* (Figure 1.2). The expansion of the sails and the setting of the sails were automatically driven by computer-controlled hydraulic units. The reported results showed overall fuel saving od more than 30%, increased passage speeds, increased stability, and reduced engine wear. The success of this led to another 17 vessels being built up to 1994 using similar technology (Schönknech & Laue, 1987).

However, the plummeting oil prices made the internal rate of return (IRR) of such technology uneconomic, especially given the cost and limits of the computer technology employed at the time. This resulted with a large discontinuation of the experiments. Despite the proven technology and the attractive fuel savings reported, wind-assisted propulsion became unappealing from an economic perspective.

1.2 Recent interest in wind-assisted propulsion

Wind assisted propulsion has recently gain interest as an attractive solution to reduce the dependence of the maritime industry from the fossil fuels, prompted by the emerging regulations on environmental exhaust emission on one hand, which add a further element of uncertainty and business risk for vessel owners, and the volatile fuel prices, driven by fuel supply and demand variations on the other.

Tier III, as part of amendments made to the International Convention for the Prevention of Pollution from Ships was adopted in 2008 and came into effect in January 2016. This regulation set stricter controls on NOx emission limits for new engines on vessels operating within special areas known as Emission Control Areas (Baltic Sea, North Sea, North America Area, United States and Caribbean Sea Area). However, engine modifications have not been enough to meet the TIER III standards, as the regulation requires some sort of exhaust after-treatment. The solution for yachts over 500GT (regulations granted a five-year exemption for vessels under 500GT) has been the use of a selective catalytic reduction (SCR), which utilizes a urea water solution to break down NOx into nitrogen and water. However, this system has proved to be ineffective at idle and low speeds since the SCR requires exhaust temperatures to reach a certain level to decompose urea exhaust fluid to water vapour an ammonia [1]. In addition, the system also has an impact on the yacht's efficiency and performance, as it makes the boats heavier, slower, and more expensive to operate and maintain.

There is also the added problem of incorporating a tank to hold urea. According to the rules and regulations, the yacht needs to carry only enough urea to run the SCR within an Emission Control Area. However, assessing the right amount is complicated. If the yacht runs out while on an Emission Control Area, it risks excessive fines for noncompliance. While, if too much urea is stored, maintenance issues may occur, as the storage life of the diesel exhaust fluid (the urea solution) is around six mounts, after that, it will crystallise and perhaps block the SCR piping if the water content vaporises [1]. In addition, a SCR system takes approximately one-third of the space taken by each engine, so the additional space required in the engine room is critical. This can be an added issue on existing vessels, where retrofitting the system could not be achieved without having to increase the size of the engine room.

The current energy efficiency regulations for new ships is contained in the Energy Efficiency Design Index (EEDI). The EEDI is non-prescriptive and performance based mechanism that leaves the choice of technologies to use, allowing ships to be built using a combination of technology and design as long as a certain efficiency level is achieved. This can be done through a combination of technologies, such as engine technology, hydrodynamic optimisation devices, or wind-assisted propulsions. The EEDI is expressed in grams of carbon dioxide (CO_2) per ship's capacity-mile, hence the smaller the EEDI the more energy efficient the ship's design. Wind-assisted propulsion is on the few technologies potentially offering double digit fuel saving today [2]. Although it cannot be considered as a primary mean of propulsion, it represents a realistic option for renewable power by reducing the required propulsion power.

1.3 RESEARCH OUTLINE

The present dissertation will examine the performance comparison between a Flettner rotor and a wing-sail for superyacht applications. The structure of this dissertation is given next. In Chapter 2 the baseline hull form is introduced. In addition, the power requirements for such vessels are calculated using the Holtrop and Mennen powering method.

Chapter 3 deals with the numerical modelling aspect of the project. The chapter begins with a literature review of critical aspects from previous numerical investigations on Flettner rotors and wing sails. The attention is then directed to the description of the turbulent models available for the project. Then, the wall treatment on the CFD simulation is introduced. Finally, the verification and validation study is described.

Chapter 4 deals with the performance investigation of a Flettner rotor. Initially, the chapter begins with the introduction to Flettner rotors ships built in the past, as well as an introduction into the principle behind the rotor, the Magnus effect. The mesh and mesh quality are then presented, as well as the CFD simulation setup. A detailed analysis of the Reynolds number effects on the aerodynamic coefficient of a two-dimensional rotating cylinder is then carried out. This section begins with a broad review of the papers published on this topic. In addition, this section also introduces the selection of an appropriate turbulence model. The results of the two-dimensional CFD simulations are then presented, with particular attention to aerodynamic lift and drag coefficients. Finally, the power required to spin the cylinder and the rotor efficiency are also included at the end of this section.

In Chapter 5 the performance investigation of the wing sail is completed. Initially, the chapter begins with the introduction to wing sail assisted ships built in the past. The mesh and mesh quality are then presented, as well as the CFD simulation setup. A detailed analysis of the Reynolds number effects on the aerodynamic coefficient of a two-dimensional NACA0012H and EPPLER 473 profiles is then carried out. This section also introduces the selection of an appropriate turbulence model. The results of the two-dimensional CFD simulations are then presented, with particular attention to aerodynamic lift and drag coefficients.

Chapter 6 deals with the approach used for the performance prediction program. In addition, the summation of the thrust provided by multiple wind-assist devices is addressed, and how the aerodynamic interaction effects are fully disregarded as a result. Furthermore, the effect of how locating the wind-assist device on ship form reduces its efficiency at all points of sail is presented.

In chapter 7 the performance of the Flettner rotor and the wing sail on the target vessel is compared. Finally, the main conclusions of this project are presented in chapter 8 together with a number of recommendations for future work.

2 TARGET VESSEL

2.1 INITIAL CONSIDERATIONS

The particulars of a superyacht were used to define the initial dimensions and location of the wing sail. The candidate type of superyacht was a 3000GT 70 metre explorer with an open deck area fore and aft of the superstructure. The mounting site was also carefully chosen to ensure that forces could also be safely transferred to the vessel's structure in a real-world application.

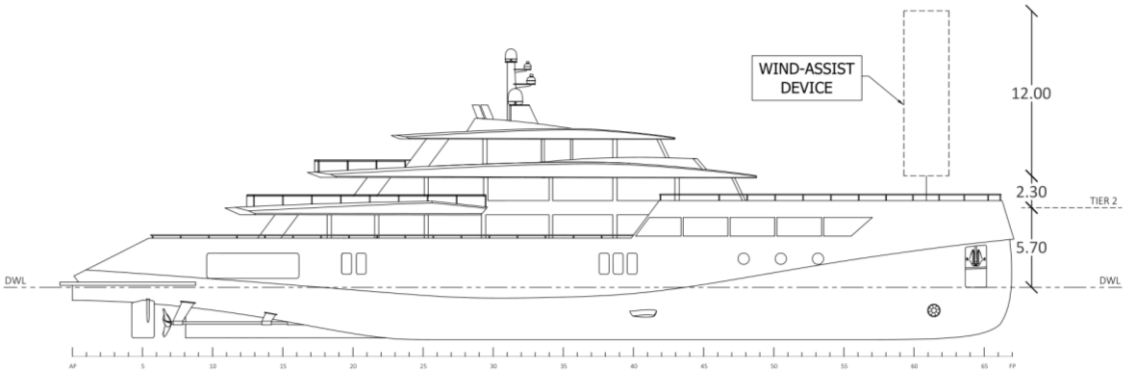

Figure 2.1: General arrangement of the target vessel.

2.2 RESISTANCE AND POWERING

The resistance and powering requirements of the baseline hull form were analysed with the use of systematic series. These series are a set of models designed to vary in a regular way a given number of parameters. Based on the results of towing tank testing these models, a regression of the resistance as a function of the parameters chosen is produced. The Holtrop and Mennen systematic series are used for the determination of the propulsive power of a vessel, which series data are based on model experiments and full-scale data.

2.2.1 ANALYTICAL TOOL

A systematic series is a set of models designed to vary in a regular way a given number of parameters. The results of test on these models were analysed, producing a regression of the resistance as a function of the parameters chosen. The Holtrop and Mennen systematic series are used for the determination of the propulsive power of a vessel, which series data are based on model experiments and full-scale data.

In order to determine the propulsive power of a ship employing the Holtrop and Mennen systematic series, a VBA (Visual Basic for Applications) based Excel spreadsheet was created. Moreover, the Wageningen B-series propellers were incorporated to study the open-water characteristics of a vessel. Due to the complexity of the formulae and the polynomials within the methods the analytical tool was written in VBA, hence allowing the tool to automatically iterate and look for the optimum values of key propeller parameters. Within the tool, two main iterations are completed: one to adjusts the blade area ratio until both K_Q values are equal, and the next iteration adjust the initial pitch of the propeller until the pitch to diameter ratio of the input value and the calculated value match. Since for a fixed pitch propeller the pitch of the propeller can only be optimized for a particular speed, the tool allows to select if the pith should be optimized for maximum or cruising speed.

2.2.2 Results

The Holtrop and Mennen tool was employed to determine the power requirements of a 68 meter superyacht. The known hull parameters were as follows:

• Length on waterline	66.60	m	• LCB (FOMS)	-0.45	%
• Breadth moulded	12.50	m	• C_M	0.918	
• Av. Moulded draft	3.40	m	• C_{WP}	0.824	
• Displacement	1650	t	• Transom area	2.64	m^2

The Holtrop and Mennen powering method established an effective power of 1817 kW to reach the maximum speed of 18 knots, and 662kW to reach the cruising speed of 14 knots. Assuming the vessel was fitted with a single propeller, an optimum diameter of 4 meters was achieved when optimized for the maximum speed. For this propeller size an open water efficiency of 57% was established according to the Wageningen B-series. Therefore, a shaft power of 3053kW was required for the vessel to reach the maximum speed. Further data is shown in Appendix 1.

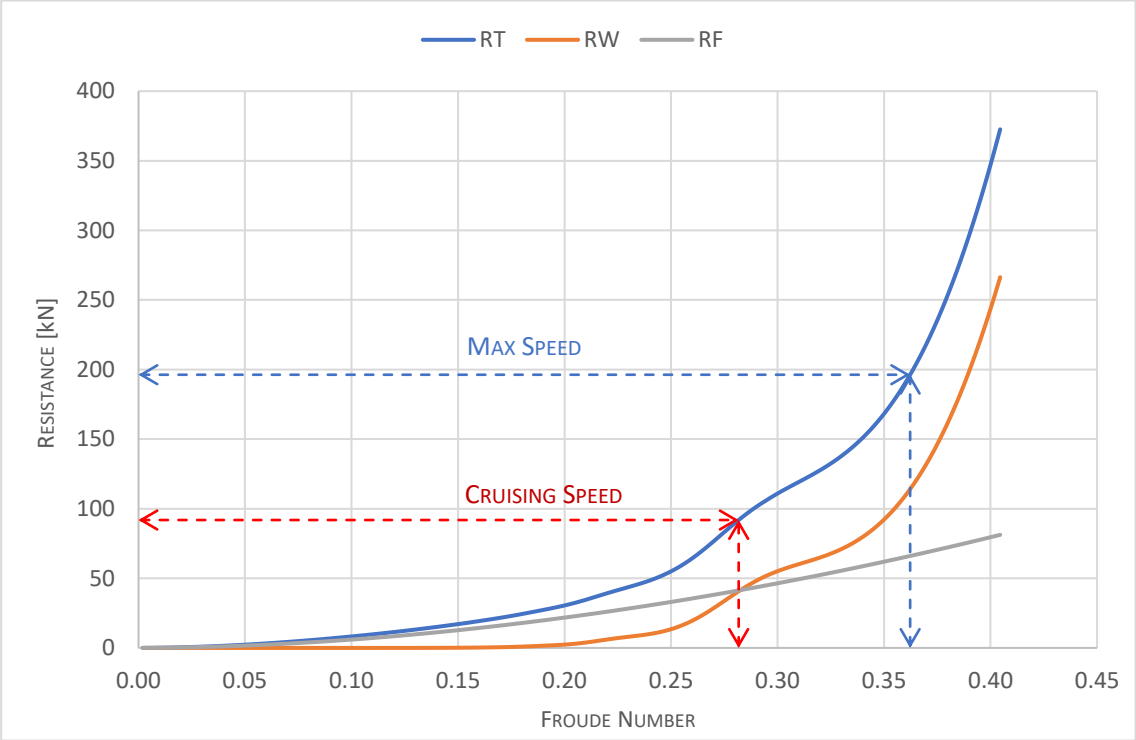

Figure 2.2: Initial resistance results for the target vessel.

3 NUMERICAL MODELLING

3.1 LITERATURE REVIEW

Computational fluid dynamics utilizes numerical analysis and data structures to analyse and solve fluid flows and the interaction of the fluid (liquid and gases) with surfaces defined by boundary conditions. Early work completed in 1983 by Ingham [3] used finite differencing scheme to model flow over a rotating cylinder at very low Reynolds numbers. The study used upwind, downwind, and central differencing schemes (CDS) to model the flow. Better results were achieved with the CDS model due to its higher order of accuracy. Further work by Badr et al. in 1985 [4] also implemented the finite differencing scheme to analyse the time-dependant flow past a rotating and translating cylinder. This work was able to capture accurate flow behaviour, as well as the movement of the stagnation point.

A similar approach was used in 1993 by Kang et al. [5] but solved the two-dimensional primitive variable Navier-Stokes equations with a Newton method. The mesh used for modelling the oscillatory rotation of a cylinder was a small O-type mesh (see Figure 3.1) which was still able to accurately capture downwind flow behaviour past the cylinder.

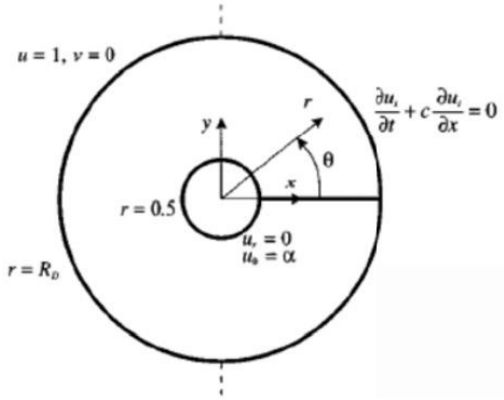

Figure 3.1: Outline of geometry for a O-type mesh (Source: Kang et al. (1999)).

In 1995 Chew et al. [6] combined two schemes on two different regions to model a generic case at Re = 1000. The first region is the near-wall viscous region around the cylinder and the second region is remaining domain area. The study used a hybrid vortex scheme which combined the use of the diffusion-vortex method in the near-wall region and the vortex-in-cell method in the far-field area. More recently, Karabelas [7] conducted a range of large eddy simulations (LES) at spinning ratios from 0 from 2 and at Re = $1.4 \cdot 10^5$. However, the open literature is poor in rotating cylinder flows at high Reynolds number regimes.

3.2 Turbulence modelling

Turbulence consist of fluctuation in the flow field in time and space, which occurs when the inertial forces in the fluid became significant compared to viscous forces. To allow turbulence effects to be predicted, turbulence models has been specifically developed to account for turbulence effects without the need of a prohibitively fine mesh and direct numerical simulation (DNS). Various turbulence models differ in how the flow close to wall is modelled, as well as the number of additional variables solved for, and what these variables represent. The different turbulence models relevant to the study are introduced next.

3.2.1 Statistical Turbulence Models

Statistical turbulence models based on the Reynolds Averaged Navier-Stokes (RANS) equations, modify the original unsteady Navier-Stokes equations with the introduction of averaged and fluctuating quantities. These models are known as statistical turbulence models due to the statistical averaging produce employed to obtain the equations. These equations will represent the mean flow quantities only, while modelling turbulence effects without a need for the resolution of the turbulent fluctuations.

3.2.2 Eddy Viscosity Turbulence Models

Eddy viscosity turbulence models (EVM) suggests that turbulence consist of small eddies which are continuously forming and dissipating, and in which the Reynolds stresses are assumed to be proportional to mean velocity gradients. EVM models can often be unsuitable for turbulent curved flows though.

Some eddy viscosity models compute the global value for the turbulence viscosity from the mean velocity and a geometric length scale using an empirical formula. Since no additional transports equation and therefore solved, these models are known as ‘zero equation’. The turbulence viscosity is modelled as proposed by Prandt and Kolmogorov as the product of a turbulent velocity scale and a turbulence length scale [8].

Two equation turbulence models such as k-ε and k-ω offer a good compromise between numerical effort and computational accuracy. Two-equation models use gradient diffusion to relate the Reynolds stresses to the mean velocity gradients and the turbulent viscosity, where the turbulent viscosity is modelled as the product of the turbulent velocity and turbulent length scale. In one hand, the k-ε model solves for two variables: k, the turbulence kinetic energy, and ε, the rate of dissipation of turbulence kinetic energy. In the other hand, the k-ω solves for k, the turbulence kinetic energy, and ω, the specific rate of dissipation of kinetic energy.

The Shear Stress Transport (SST) model accounts for the transport of the turbulent shear stress and gives highly accurate prediction of the onset and the mount of the flow separation under adverse pressure gradients. This model is a combination of the k-ε model in the free stream and k-ω model near the walls.

3.2.3 Reynolds Stress Turbulence Models

The Reynolds Stress Turbulence models are based on transport equations fir all components of the Reynolds stress tensor and the dissipation rate. These models do not use the eddy viscosity hypothesis but solve the transport of Reynolds stress in the fluid with an equation, for the individual stress components.

3.2.4 Model Comparison

The near wall treatment of the k-ω formulation is one of the advantages of this turbulence model for low-Reynolds number computations. The model does not involve the complex nonlinear damping function required for the *k*-εmodel. However, the *k*-εmodel does not predict the onset and amount of flow separation from smooth surfaces, because the model does not account for the transport of the turbulent shear stress. As a result, this leads in an overprediction of the eddy-viscosity.

3.3 Wall treatment

The presence of walls strongly affects the turbulent flow field. The walls are assumed to be a non-slip boundary, therefore the relative velocity between the fluid and the wall is zero. The flow velocity increases rapidly moving outwards perpendicular to the wall until it reaches the velocity of the free stream. The rate of change of velocity across the wall is not linear, as due to the large gradients in velocity the generation of turbulent kinetic energy is largest close the walls. This flow filed is divided into three regions. The viscous sub-layer is closest to the wall, where the viscous forces are predominant, significantly dampening turbulence and causing the flow to be mostly laminar. The buffer layer represents the intermediate region away from the wall, where the molecular viscosity and turbulence are of equal significance [9]. The outermost region is called the fully turbulent sub-layer, where the turbulent forces dominate, and viscous forces become negligible.

The near-wall boundary layer is therefore a critical aspect for the prediction of turbulent flows close to solid walls. A non-dimensional wall distance for a wall-bounded flow was defined as flows:

$$y^+ = \frac{y \cdot u_*}{v} \qquad \textit{(Equation 1)}$$

Where $u_* = \sqrt{\tau_\omega/\rho}$ is the friction velocity at the nearest of the wall and τ_ω is the wall shear stress. The location of the first layer cell within the boundary layer is given by:

- $0 < y^+ < 5$ Viscous sublayer
- $5 < y^+ < 30$ Buffer sublayer
- $30 < y^+ < 400$ Fully turbulent sublayer

The wall treatment must be specified for each turbulence model, since specific assumptions need to be made; for the wall boundary conditions and the turbulence quantities, to that model. Furthermore, wall treatments share the need to specify profiles of the mean flow quantities on the near-wall turbulent boundary layers. The mathematical description for mean flow quantities is defined by a wall law in turbulent boundary layers. The most common types of wall laws are: standard walls laws and blended walls laws. On one hand, the standard wall laws are slope-discontinuous between the laminar and turbulent profiles. In the other hand, the blended wall laws include a buffer region that smoothly blends the laminar and turbulent flow together [10]. Since the current study operated with a non-dimensional wall distance, the blended walls law was used by default.

3.4 Verification and validation

3.4.1 Validation

In the validation process, a simulation result (solution) is compared with an experimental result (data) which are conducted for specified variables at given locations, known as validation points. The nomenclature used in the validation approach is presented in Figure 3.2.

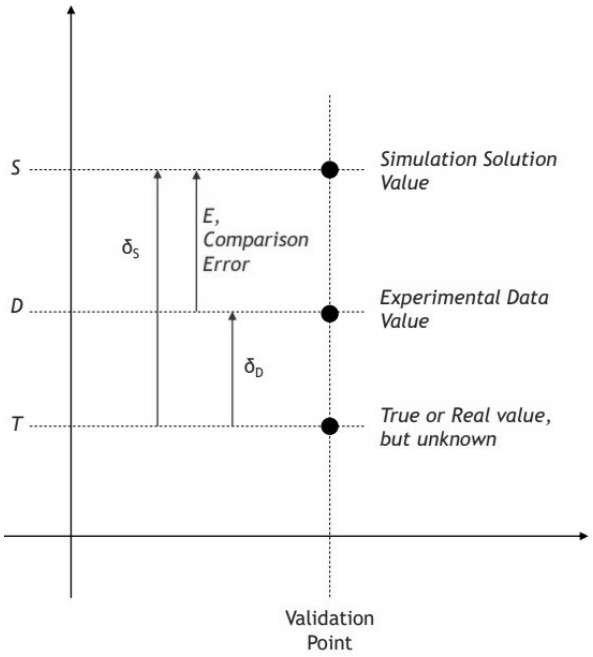

Figure 3.2: Schematic showing nomenclature for validation approach (Source: ASME V&V 20-2009).

The validation comparison error *(E)* is described as the difference between the simulation solution value *(S)* and the experimental data value *(D)*. As a result, the error in the solution value (δ_s) is the difference between the solution value and the true value *(T)*, and similarly the error in experimental data value (δ_D) is the difference between the experimental data value and the true value *(T).* The true value is a quantity of interest defined by the observer and is an abstraction [11]. The experiment is considered as the reality of interest, and thus the conditions of the actual experiment are the validation points simulated. The validation comparison error *(E)* is therefore the combination of all errors in the simulation results and in the experimental results (Equation 2).

$$E = (T + \delta_S) - (T + \delta_D) = \delta_S - \delta_D \qquad \textit{(Equation 2)}$$

Error in the simulation solution can be from errors from model assumptions and approximations δ_{MODEL}, errors from numerical solutions to equations δ_{NUM}, and errors in input values δ_{INPUT}. The objective of validation is to estimate the δ_{MODEL} within an uncertainty range. Since the signs and magnitude of δ_{NUM}, δ_{INPUT}, and δ_{MODEL} are unknown, the uncertainties corresponding to these errors are u_{NUM}, u_{INPUT}, and u_D. The validation standard uncertainty u_{VAL} is defined as an estimate of the standard deviation of the combination of errors ($\delta_{NUM} + \delta_{INPUT} - \delta_D$) as given in E. u_{NUM} can be estimated with verification that the code is mathematically correct for the simulations of interest, so that as the discretisation is refined the solution converges to a value (ie, as the mesh size increases, the results remain constant).

$$u_{VAL} = \sqrt{{u_{NUM}}^2 + {u_{INPUT}}^2 + {u_D}^2} \qquad \textit{(Equation 3)}$$

3.4.2 VERIFICATION

Code Verification

The objective of verification is to establish a numerical accuracy, which is independent from the physical (modelling) accuracy, as this is subject of validation. Verification establishes the numerical accuracy of the code ensuring that the code is "debugged", and that the solution is consistent, evaluating error estimation as the grid changes.

Solution Verification

While code verification provides an evaluation of error, solution verification provides only an estimate of error. The Grid Convergence Index (GCI) is a standardised method of verification to determine the quality of the convergence with the grid quality. More specifically, the GCI is a measure of the difference between the computed value and the asymptotic numerical value. This method for examining the special and temporal convergence of CFD simulations was presented by Roache [12], which is based on Richardson's extrapolation method. This extrapolation method is employed for obtaining a higher-order estimate of the value at zero grid spacing (continuum value) from a series of lower-order discrete values.

The method involves performing the simulation on two or more successively finer grids. The GCI can be computed using two levels of grid; however, three levels are recommended in order to accurately estimate the order of convergence and to ensure the solutions are within in the asymptotic range of convergence. In this process, different *n* levels of coarser grids are generated, with the number of grid points in each coordinate satisfying the following relation (where *m* is an integer):

$$N = 2^n\, m + 1 \qquad \textit{(Equation 4)}$$

A minimum grid refinement factor of $r \geq 1.1$ must be employed to allow the discretization error to be differentiated from other error sources, such as iterative errors, and computer round-off errors. However, practical experience [Roache] has shown good results with non-constant grid refinement ratios greater than 1.3 using GCI. The GCI on the fine grid is defined as follows:

$$GCI_{fine} = \frac{F_s|\varepsilon|}{(r^p - 1)} \qquad \textit{(Equation 5)}$$

where F_s is a factor of safety, and $|\varepsilon|$ is the approximate relative error derived from the extrapolated solution values of the grids. A factor of safety is applied for reporting purposes, which is recommended to be F_s=3 for comparisons of two grids and F_s=1.25 for comparisons of three or more grids. Since the analysis will involve many CFD simulations, the use of a coarser grid may result in reduced computing time. It is therefore necessary to quantify the error for the coarser grid. The GCI on the course grid is defined as follows:

$$GCI_{course} = \frac{F_s|\varepsilon|r^p}{(r^p - 1)} \qquad \textit{(Equation 6)}$$

4 FLETTNER ROTOR

4.1 INTRODUCTION

The Flettner rotor is a form of wind based propulsion that utilizes the Magnus effect, a phenomenon which generates a sidewise force on a spinning cylindrical solid immersed in a fluid when there is relative motion between the spinning body and the fluid [13]. This propulsion was invented by the German engineer Anton Flettner (Flettner, 1925), and it was first used in 1925 onboard a ship named *Backau* as a form of propulsion (Figure 4.1). This vessel was a refitted schooner which carried two rotors approximately 15 metres high, and 3 metres in diameter, driven by an electric propulsion system of 37kW of power. During the sea trials of the Backau, the vessel showed that it could be sailed much closer to the wind that was possible with the conventional sail plan. In addition, it was also possible to steer the vessel by changing the rotational speed of the rotor sails and even to sail in reverse. The *Backau* successfully completed its first voyage across the Atlantic in 1926. The rotor sails actually proved to enhance the safety of the ship on heavy weather, since they served to retain steering control while the wheel and rudder were useless during a running sea. Despite the proven concept, the increasing adoption of diesel engines and the low oil price of that time, the rotor ship was fast abandoned.

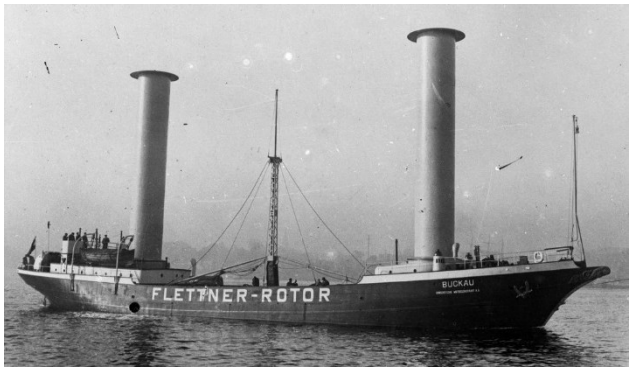

Figure 4.1: The Backau rotor ship. (Source: DLR Central Archive)

In recent years there has been several examples of Flettner rotors in used on commercial ships. In 2008, the wind energy company Enercon designed and began construction on the cargo ship *E-ship 1*. This vessel was fitted with 4 individual 25 metre height rotors, two fore and two aft, as a form of assisted propulsion. According to Enercon, this vessel has achieved operational fuel savings of up to 25% compared to same-sized conventional freight vessels [14]. In 2015, the Ro-Ro cargo ship *MV Estraden* was retrofitted with two 18 metres high and 3 metres in diameter, Flettner rotors. Based on verified measurements by NAPA, the rotor sail solution achieved a fuel consumption reduction of 6.1% [15]. In 2018, the *Maersk Pelican* was retrofitted with two 30 metres high and 5 metres in diameter Flettner rotors. Based on independent measurements conducted by Lloyd's Register fuel savings of 8.2% during the first year of operation were confirmed.

4.2 Flow past a smooth cylinder

When a cylinder is made to rotate rapidly in an airstream directed against its axis, the resulting force is formed by the resistance or drag in the direction of the wind and a lateral force towards the side where the direction of the wind coincides with the direction of rotation. This force is called the Magnus effect, initially observed and scientifically explained by Professor G.Magnus in 1851.

The flow past a non-rotating cylinder is known to produce a Von Kármán vortex street behind the cylinder, as shown in Figure 4.2. However, the flow past a rotating cylinder shows quite a different behaviour that the observed in a non-rotating situation. Such vortex street may also be developed for rates less that the critical velocity ratio. Experimental results have showed in almost all cases the flow steadies once the velocity ratio reaches a critical rate of $\alpha_L \approx 2$. Recent work completed by Karabelas [7] indicate that the flow in the turbulent regime drops the critical rate to roughly $\alpha_L \approx 1.3$. As the cylinder rotates within a uniform flow, one side of the cylinder perpendicular to the uniform flow will move against the flow and the opposite will move with the flow . As a result, a difference in velocity between the sides will essentially mean a pressure drop across the cylinder. Much like on an airfoil, the pressure difference forces the flow to bend towards the low pressure side. In addition, the asymmetry about the centreline shows that the stagnation point at the leading edge of the cylinder rotated in the direction of the rotation.

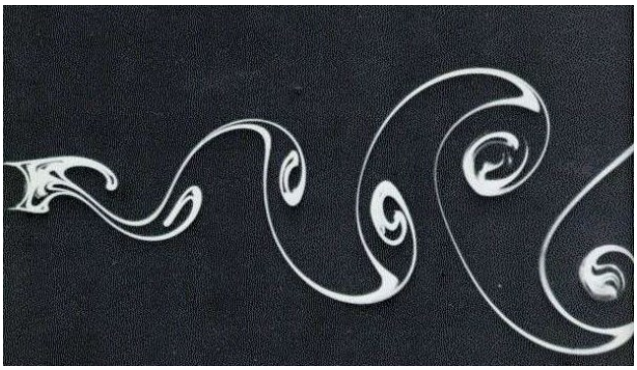

Figure 4.2: Von Kármán vortex street at Re = 140. (Source: Von Dyke 1982.)

The fundamental principles of the magnus effect were initially explained by the Kutta-Joukowsky theorem. This theory states that, the magnitude of the force can be computed by the integrating the surface pressure times the area around the cylinder [16]. Assuming a rotating cylinder in the potential flow, the lift force F_L from the Kutta-Joukowsky theorem can be calculated using the following equation:

$$F_L = \rho(\Gamma \cdot U_\infty) \qquad \textit{(Equation 7)}$$

The circulation Γ around the cylinder is calculated as follows

$$\Gamma = \oint V ds = 2\pi\Omega R^2 \qquad \textit{(Equation 8)}$$

Where $\oint ds$ is the contour integration of the full circumferential length of the cylinder wall and V is the tangential velocity along the path of integration. As a result, the final expression of lift force L for a rotating cylinder per unit length is obtained as

$$F_L = 2\pi\rho U_\infty \Omega R^2 \qquad \textit{(Equation 9)}$$

This formulation was employed to initially size the rotor geometry, based on a target lift force of 20% of the total resistance of the vessel. As a result, for a vessel speed of 18 knots a rotor diameter of 1 metre was established.

4.3 COMPUTATIONAL GRID

4.3.1 MESH

The grid generation and grid quality are essential elements of the whole discretization process., as the accuracy of the calculated numerical results is dramatically dependent on the mesh quality. An O-type mesh with hexahedral elements was constructed for the field surrounding the rotor, with a total number of cells of 281000. The domain diameter size was 20 times rotor diameter and 0.1 rotor diameters high. The reference system was built so that the origin lies on the centre of the rotor, the x-axis has the leading-to-trailing edge direction, and the z-axis is directed upward.

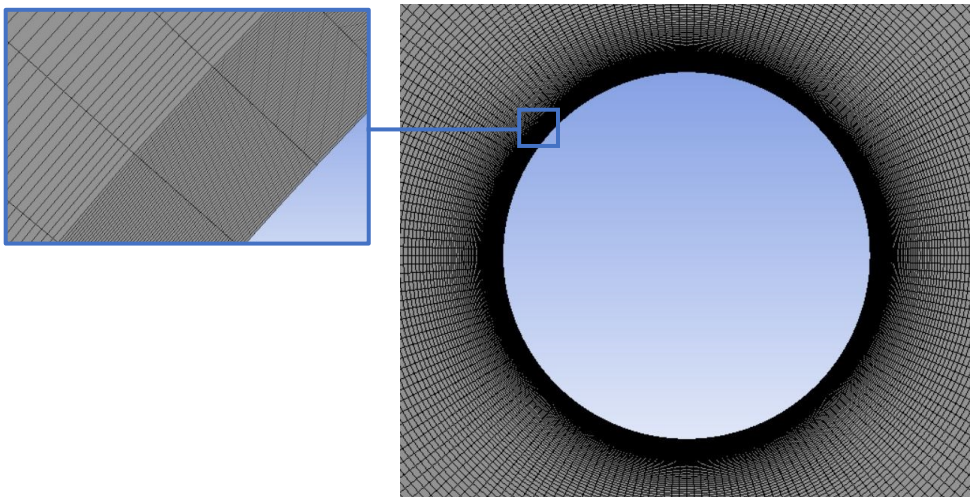

Figure 4.3: Rotor geometry and structured mesh with $y^+ = 3$.

Simulations were completed with the SST k-ω turbulence model (see Section 4.4), which utilizes the k-ω turbulence model in the near wall region. Since the k-ω turbulence model is capable of resolving the near-wall region down to the viscous sub-layer, a resolution corresponding to a non-dimensional wall distance of $y^+ = 1$ was targeted, although values up to $y^+ = 4$ were acceptable. In addition, the boundary layer resolution must be sufficiently high in the near-wall boundary layer. Therefore, 20 control layers were positioned in the near-wall boundary layer.

Obtaining a sensible y^+ value required several simulations with an initial non-dimensional wall distance of 10, positioned for the log low region. Postprocessing the results, the y^+ value was then adjusted based on the regions with high-velocity gradient. The y^+ value was much reduced to close the grid to the wall and hence expose regions to more intensified turbulent flow. A first layer height of $1.37 \cdot 10^4$ meters was established, corresponding to a y^+ value of 3.

4.3.2 MESH QUALITY

The quality of the mesh pays a significant role in the accuracy of the numerical computation since many aspects of the mesh have a vital contribution to simulation accuracy. A good quality mesh should incorporate the following aspects:

- A meshing valid for the studied physics. Therefore, a good boundary resolution must be present to capture frictional effects on the walls.
- A grid independent solution.
- Important geometric details well captured.
- A mesh quality criterion within correct range. The attributes associated with mesh quality are orthogonality, the skewness, and the aspect ratio.

Orthogonality

The measure of mesh orthogonality relates to the distance between adjacent element edges (or adjacent element faces) are to some optimal angle (depending on the relevant topology). The orthogonality is measured from 0 (poor) to 1 (good) [17]. For a cell it is the minimum of:

$$\frac{A_i \cdot f_i}{|A_i||\overrightarrow{f_i}|} = \frac{A_i \cdot c_i}{|A_i||\overrightarrow{c_i}|} \qquad \textit{(Equation 10)}$$

Where A_i is the face normal vector, f_i is a vector from the centroid of the cell to the centroid of that face, and c_i is a vector from the centroid of the cell to the centroid of the adjacent cell. The orthogonal quality reported form this mesh shows a minimum value of 0.998, which therefore results in a good mesh orthogonality.

Skewness

Skewness is defined as the difference between the shape of the cell and the shape of an equilateral cell of equivalent volume [17]. This is captures according to the Normalized Angle deviation (Equation 11) by finding the minimum angle between two lines joining opposite mid-sides of the element. The skewness is measured from 0 (good) to 1 (poor).

$$skewness = max\left[\frac{\theta_{max} - \theta_e}{180 - \theta_e}, \frac{\theta_e - \theta_{min}}{\theta_e}\right] \qquad \textit{(Equation 11)}$$

Where θ_e is the equiangular face/cell, 90 degrees for hexahedral elements or 60 degrees for tetrahedral elements. As a general rule, the maximum skewness should be kept below 0.95, with an average value that is less than 0.33. The skewness reported form this mesh shows a maximum and average value of 0.01, which therefore results in a good mesh skewness.

Aspect ratio

The aspect ratio is the measure of the stretching of a cell. Generally, it is best to avoid aspect ratios in excess of 5:1 away from the walls, and aspect ratio greater than 10:1 on hexahedral cells inside the boundary layer [10]. Furthermore, in order to achieve good stability of the energy solution, the maximum aspect ratio should be kept below 35:1. The aspect ratio reported form this mesh shows an aspect ratio of 18.8 in the bulk flow. However, higher than recommended aspect ratio values are found in the boundary layer region, due to the geometry depth. With regard to the stability of the flow solution it does not signify an issue, but it may impede good stability of the energy solution. However, simulations have shown a good converge along the different set of conditions.

4.4 Setup

4.4.1 Boundary conditions

A velocity inlet boundary condition was defined on the front part of the domain with the prescribed velocity for each run. On the rear part of the domain, a pressure outlet boundary condition was set with a relative pressure of 0 Pa. On the sides of the domain, a symmetry boundary condition was also used. The wall boundary conditions on the cylinder were set to non-slip and zero roughness and the rotation of the rotor was modelled as a moving-wall boundary condition.

4.4.2 Simulation settings

Simulations were completed with the SST k-ω turbulence model which has previously been used in similar studies [9] [18]. This model applies different sub-models in different parts of the turbulent sub-layers. It utilizes the k-ω turbulence model in the near wall region and switches to the k-ε turbulence model (using a k-ω formulation) in the free stream. As a result, the SST k-ω turbulence model incorporates the strength of the two respective models.

All the simulations were completed with a variable time step, as a function of the Courant number. This represents the measure of how much flow particles traverses a computation grid cell in a given time-step. Ideally, the time-step should be scaled for a Courant number lower than one. Otherwise, fluid particles move through two or more cells at each time-step and this can affect convergence negatively. However, as the time-steps are reduced, and the simulation time is increased. The computational time for each simulation with a Courant number of one was estimated at 56h, therefore, the time-step scale was increased. Although, the simulations targeted a high courant number, good convergence was reported.

4.5 Verification and validation

4.5.1 Grid Convergence Index

The Grid Convergence Index (GCI) method was employed to determine the quality of the convergence with the grid quality. As stated in Section 3.4.2, the method involves performing the simulation on two or more successively finer grids. Three levels of grid refinement were used to accurately estimate the order of convergence and ensure the solutions are within the asymptotic range of convergence. The grid convergence results on a sequence of grids are presented here:

Grid	Grid Size	Edge Cells	Cell Size
Fine	475600	689.64	1.45E-03
Medium	365000	604.15	1.66E-03
Coarse	281000	530.09	1.89E-03

Table 1: GCI grid definitions.

GCI calculations were completed for the hight free-stream velocity run. Furthermore, the lift and drag coefficient were analysed on the study. Considering that three levels of grid refinement were analysed, a factor of safety of 1.25 was applied [19] [20]. GCI results (see Figure 4.4) showed that the lift and drag coefficient on the finest grid were estimated to be within ≈2% of the value obtained by a grid double the size. Therefore, the grid refinement was considered as appropriate for the study. Further details are shown in Appendix 2.

RPM	C_L	C_D
225	1.96%	0.31%
450	0.50%	0.43%

Figure 4.4: GCI results summary.

4.5.2 Mesh independence

The mesh independence study was done by comparing the three different mesh resolutions (see Table 1) for five different velocity ratios. Results are presented in Figure 4.5, for the lift and drag coefficients against the range of velocity ratios for the different mesh resolutions. As the mesh resolution was increased the lift and drag coefficients did not present any changes in the examined speed ratio range. According to the results from the mesh independence study, the near wall boundary layer is well resolved, and the free-stream resolution does not require to be increased at the lowest mesh resolution. The mesh independence study results are therefore in accordance with the mesh results obtained with the GCI (see Section 4.5.1).

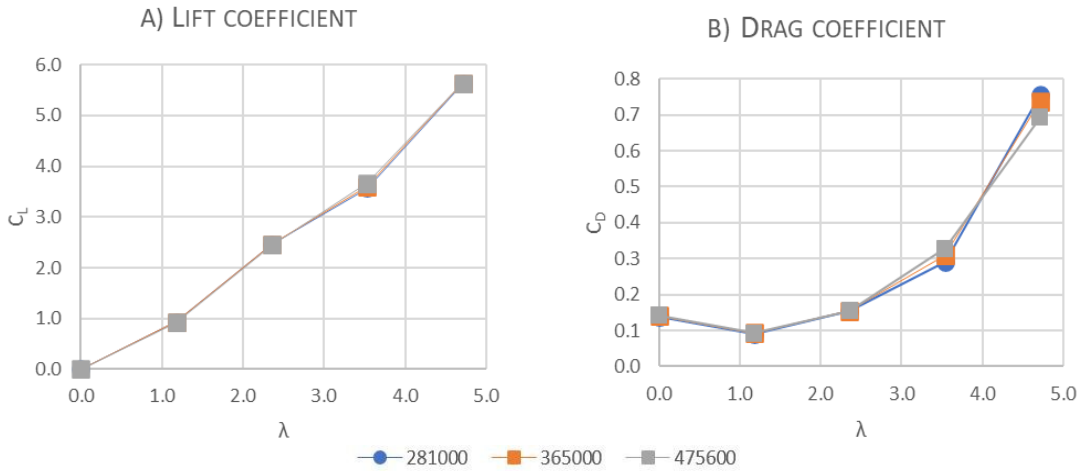

Figure 4.5: Lift and drag coefficients as a function of speed ratio for different mesh resolutions.

4.5.3 Boundary layer resolution

Boundary layer resolution was analysed based on the eddy viscosity ratio. The eddy viscosity ratio is defined as the eddy viscosity divided by the dynamic viscosity. The simulation results represented in Figure 4.6 shows that the established y^+ value prescribed at the first cell lays within the logarithmic composite region of the turbulent boundary region [21]. Moreover, the increase in turbulent viscosity between the inner layer and the outer layer of the logarithmic region is also captured. Furthermore, the turbulence gradually dissipates closer to the free stream conditions as expected. Therefore, the previously established non-dimensional wall distance (Section 4.3.1) were considered valid for the study.

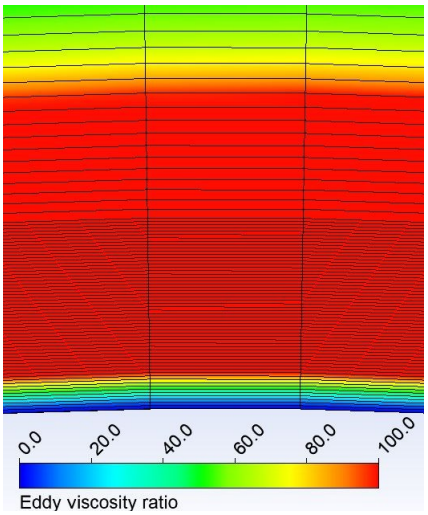

Figure 4.6: Eddy viscosity ratio plot at U=12 m/s and V_R = 0.6 for y^+ = 3.

4.6 Reynolds number effect on the aerodynamic performance

4.6.1 Literature review

The determination of the air forces acting on rotating cylinder with axes perpendicular to the direction of the motion were first studied at the Langley NACA Laboratory by Reid [22] in 1924. The experiments were carried out on a rotating cylinder of physical aspect ratio, $AR = 13$, without endplates, at Reynolds numbers varying between $Re = 3.9 \cdot 10^4$ and $Re = 1.1 \cdot 10^5$. The experiments showed that for the range considered, the Reynolds number has a minimal influence on C_L and C_D. However, the results of Reid also indicate that beyond a velocity ratio, $\lambda = 0.5$, the lift forces increase steadily and between $\lambda = 0.5$ and $\lambda = 2.0$, there is practically no variation in drag. In addition, for velocity ratios greater than 2.0 the drag increased and the maximum lift to drag ratio (7.8) is attained when $\lambda = 2.5$, approximately.

Later in 1934, Thom [23] presented an experimental work on rotating cylinders, with a large series of force and pressure measurements with emphasis on the effects of the surface roughness, aspect ratio, end plate disk and the Reynolds number. With regard to the scale effects, the work of Thom measured the C_L and C_D values on a rotating cylinder of physical aspect ratio, $AR = 12.5$, with endplates, at Reynolds numbers varying between $Re = 5.3 \cdot 10^4$ and $Re = 8.8 \cdot 10^4$. The results show no effects on the aerodynamic coefficients at the Reynolds numbers considered. Later work of Thom completed in 1934 [24] studied placing evenly spaces disks along the span of the Flettner rotor to increase lift and decrease drag, which resulted with no increase in lift but did prolong the drop in C_D with increasing angle of attack.

Swanson [25] provided in 1961 a detailed summary of the experiments on Flettner rotors carried out until that time. The study was performed for a set of two-dimensional tests at a Reynolds number range $3.5 \cdot 10^4 < Re < 5.0 \cdot 10^5$ for velocity ratios $0 \leq \lambda \leq 1$. The study indicated that as the velocity ratio $\lambda > 1$, the drag increases to a value greater than the drag on the non-rotating cylinder, even though the wake area is increasing. The increase in drag is due to "the movement of the trailing stagnation point and the wake in a counterclockwise direction into the region near the bottom of the cylinder. Further increase in λ produces an additional rotation of the wake towards the front of the cylinder. The resulting flow pattern and pressure distribution produce a lower C_D, and more favourable lift to drag ratio are obtained in the velocity ratio $\lambda \approx 4$ [25].

In 1985, Clayton [26] performed several tests on a rotating cylinder of aspect ratio $AR = 10.4$ with two endplates of size $1.4D$ and $2D$, at two Reynolds number: $Re = 1.7 \cdot 10^4$ and $Re = 4.9 \cdot 10^4$. The results from the author indicate that when the larger size endplate is employed, the effects of different Reynolds number on the aerodynamic performance is negligible. However, for the smaller endplate, a reduction of Reynolds number reduces C_L and increases C_D for $\lambda > 2$, while for higher λ values there is a tendency for C_L / C_D to be higher for the lower Reynolds number case. However, the maximum C_L / C_D is archived at the higher Reynold number at a low λ.

Tokumaru and Dimotakis [27] completed in 1993 a series of test to investigate the mean lift coefficient of a rotating cylinder with aspect ratio $AR = 18.7$, with no endplates, at a Reynolds number $Re = 3.8 \cdot 10^3$. The experiment yielded estimates for C_L which agree with the data published by Thom [23] when $\lambda > 1$. However, for $\lambda < 1$ the measurements showed values that are higher. The discrepancy is attributed to a lower Reynolds number used in their investigation.

4.6.2 Lift coefficient

The two-dimensional lift coefficients are presented in Figure 4.7. In the range $0 < \lambda < 2.5$, higher Reynolds numbers lead to higher lift coefficients. This holds true until Re = 3.2·105, since for the higher Reynolds number studied such effects are not noticeable. Furthermore, the slope the lift coefficient at velocity ratios $\lambda < 4$ is less steep at the lower Reynolds numbers. Therefore, the Reynolds number does have a significant effect for an incremental velocity ratio. On the order hand, at a certain velocity ratio the lift coefficient does not seem to be affected by the Reynolds number. This is also supported by the fact that the lift coefficient at the highest Reynold number is not affected at any velocity ratio. Furthermore, the results of the lift coefficient obtained in the present study were compared to similar studies (Figure 4.7). In the experimental work of Badalamenti [28] the lift coefficient curve follows a similar trend to the results presented in this study. However, the slope of the curve presented by the author decreeses at $\lambda = 2.5$, while the numerical results completed on this study decreeses at $\lambda = 4$. In the work of Bordogna [29] the lift coefficient curve follows a similar trend for $Re = 3.6 \cdot 10^5$, while the lift coefficient curve for $Re = 1 \cdot 10^6$ is considerably lower. This is likley to be due to the lower Reynold number used in the experiments.

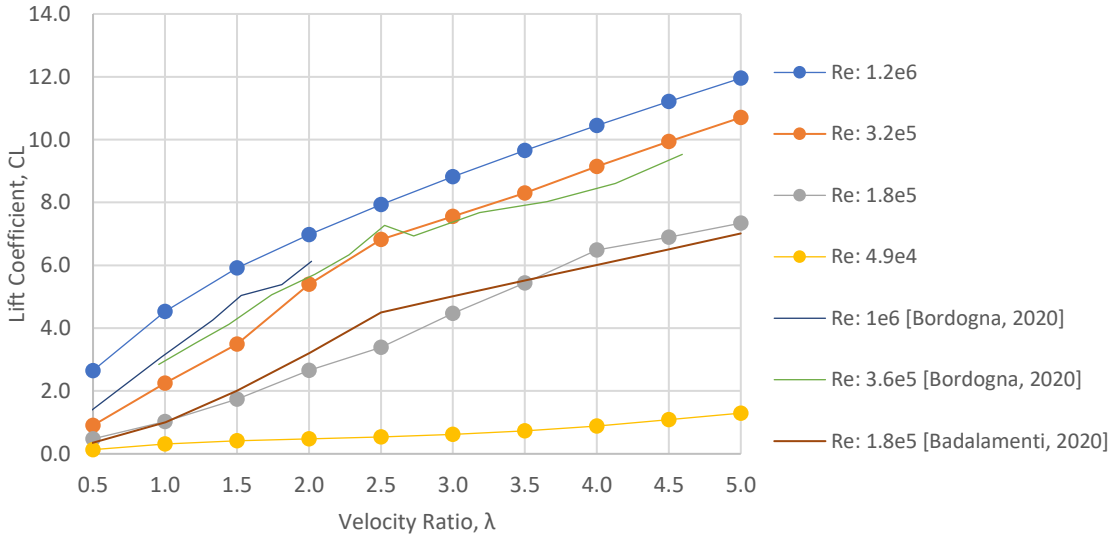

Figure 4.7: Lift coefficient vs velocity ratio.

The results presented in this section represent the two dimensional lift coefficients, which are then scaled to three dimensional values based on the rotor height and aspect ratio. However, studies of three-dimensional cylinders without end plates indicate that the lift coefficient ceases to increase after a certain velocity ratio [28] [30], depending on the aspect ratio of the rotor. In the work of Badalamenti [28] a rotor with an aspect ratio AR = 5.1 shows that the slope of the lift coefficient curve decreases at $\lambda = 2.5$ and for $\lambda > 5$ a plateau is found [29].

4.6.3 Drag coefficient

The drag force obtained from the CFD simulations were time-averaged as a function of the speed ratio, since the drag results changed overtime. This is due to the fact that the drag is very sensitive to changes in pressure distribution, caused by the non-periodic vortex shedding located in the wake of the cylinder (Section 4.6.4). The two-dimensional drag coefficients are presented in Figure 4.8.

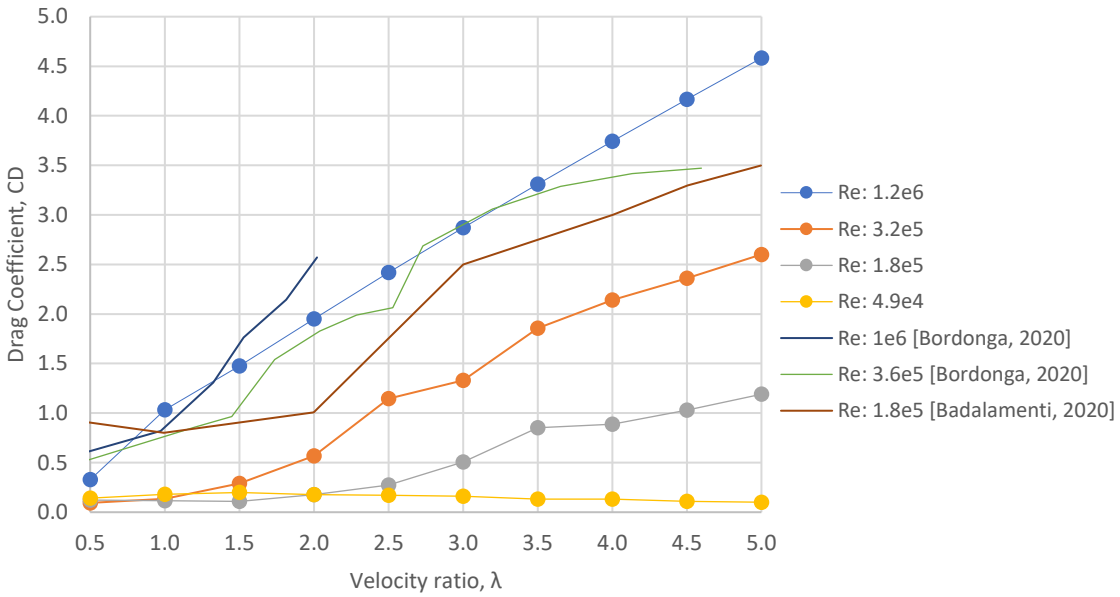

Figure 4.8: Drag coefficient vs velocity ratio.

From the numerical results obtained from this study, the Reynolds number influence is evident at velocity ratios up to $\lambda = 3.5$. Similar to the lift coefficient, the drag coefficient at the highest Reynold number is not affected at any velocity ratio. At $0.5 < \lambda < 2$ the difference between the drag coefficient obtained at $Re = 4.9 \cdot 10^4$ and $Re = 1.8 \cdot 10^5$ do not show any remarkable difference. However, at $\lambda > 3.5$ the difference becomes significant. The results in the present study shows a similar trend compared to the findings of Bordogna [29]. However, when compared to the study of Badalamenti [28] the results significantly differ.

The work of De Marco et.al [31] shows that similarly to the lift coefficient, the drag coefficient on three-dimensional cylinders without end plates ceases to increase after $\lambda < 2$. Furthermore, in case the cylinder was equipped with endplates, the drag keeps increased with velocity ratio. This is also supported by Badalamenti [28] and Zhang et al. [32], by the fact that for velocity ratios $\lambda > 3$, rotating endplates generate more drag that a cylinder without endplates.

4.6.4 Flow Vorticity

Figure 4.9 shows a contour plot of vorticity of the vortex street for λ = 5 at Re = $1.2 \cdot 10^6$. The vorticity describes the local spinning motion of the fluid, as defined by the curl of the flow vector [9], and given by:

$$\vec{\omega} = \frac{\partial u_y}{\partial x} - \frac{\partial u_x}{\partial y} \qquad \textit{(Equation 12)}$$

The high spinning ratio of the cylinder and viscous effects close to the wall cause the wake to be drawn towards the direction of rotation (A). The free-stream flow causes an extension of the wake (B) which then formats a negative vortex (C), which eventually separates (D). This process is repeated successively. This vortex shedding is different than for a non-rotating cylinder or slowly spinning cylinder, as there is single vortex shedding and it occurs below the cylinder. In addition, the frequency of the vortex shedding is much lower than for von Kármán shedding (Section 4.2). As a result of this transient flow behaviour, the lift and drag forces change periodically, since the wake location and structure change.

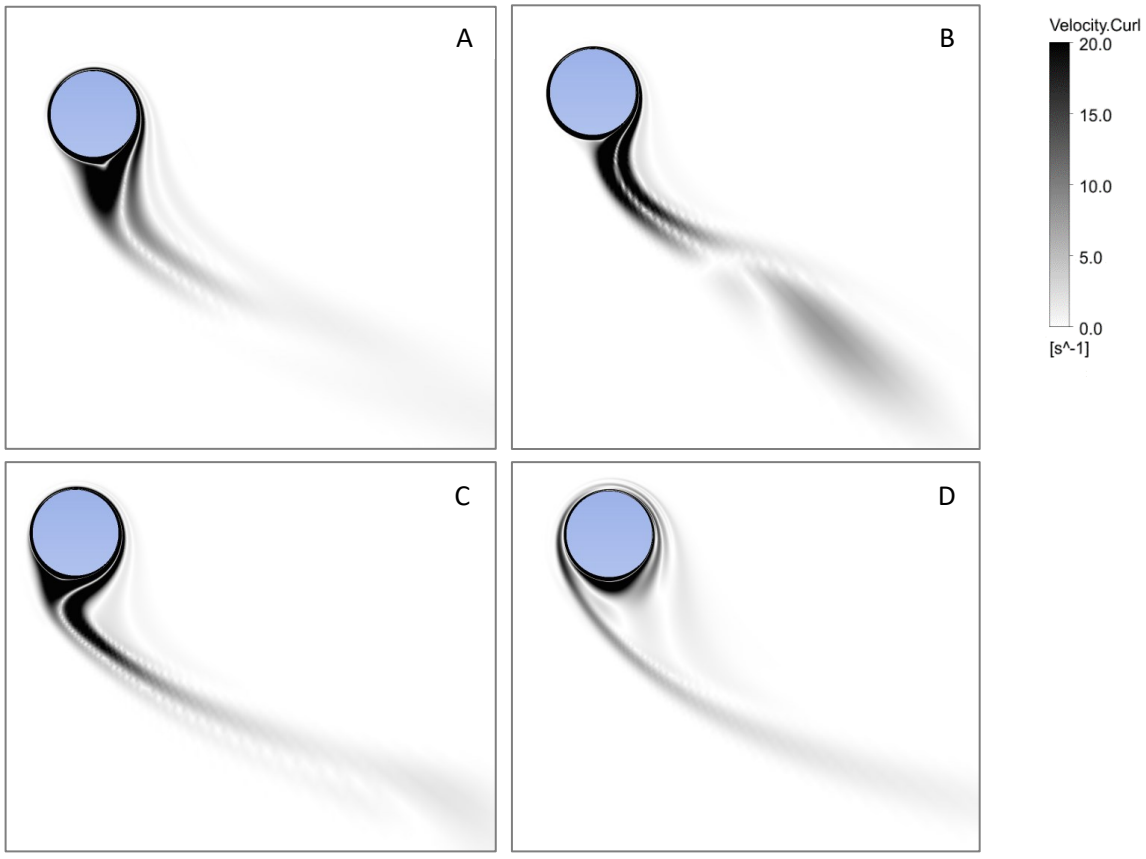

Figure 4.9: Contours of vorticity showing the development of a vortex street for λ = 5.

A similar flow structure is observed at lower velocity ratios. In addition, a second vortex shedding mode is observed at λ = 5, with a lower shedding frequency than von Kármán shedding. As a result, a sudden increase in drag is experienced as the spin ratio approached the second shedding mode. Stojković [33] also reported this second shedding mode for 4.35 < λ < 6.25. Furthermore, the author also indicates that the onset of the second shedding mode occurs for a lower spin ratio as the Reynolds number is increased.

4.6.5 Rotor efficiency

The efficiency of the rotor was not substantiated by the L/D ratio since it does not provide a relevant quantity in terms of the rotor contribution to the ship's propulsion. In this context, the thrust power produced by the rotor in relation to the rotational power required to drive it was the most import metric form to assess the efficiency. For the purposes of assessing rotor performance in isolation, a pseudo power multiplication factor was employed, defined as:

$$\varepsilon = {F_L \cdot U_\infty}/{P_R} \qquad \textit{(Equation 13)}$$

Where F_L is the rotor lift force, U_∞ the freestream velocity, and P_R the power required to rotate the rotor. When ε > 1, the rotor provides more thrust energy than the power required to rotate it. Plotting the results in dimensional form (Figure 4.10) illustrated that the higher the velocity ratio, the less thrust was produced by the rotor, but the less power was required to drive the rotor. Furthermore, the Reynolds number influence is evident.

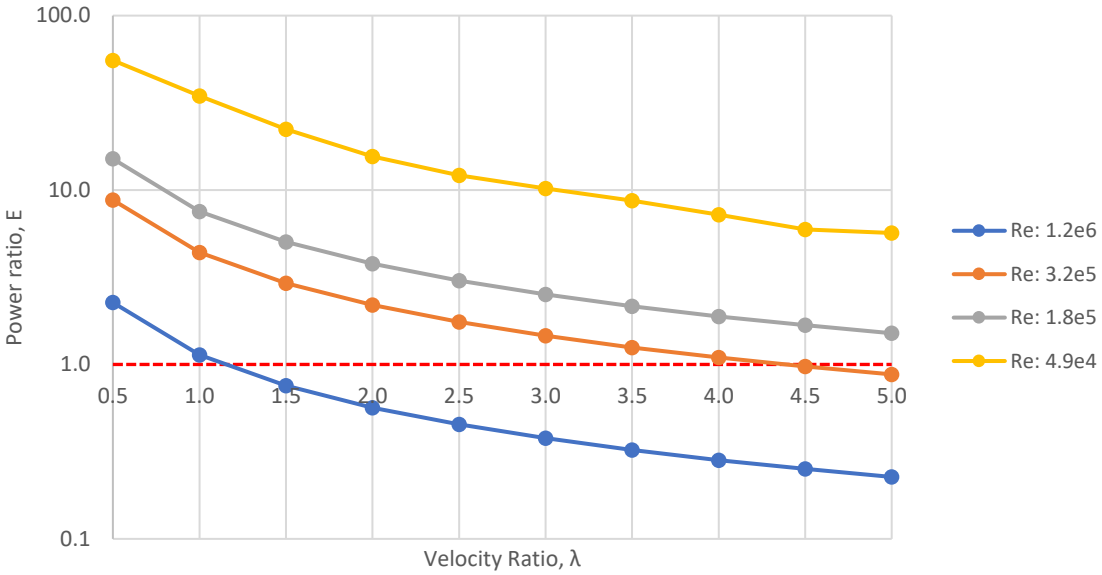

Figure 4.10: Variation of power multiplication factor with velocity ratio.

4.6.6 Conclusions

The present chapter deals with a series of CFD simulations aim at a better understanding of the Reynolds number effects on the lift and drag coefficients of Flettner rotors. The results indicate that there is a significant influence of the Reynolds number on the lift coefficient below a velocity ratio λ = 2.5, and below a velocity ratio λ = 3.5 on the drag coefficient. Moreover, both the lift and the drag coefficients are not affected at any velocity ratio at the highest Reynold number. The results from the present study were also compared with similar studies. Despite the difference in results caused by different Reynolds number used, similar qualitative conclusions are shared with the findings of Badalamenti [28] and Bordogna [29]. The stability of the wake was found to be highly dependant on the velocity ratio, with the von Kármán vortex shedding developing from 0 < λ < 1.4 and ceasing at 1.6 < λ < 2.7. In addition, at λ = 5 a second vortex shedding mode was observed.

5 WING SAIL

5.1 INTRODUCTION

A wing sail is a vertical airfoil cross-section structure, much like an airplane wing, which utilizes the change in pressure between each side surfaces of the wing to generate lift. Historically wing sails were early studied in small sailing dinghies to investigate replacing cloth sails with similar size and shape wing sail, aiming on better performance. One of the first known to implement the use of wing sails on a boat was *Utne* in 1941 with the construction of the *Flaunder*. This boat was a modified one-man sailing kayak that utilized a self-trimming rotating wing sail. However, due to the outbreak of World War II, the *Flaunder* was destroyed as a potential war machine, and no further progress was noted.

Later in 1968, Walker [34] designed and built a series of self-trimming wing sailed trimarans. One of which was the trimaran *PlaneSail*, which used four NACA0012H section wings arranged as quadra-plane with a trailing tail for self-trimming. This designed was refined with another trimaran the *Flyer* in 1972, which used a single multi-element wing with both leading and trailing edge devices. Interest on wing sails arised when the C-Class racing catamaran *Miss Nylex* won the International Catamaran Challenge Trophy in 1974. Up until this this point in time, wing sails had remained a rarity in the sailing world. This C-Class racing catamaran used a rigid wing sail with two trailing edge flaps. Furthermore, the implementation of wing sails in the last three editions of the America's Cup, has yet increased wing sail visibility.

In recent years there has been several examples of wing sails in used on commercial ships. In 2019, the 3600 DWT general cargo *MV Ankine* shipping vessel (see Figure 5.1) was retrofitted with twin wing sails. This vessel is expected to reduce fuel cost over a period of approximately three years, which will equal the cost of the system. Furthermore, recent studies on wing sail implementation for commercial purposes has shown potential fuel savings of up to 30%, and recorded fuel savings of 22.9% when motor powered and with the wing sail operation.

Figure 5.1: Ankine vessel fitted with twin wing sails (Source: Econowind).

5.2 INITIAL CONSIDERATIONS

The profile of a wing sail is able to greater a great amount of lift and hence provide a strong propulsive force, while maintaining a low induced drag which would slow the speed of the vessel. Its operating principles is to maximise the aerodynamic lift force by rotating the wing to the optimum angle of attack. An airfoil section can be made either symmetrical or asymmetrical. An asymmetrical section can offer a higher maximum lift coefficient and a higher lift/drag ratio than a symmetric section. However, since the vessel is required to sail equally well on both port and starboard tacks, the section must be symmetrical.

5.3 Computational grid

5.3.1 Mesh

The simulations were intended to be performed on two airfoil sections, named NACA-0012 and EPPLER-473, at the angles of attack ranging from 0° to 20° in steps of 2° degrees. Therefore, each angle of attack required its own mesh (for each mesh). Geometry dimensions are shown in Figure 5.2. In addition, the airfoils were 1 metre in chord length, with a 0.1 metre geometry depth.

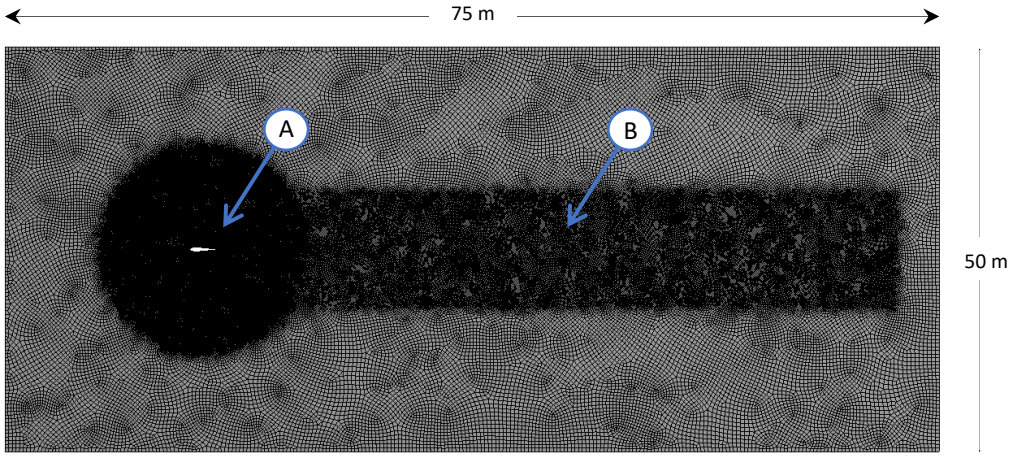

Figure 5.2: EPPLER-473 airfoil mesh at an angle of attack α = 0°.

The rectangular type mesh with tetrahedral elements was constructed for the field surrounding the airfoil, with a total number for cells of ≈340000. Two geometric bodies were used to control the mesh refinement around the airfoil (A) and along the wake (B). In the intersection region, this feature created a finer number of grid points. The area around the airfoil was refined with a node increment of 1.3, and the wake was refined with a node increment of 1.2.

With relatively complex geometries like an airfoil, a tetrahedral element order can offer a mesh with much fewer cells that the equivalent mesh consisting of hexahedral elements. This is because the tetrahedral mesh allows clustering of cells in selected regions of the flow domain. However, a large aspect ratio in tetrahedral mesh will invariably affect the skewness of the cell and may hinder accuracy and convergence. Therefore, an unstructured hexahedral mesh of high aspect ratio was used, as the mesh had far fewer cells than a tetrahedral mesh would, and convergence will generally be faster, hence saving computational expense.

5.3.2 Mesh quality

As previously explained in Section 4.3.2, the mesh quality pays a significant role in the accuracy of the numerical computation. The same mesh quality criterion previously used was employed to assess the mesh quality of the airfoil meshes:

- The orthogonal quality reported form this mesh shows a maximum value of 0.99, which therefore shows a good mesh orthogonality.
- The skewness reported form this mesh shows a maximum and average value of 0.12, which is therefore results in a good mesh skewness.
- The aspect ratio reported form this mesh shows an aspect ratio of 3.2 in the bulk flow. However, higher than recommended aspect ratio values are found in the boundary layer region, due to the geometry depth. With regard to the stability of the flow solution it does not signify an issue if it does not impede good stability of the energy solution. However, simulations showed good converge along the different set of conditions.

5.4 Setup

5.4.1 Boundary conditions

A velocity inlet boundary condition is defined on the front part of the domain with the prescribed velocity for each run. On the rear part of the domain, a pressure outlet boundary condition is set with a relative pressure of 0 Pa. On the sides of the domain, a symmetry boundary condition was also used. The top and bottom walls of the domain were set to free-slip, while the airfoil wall were set to non-slip and zero roughness.

5.4.2 Simulation settings

Simulations were completed with the k-ε turbulence model (Section 3.2.2). This model is a two-equation model which consist of transport equations for the turbulent kinetic energy and for the turbulent energy dissipation rate. All the simulations were completed with a variable time step, as a function of a target Courant number, which represents the measure of how much flow particles traverses a computation grid cell in a given time-step. Ideally, the time-step should be scaled for a Courant number lower than one. Otherwise, fluid particles move through two or more cells at each time-step and this can affect convergence negatively. However, as the time-steps are reduced, and the simulation time is greatly increased. An initial set of simulation were completed with different target Courant numbers. Due to the long processing time involved in each simulation, a target Courant number of was specified, with residuals RMS of $1 \cdot 10^{5}$. Although the simulations targeted a high courant number, good convergence was reported.

A critical aspect for the prediction of turbulent flows close to solid walls is the formulation and numerical treatment of the equations in these regions, as it has an important influence on the development of the boundary layer. The approach used to model the flow in the near-wall region was the wall functions method.

5.4.3 Wall functions

The approach used to model the flow in the near-wall region was the wall functions method, since the k-ε turbulence model was employed. With the scalable wall function approach, the viscosity affected by the sublayer region is solved by employing empirical formulas to provide near-wall boundary conditions for the mean flow and turbulence transport equations [6].

The k-ε turbulence model is not valid in the near wall region, since the viscous and buffer sub-layers are not resolved. Instead, empirical wall functions are employed to estimate the near wall and the fully turbulent region. This wall functions use the law of the wall (Section 3.3) to determine the mean velocity in the viscous and buffer sub-layers, expressed as:

$$U^* = \frac{1}{\kappa}\ln(Ey^*) \qquad \textit{(Equation 14)}$$

Where U^* is the dimension less velocity, κ is the Von Kármán constant and E is an empirical constant. In addition, the calculation of turbulent quantities is assumed to be under local equilibrium. Therefore, the production of turbulent kinetic energy equals the dissipation rate closest to the wall. This standard wall functions provide good results for a broad range of flows, such as the air flow around an airflow at low angles of attack. However, it fails for flows where the assumptions of constant shear and local equilibrium does not apply, such us when adverse pressure gradient are present [17].

5.5 Verification and validation

5.5.1 Grid convergence index

As per the rotor simulations, the Grid Convergence Index (GCI) method was employed to determine the quality of the convergence with the grid quality on the airfoil meshes. As stated in Section 3.4.2, the method involves performing the simulation on two or more successively finer grids. Three levels of grid refinement were used to accurately estimate the order of convergence and ensure the solutions are within the asymptotic range of convergence. The sequence of grids is presented here:

Grid	Grid Size	Edge Cells	Cell Size
Fine	472771	687.4	1.46E-03
Medium	332830	576.8	1.73E-03
Coarse	249916	499.8	2.00E-03

Table 2: Airfoil GCI grid definitions.

GCI calculations were completed with an inlet of speed of 5 m/s. Furthermore, the lift and drag coefficient were analysed on the study. Considering that three levels of grid refinement were analysed, a factor of safety of 1.25 was applied [19] [20]. GCI results (Table 3) showed that the lift and drag coefficient on the finest grid were estimated to be within ≈3% of the value obtained by a grid double the size. Therefore, the grid refinement was considered as appropriate for the study. Further details are shown in Appendix 13.

AoA	C_L	C_D
0°	18.76%	2.61%
10°	0.33%	1.51%
20°	1.14%	0.13%

Table 3: Airfoil GCI results summary.

5.5.2 Mesh independence

The mesh independence study was done as previously in Section 4.5.2, by comparing the three different mesh resolutions (Table 2) for three angles of attack. Results are presented in Figure 5.3, for the lift and drag coefficients against the range of angles of attack for the different mesh resolutions. As the mesh resolution was increased the lift and drag coefficients did not present any changes in the examined speed ratio range. According to the results from the mesh independence study, the near wall boundary layer is well resolved, and the free-stream resolution does not require to be increased at the lowest mesh resolution. The mesh independence study results are therefore in accordance with the mesh results obtained with the GCI (Section 5.5.1).

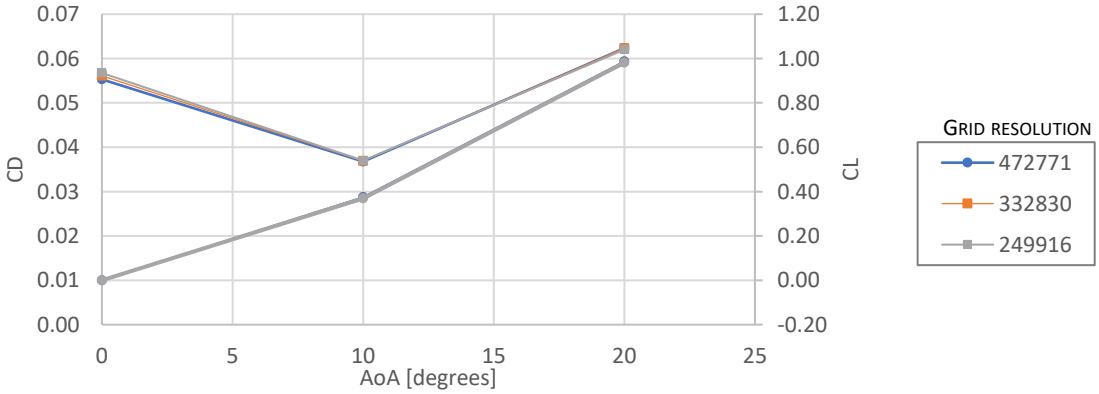

Figure 5.3: Lift and drag coefficients as a function of speed ratio for different airfoil mesh resolutions.

5.6 Reynolds number effect on the aerodynamic performance

5.6.1 Literature review

The NACA-0012 airfoil has been extensively studied and its aerodynamic features are well known. Abbot and von Doenhoff [35] presented a large experimental data for a range of two-dimensional airfoils. This study reported a maximum C_L of 1.1-1.6 for a chord based Reynolds number ranging from $3{\cdot}10^6$ to $9{\cdot}10^6$, and stall angles between 12° and 16°. Furthermore, the lift coefficient is not affected by the position of minimum pressure, and it increases linearly with the angle of attack at constant slope $\Delta C_L/\Delta\alpha$. Shailes et al. [36] investigated the effect of Reynolds number on a NACA-0012 airfoil section both experimentally and numerically, at Re = $2.21{\cdot}10^5$ and Re = $2.81{\cdot}10^5$. The study indicates that a large pressure coefficient is observed between the top and bottom surfaces at lower Reynolds numbers, therefore meaning that higher lift is generated at the lower Reynolds number than at the higher Reynolds numbers. In addition, this study indicates that leading edge vortex shedding has a negative effect on the lift of the airfoil.

Studies with an EPPLER-473 airfoil section are rarely available, and a detailed experimental or numerical study to understand the flow and aerodynamic characteristics of such airfoil section scares. The aerodynamic characteristics for this section were acquired from the XFoil program, written by Drela [37]. The results obtained from this program are calculated with an inviscid linear-vorticity panel method with a Karman-Tsien compressibility correction, with the viscous layer influence modelled with source distribution superimposed on the airfoil and wake permit modelling. The XFoil results reported a maximum C_L of 1.37-1.46 for a chord based Reynolds number ranging from $5{\cdot}10^4$ to $1{\cdot}10^6$, and stall angles between 18.25° and 18.5°. Furthermore, the lift coefficient is not affected by the Reynolds number up to an angle of attack of $\alpha = 10$. The XFoil study also indicates that the drag coefficient is lower at the highest Reynolds number, hence the C_L/C_D ratio is greater for the higher Reynolds number. Moreover, for angles of attack $\alpha > 10$, the C_L/C_D is significantly greater at the highest Reynolds number.

5.6.2 Results – NACA0012H

Lift Coefficient

The lift coefficient versus the angle of attack are presented in Figure 5.4 for the NACA0012H airfoil section. The lift coefficient C_L increases linearly with the angle of attack at constant slope $\Delta C_L/\Delta\alpha$ at the lowest Reynolds numbers Re = $6.4{\cdot}10^4$, since viscous effects are relatively high at low Reynolds numbers. At the higher Reynolds numbers the increase in lift coefficient C_L with the angle of attack is noticed up to 16° angle of attack. The simulations revealed that flow remains attached to the airfoil up to an angle of attack of 16°, after this the flow on the upper surface of the airfoil separates. This leads to from the vortex behind the airfoil and the stalling conditions begins.

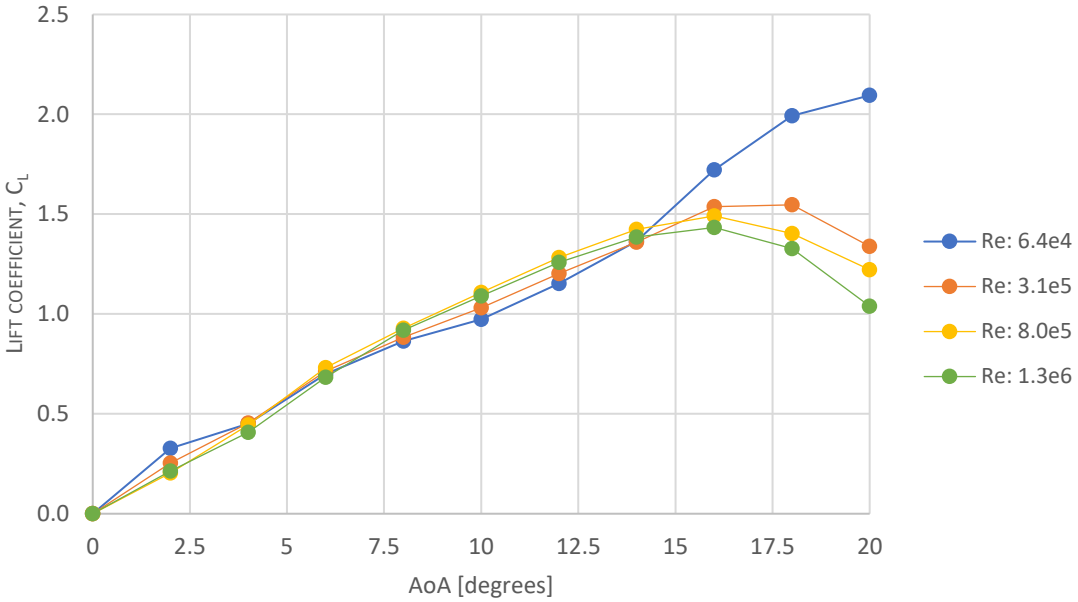

Figure 5.4: Lift coefficient vs angle of attack for NACA0012H airfoil section.

Drag Coefficient

The drag coefficient versus the angle of attack are presented in Figure 5.5 for the EPPLER 473 airfoil section. At low and moderate angles of attack where there is no appreciable separation on flow, and the drag is mainly caused by skin friction. Under these circumstances, the value of the drag coefficient depends upon the relative extent of the laminar boundary layer and the induced velocities over the surfaces of the section. However, at an angle of attack $\alpha < 10°$, the flow separation is appreciable at the lower Reynolds numbers $Re = 6.4 \cdot 10^4$ and $Re = 3.1 \cdot 10^5$, which substantially increases the drag coefficient C_D. At the higher Reynolds numbers $Re = 8 \cdot 10^5$ and $Re = 1.3 \cdot 10^6$, flow separation is found at angles of attack $\alpha < 16°$.

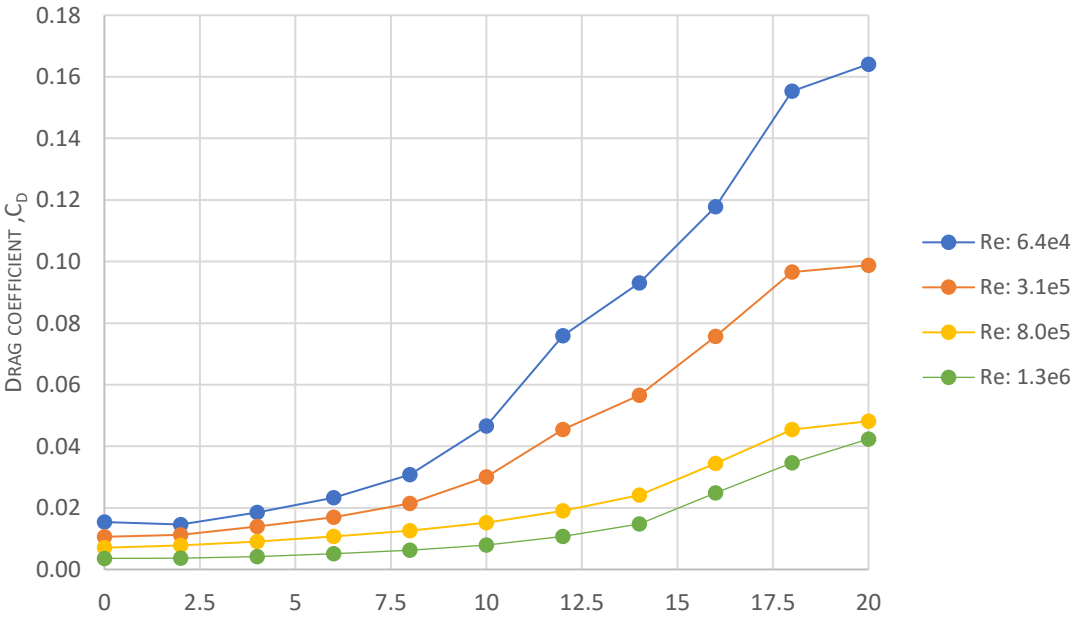

Figure 5.5: Drag coefficient vs angle of attack for NACA0012H airfoil section.

5.6.3 Results – EPPLER 473

Lift Coefficient

The lift coefficient versus the angle of attack are presented in Figure 5.6 for the EPPLER 473 airfoil section. The lift coefficient C_L increases linearly with the angle of attack at constant slope $\Delta C_L/\Delta\alpha$ at the lowest Reynolds numbers Re = $6.4{\cdot}10^4$ and Re = $3.1{\cdot}10^5$, since viscous effects are relatively high at low Reynolds numbers. At the higher Reynolds numbers Re = $8{\cdot}10^5$ and Re = $1.3{\cdot}10^6$, the increase in lift coefficient C_L with the angle of attack is noticed up to 14° angle of attack. The simulations revealed that flow remains attached to the airfoil up to an angle of attack of 14°, after this the flow on the upper surface of the airfoil separates. This leads to from the vortex behind the airfoil and the stalling conditions begins.

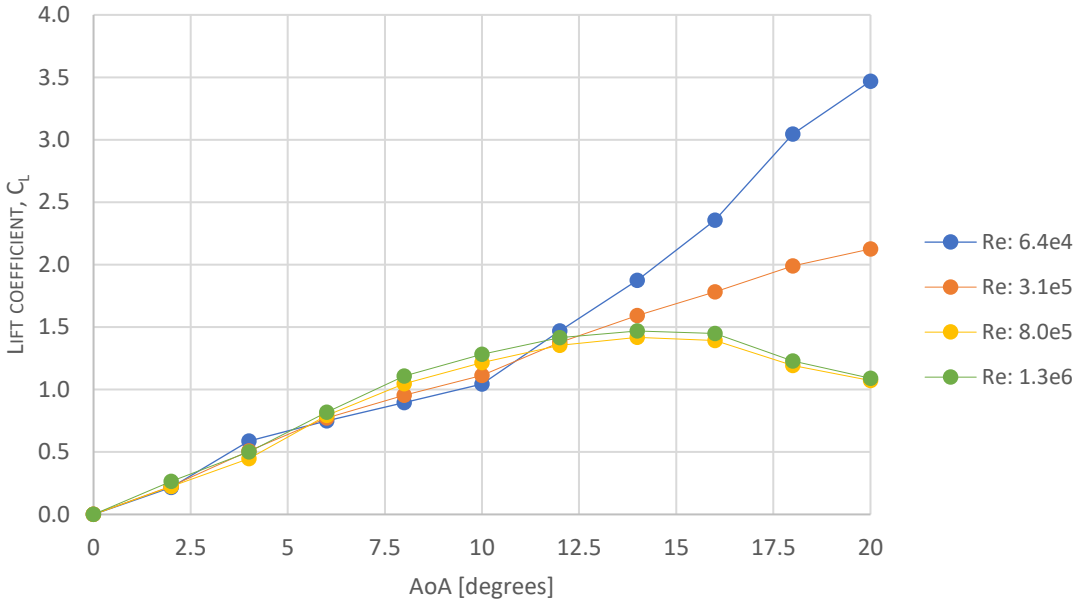

Figure 5.6: Lift coefficient vs angle of attack for EPPLER 473 airfoil section.

Drag Coefficient

The drag coefficient versus the angle of attack are presented in Figure 5.7 for the EPPLER 473 airfoil section. At low and moderate angles of attack where there is no appreciable separation on flow, and the drag is mainly caused by skin friction. Under these circumstances, the value of the drag coefficient depends upon the relative extent of the laminar boundary layer and the induced velocities over the surfaces of the section. However, at an angle of attack $\alpha < 10°$, the flow separation is appreciable at the lower Reynolds numbers Re = $6.4{\cdot}10^4$ and Re = $3.1{\cdot}10^5$, which substantially increases the drag coefficient C_D. At the higher Reynolds numbers Re = $8{\cdot}10^5$ and Re = $1.3{\cdot}10^6$, flow separation is found at angles of attack $\alpha < 16°$.

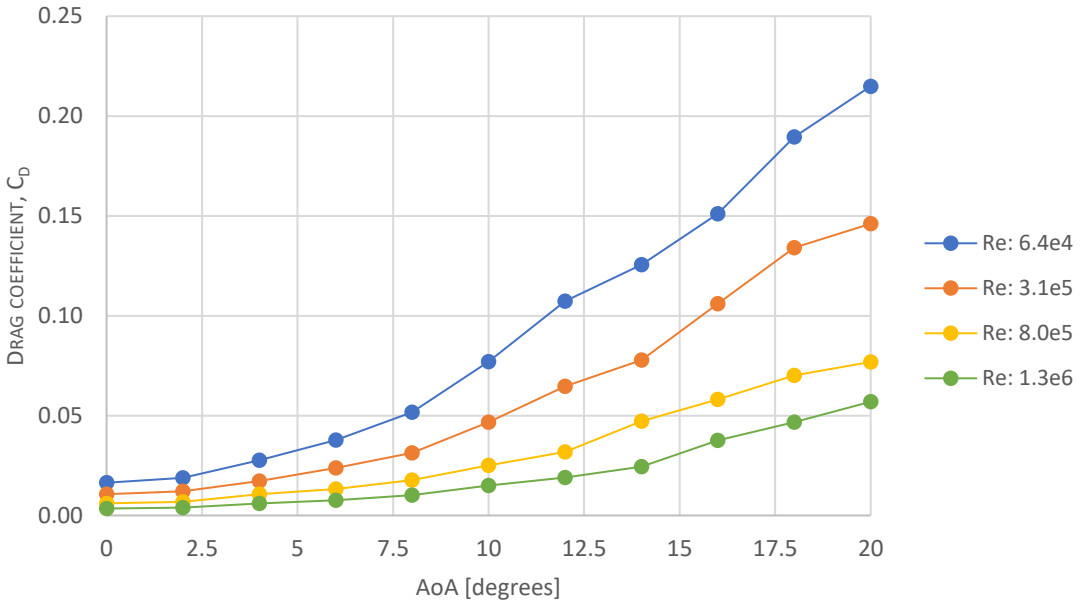

Figure 5.7: Drag coefficient vs angle of attack for EPPLER 473 airfoil section.

5.6.4 AIRFOIL SECTION COMPARISON

At the highest Reynolds numbers Re = $1.3 \cdot 10^6$, both airfoil result in a similar lift coefficient. However, the drag coefficient results in a much lower value for the NACA0012H section. Therefore, a better C_L/C_D ratio is achieved with the NACA0012H section at the higher Reynolds number. Moreover, at the lowest Reynolds number Re = $6.4 \cdot 10^4$ a similar situation is found, with the NACA0012H section obtaining a better C_L/C_D ratio. It is at the middle range of the Reynold number studied (Re = $3.1 \cdot 10^5$ and Re = $8 \cdot 10^5$) when the EPPLER473 section results with the better C_L/C_D ratio. The EPPLER473 section shows the commence of flow separation on the trailing edge at an angle of attack of 10°, while this phenomenon is not found on NACA0012H section up to an angle of attack of 12°.

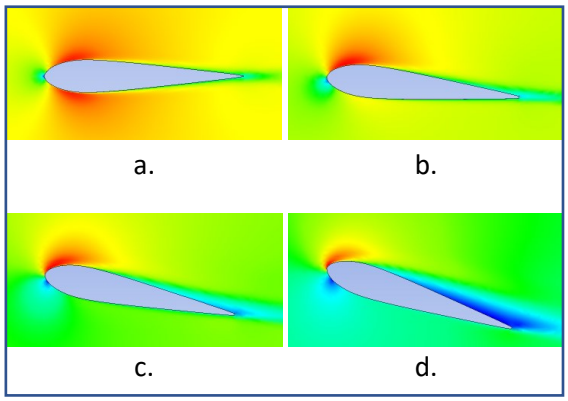

Figure 5.9: NACA0012H profile - Velocity distribution Angle of attack a. 0° b. 6° c. 12° d. 16°

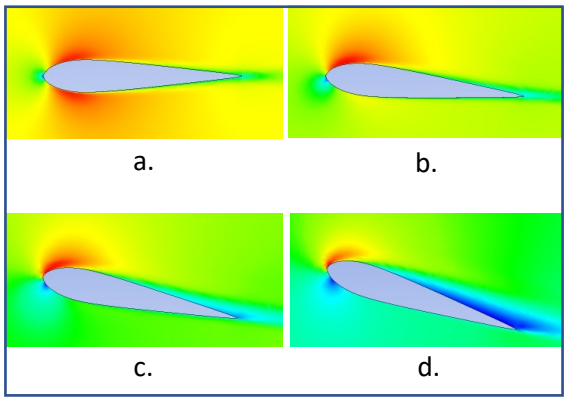

Figure 5.9: EPPLER 473 profile - Velocity distribution Angle of attack a. 0° b. 6° c. 12° d. 16°

6 Performance Prediction

6.1 Initial considerations

In order to assess the aerodynamic performance resulting from CFD generated data, a velocity prediction (VPP) approach was used. The forces acting on the wind-assisted vessel were divided into two groups: aerodynamic forces, and hydrodynamic forces. The hydrodynamic force model was developed based on the resistance and powering calculations completed in Section 2.2 with the Holtrop and Mennen systematic series. The aerodynamic force model was created based on the previously presented CFD derived data. The simulations were carried out with a single rotor or wing sail in isolation. Further information on this topic is presented in Section 6.2. In order to conduct the performance prediction analysis a number of assumptions were made, these include:

- A constant fully loaded displacement condition was used for all simulations.
- A maximum rotation velocity of 450 rpm was used for a 1 metre in diameter rotor.
- The powering of the rotor was accounted for in the power saving calculation and efficiency factor were used for the conversion of effective to delivered power.
- No reduction factor of rotor or wing sail performance due to siting upon the vessel's geometry was included. Further information on this topic is presented in Section 6.3.
- The wind-assist device was assumed to be continuously placed in its operation position, and therefore, the aerodynamic windage when not in use was included.
- Due to the location of the rotor, the use of the vessel's lift generating appendages to maintain course were ignored.
- The impact of ship motions on the aerodynamic and hydrodynamic models were ignored.

6.2 Aerodynamic interaction between multiples devices

To increase the fuel-saving potential of the designated vessel, multiple wind-assist devices should be employed in real-life applications. However, as previously stated the performance prediction program only considerers a single wind-assist device, as the interaction between multiples devices has not been investigated in this study. The aerodynamic thrust generated by a set of devices is commonly calculated as the summation of the thrust provided by each of the installed devices [30] [38]. However, the aerodynamic interaction effects are fully disregarded as a result.

The position of the multiple wind assist devices with respect to the incoming wind direction plays an important role. When two devices come close to being aligned with the incoming wind direction, the aerodynamic coefficients of the downstream device are strongly influenced by the interaction effects. Studies on this topic have shown that these effects are mainly noticeable for $150° \leq AWA \leq 180°$ as well as for $15° \leq AWA \leq 30°$ [29]. In this apparent wind angles the downstream wind device is partially immersed in the wake generated by the upstream device, and it is therefore where the more prominent variations of lift and drag occur.

The aim of this study is to compare the aerodynamic performance of a Flettner rotor and a wing sail; therefore, the devices must be under the same operational conditions. The use of multiple devices has not been considered within the velocity prediction program, as it would have not considered interaction effects. This would have made the operational conditions different for each device, and therefore incomparable.

6.3 Influence of the ship's hull on the aerodynamic performance

The effect of locating the wind-assist device on ship form is to reduce the wind-assist device efficiency at all points of sail. The effects are greatest when the true wind angle is ±90° and -135°, as the vessel presents a large frontal area at these angles. This creates a large wake over deck, with a large region of decelerated flow. As a result, the efficiency of the device is reduced. When the vessel is oriented to a true wind angle of 0 or 180, the device does not lie in the large wake produced by the deck. However, since the lift is produced perpendicular to the wind direction, the thrust produced would not be usable. Therefore, in practice the flow around a wind-assist device may differ significantly from simple uniform or power law boundary layers [20].

7 Performance Comparison

The VPP analysis was done for specific constant ship speed at a range of true wind speed and angels. Furthermore, it used a simplified assessment approach to represent the results in terms of power saving, i.e. the percentage reduction in delivered engine power. Each wind-assist device provided the highest effective power savings at a particular wind speed and wind angle. On one hand, at a true wind speed between 5-10 knots the Flettner rotor resulted with the largest power savings at all the angles analysed, with power savings up to 8.9%. In the other hand, at a true wind speed between 15-20 knots the largest power saving were provided by the wing sail for true wind angles up to 90°(power savings up to 17.5%), and by the Flettner rotor for angles greater than 99° (power savings up to 17.7%).

		True Wind Speed [knots]			
		5	10	15	20
True Wind Angle [degrees]	0	0.39%	0.70%	1.11%	1.62%
	9	-0.25%	-0.52%	-0.69%	-0.76%
	18	-0.88%	-1.74%	-2.65%	-3.44%
	27	-1.49%	-3.05%	-4.65%	-6.05%
	36	-2.07%	-4.35%	-6.54%	-8.53%
	45	-2.61%	-5.57%	-8.28%	-10.82%
	54	-3.09%	-6.65%	-9.84%	-12.87%
	63	-3.55%	-7.56%	-11.16%	-14.63%
	72	-3.91%	-8.26%	-12.23%	-16.04%
	81	-4.15%	-8.72%	-13.04%	-17.07%
	90	-4.28%	-8.91%	-13.58%	-17.69%
	99	-4.24%	-8.83%	-13.29%	-17.71%
	108	-4.03%	-8.47%	-12.59%	-16.83%
	117	-3.73%	-7.85%	-11.62%	-15.57%
	126	-3.32%	-6.99%	-10.41%	-13.98%
	135	-2.83%	-5.95%	-8.99%	-12.09%
	144	-2.29%	-4.75%	-7.38%	-9.95%
	153	-1.72%	-3.46%	-5.59%	-7.61%
	162	-1.13%	-2.20%	-3.61%	-4.96%
	171	-0.52%	-1.07%	-1.45%	-2.07%
	180	0.11%	-0.03%	0.01%	0.00%

Figure 7.1: Breakdown of percentage power savings at cruising speed with the Flettner rotor configuration.

8 Conclusions and Recommendations

The aim of this project was to complete a numerical investigation for the comparison between a Flettner rotor and a wing-sail for superyacht applications. The performance of full scale Flettner rotor and wing-sail are investigated using computational fluid dynamics for a variety of wind conditions and geometries and validated with published experimental data.

The results from the two-dimensional simulations showed good agreement with published data, but underestimated drag forces for higher velocity ratios. The stability of the wake was found to be highly dependant on the velocity ratio, with the von Kármán vortex shedding developing from $0 < \lambda < 1.4$ and ceasing at $1.6 < \lambda < 2.7$. In addition, at $\lambda = 5$ a second vortex shedding mode was observed. The analysis completed on the Reynolds number effects on the aerodynamic coefficients of Flettner rotors indicate that there is a significant influence of the Reynolds number on the lift coefficient below a velocity ratio $\lambda = 2.5$, and below a velocity ratio $\lambda = 3.5$ on the drag coefficient. In addition, both the lift and the drag coefficients are not affected at any velocity ratio at a Reynold number $Re = 1.2 \cdot 10^6$.

The analysis completed on the Reynolds number effects on the aerodynamic coefficients of the airfoil profiles showed that at a Reynolds numbers $Re = 1.3 \cdot 10^6$, both the NACA0012H and the EPPLER 473 sections result in a similar lift coefficient. On one hand, at Reynolds numbers $Re = 6.4 \cdot 10^4$ and $Re = 1.3 \cdot 10^6$ the NACA0012H section results in a lower drag coefficient, and hence a better C_L/C_D ratio is achieved. On the other hand, at Reynolds numbers $Re = 3.1 \cdot 10^5$ and $Re = 8 \cdot 10^5$, the EPPLER473 section results in a better C_L/C_D ratio.

A velocity prediction (VPP) approach was used to assess the performance of the wind-assisted vessel. The hydrodynamic force model was developed based on the resistance and powering calculations completed with the Holtrop and Mennen systematic series. This established an effective power of 1817 kW to reach the maximum speed of 18 knots, and 662kW to reach the cruising speed of 14 knots. The aerodynamic force model was created based on the previously presented CFD derived data. The velocity prediction program assumed a single rotor or wing sail in isolation, constantly vertically mounted on the foredeck of the vessel. On one hand, at a true wind speed between 5-10 knots the Flettner rotor resulted with the largest power savings at all the angles analysed, with savings up to 8.9%. In the other hand, at a true wind speed between 15-20 knots the largest power saving were provided by the wing sail for true wind angles up to 90°. For angles greater than 99° the Flettner rotor provided the greater higher power savings with 17.7%.

Three-dimensional simulations should be done to further evaluate the effect of the Reynolds number on the Flettner rotor and the wing sail. In addition, surface roughness surface roughness would increase in real-life applications, and a further study of how this would affect the results could be of interest. To increase the fuel-saving potential of the designated vessel, multiple wind-assist devices should be employed in real-life applications. In order to do so, the interaction between multiples devices should be investigated. The effect of locating the wind-assist device on ship form is to reduce the wind-assist device efficiency at all points of sail. Therefore, in practice the flow around a wind-assist device will differs significantly. This should also be considered for further work.

9 BIBLIOGRAPHY

[1] K. Lardy, "Boat International," 10 02 2020. [Online]. Available: https://www.boatinternational.com/yachts/news/superyacht-emissions-regulations--42719. [Accessed 05 08 2020].

[2] D.Argyros, "Wind-powered shipping: a review of the commercial, regulatory and technical factors affecting uptake of wind-assisted propulsion.," Lloyd's Register, 2015.

[3] T. D.B. Inham, "A numerical investigation into the steady flow past a rotating circular cylinder at low and intermediate Reynolds numbers," Department of Applied Mathematical Studies, University of Leeds, Leeds, 1988.

[4] B. H.M., D. S.C.R. and Y. P.J.S., "Steady and unsteady flow past a rotating circular cylinder at low Reynolds numbers," *Computers and Fluids,* vol. 17, no. 4, pp. 759-609, 1989.

[5] S. Kang, "Laminar flow over a steadily rotating circular cylinder under the influence of uniform shear," *Phys. Fluids,* vol. 18, no. 4, pp. 047106-1-047106-12, 2006.

[6] M. C. a. S. L. Y.T. Chew, "A numerical study of flow past a rotating cylinder using a hybrid vortex scheme," *J. Fluid Mech.,* vol. 299, pp. 35-71, 1995.

[7] S. Karabelas, "Large eddy simulation of high-Reynolds number flow past a rotating cylinder," *Int. J. Heat Fluid Flow,* vol. 31, pp. 518-527, 2010.

[8] "Chapter 5 - Statistical turbulence models," [Online]. Available: https://www.io-warnemuende.de/tl_files/staff/burchard/pdf/Turb_Chap5_WS08.pdf. [Accessed 18 09 2020].

[9] M. Budesinsky, "CFD simulation of hydrodynamic loads on a floating vertical axis wind turbine," Chalmers University of Technology, Gothenburg, 2019.

[10] M. P. I. Alza, "Numerical and Experimental Studies of Sail Aerodynamics," Universidad Olitécnica de Madrid, Madrid, 2012.

[11] A. R. M. A. a. D. L. H. Kirkham, "The nature of measurement, and the true value of a measured quantity," *IEEE International Instrumentation and Measurement Technology Conference (I2MTC),* pp. 1-6, 2018.

[12] P. J. Roache, Fundamentals of Computational Fluid Dynamics, Tobiska, Lutz: SIAM Review, 2002.

[13] Encyclopaedia Britannica, “Magnus effect | Definition, Examples, & Facts,” 2020. [Online]. Available: https://www.britannica.com/science/Magnus-effect. [Accessed 07 April 2020].

[14] Reve, “Evewind,” 30 07 2013. [Online]. Available: https://www.evwind.es/2013/07/30/enercon-rotor-sail-ship-e-ship-1-saves-up-to-25-fuel/34733. [Accessed 18 09 2020].

[15] Offshore-energy, “Viking Grace to Become 1st Ship with Wind Propulsion System,” 25 1 2017. [Online]. Available: https://www.offshore-energy.biz/viking-grace-to-become-1st-ship-with-wind-propulsion-system/. [Accessed 18 09 2020].

[16] A. nerds, “LIFT GENERATION BY KUTTA JOUKOWSKI THEOREM,” [Online]. Available: https://www.aircraftnerds.com/2019/07/kutta-joukowski-theorem.html. [Accessed 18 09 2020].

[17] A. Inc., “ANSYS Fluent 17.2 Theory Guide,” 2600 ANSYS Drive, Canonsburg, 2016.

[18] L. VIta, “Offshore Floating Vertical Axis Wind Turbines with Rotating Platform,” Danish Technical University, 2011.

[19] American Society of Mechanical Engineers, “Standard for verification and validation in computational fluid dynamics and heat transfer,” A. S. o. M. Engineers, Ed., New York, NY, 2009, pp. 1-42.

[20] L. Jones, M. Prince, D. Hudson and J. Cocks, “Predicted fuel-savings for a flettner rotor assisted tanker using computational fluid dynamics,” London, 2019.

[21] LEAP CFD TEAM, “Turbulence Part 4 - Reviewing how well you have resolved the boundary layer.,” 2013. [Online]. Available: https://www.computationalfluiddynamics.com.au/tips-tricks-turbulence-part-4-reviewing-how-well-you-have-resolved-the-boundary-layer/. [Accessed 22 04 2020].

[22] E.G.Reid, “Test of rotating cylinders,” Technical report tn-209, NACA, 1924.

[23] A.Thom, “Experiments on the flow past a rotating cylinder.,” Reports andmemoranda no. 1410, Aeronautical Research Committee, 1931.

[24] A.Thom, “Effects of discs on the air forces on a rotating cylinder,” Reports andmemoranda no. 1623, Aeronautical Research Committee, 1934.

[25] W. Swanson, “TheMagnus effect: asummary of investigations to date,” *Journal of Basic Engineering,* no. 83, p. 461–470, 1961.

[26] B.R.Clayton, “Bwea initiative on wind assisted ship propulsion WASP,” *ournal of Wind Engineering and Industrial Aerodynamics,* no. 19, p. 251–276, 1985.

[27] P. Tokumaru and P. Dimotakis, “The lift of a cylinder executing rotatory motions in a uniform flow,” *Journal of FluidMechanics,* no. 255, pp. 1-10, 1993.

[28] C. Badalamenti and S. Prince, “The effects of endplates on a rotating cylinder in crossflow.,” in *roceedings of the 26th AIAA Applied Aerodynamics Conference*, 2008.

[29] G. Bordogna, “Aerodynamics of wind-assisted ships,” Delft University of Technology, Deflt, 2020.

[30] S. M. a. C. P. A. De Marco, “Preliminary analysis for marine application of Flettner rotors,” *Proceedings of the 2nd International Symposium on Naval Architecture andMaritime,* 2014.

[31] A. De Marco, S. Mancini, C. Pensa and F. De Luca, “Flettner rotor concept for marine applications: asystematic study,” *International Journal of RotatingMachinery,* no. 2016, p. 12, 2016.

[32] R. B. M. G. V. C. W. Zhang, “Flow past a rotating finite length cylinder: numerical and experimental study,” *roceedings of the 51st AIAA Aerospace SciencesMeeting including the New Horizons Forum and Aerospace Exposition,* 2013.

[33] A. R. J. L. M. T. J. S. K. H. A. Rao, “A review of rotating cylinder wake transitions,” *Journal of Fluids and Structures,* Vols. Special Issue on Unsteady Separation in Fluid-Structure Interaction–II, no. 53, pp. 2-14, 2015.

[34] J. Walker, “Walker wingsail systems,” [Online]. Available: http://www.change-climate.com/Transport_Land_Sea_Sustainable/Assisted_Ships_Sails_Solar_Projects_Marine_Pollution/Walker_WingSails.htm. [Accessed 18 09 2020].

[35] A. Ira H. and V. D. Albert E., Theory of wing sections, New York: Dover Publications, Inc., 1959.

[36] J. Shailesh, G. Uddipta, N. S and K. D. LA, “Effect of Reynolds Number on the Aerodynamic Performance,” Indian Institute of Technology (Indian School of Mines) Dhanbad , Jharkhand, 2018.

[37] M. Drela, “XFOIL: An analysis and design system for low reynolds number airfoils,” MIT Dept. of Aeronautics and Astronautics, Cambridge, Massachusetts, 1989.

[38] D. Pearson, “The use of flettner rotors in efficient ship design,” *Proceedings of the Influence of EEDI on Ship Design Conference,* 2014.

[39] National Aeronautics and Space Administration, “Examining Spatial (Grid) Convergence,” 2008. [Online]. Available: https://www.grc.nasa.gov/WWW/wind/valid/tutorial/spatconv.html. [Accessed 07 04 2020].

[40] Á. Sevilla Padrón, “Study and review of the current understanding of the models for the simulation of vertical turbulent bubbly flow with CFD.,” Sevilla.

[41] I. Syarif Arief, A. Santoso and A. Abdullah, “Design of flettner rotor in container carrier 4000 DWT with CFD,” *International Journal of Marine Engineering Innovation and Research,* vol. 2, no. 2, pp. 133-139, 2018.

[42] S.R.Boonstra, “An investigation of the internal airflow system behavior of a Turbosail,” Delft University of Technology, Delft, 2020.

[43] D. Pearson, “The use of flettner rotor in efficient ship design,” The royal institution of naval architects, London, 2014.

[44] F. Garzón and A. Figueroa, “The study on the flow generated by an array of four flettener rotors: theory and experiment,” *Appied Mathematics,* vol. 8, pp. 1851-1858, 2017.

[45] P. Chandra Shukla and K. Ghosh, “Revival of the modern wing sails for the propulsion of commercial ships,” *International Journal of Physical and Mathematical Sciences,* vol. 3, no. 3, pp. 207-212, 2009.

[46] Norsepower, “Norsepower rotor sail solution,” Norsepower, Helsinki, 2019.

[47] Lloyds's Register, “Guidance Notes for Flettner Rotor Approval,” Lloyd’s Register, London, May 2015.

[48] A. W.Blakeley, R. G.J.Flay, H. Furukawa and P. J.Richards, “Evaluation of multi-element wing sail aerodynamics from two-dymensional wind tunnel investigations,” Auckland, 2015.

[49] D. W.Atkins, “The CFD assisted design and experimental testing of a wingsail with high lift devices,” The reseach institute for design manufacture and marketing university of Salford, Salford, 1996.

[50] S. J.Otto, “Aerodynamics of high performance wing sails,” *Marine Technology,* vol. 11, no. Part 3, 1974.

[51] A. Kenneth, “A reversible asymetry rigid aerofoil for sailing vessels,” Oxford University, Oxford.

[52] G. Firestein, “Dynamic response of wingsail mast to unsteady aerodynamic loads including ship motion effetcs,” *Wind Engineering and Industrial Aerodynamics,* vol. 19, 1985.

[53] Y. T. Y. Q.LI, “A study on the performance of cascade hard sails and sail-equipped vessels.,” *Ocean Engineering,* no. 98, pp. 23-31, 2015.

[54] A. B. P. G. S. M. P. S. C. W. a. R. W. M. Traut, “Low c for the high seas: Flettner rotor power contribution on a route brazil to uk,” *Proceedings of the Low Carbon Shipping Conference,* 2012.

10 APPENDIX

Appendix 1 RESISTANCE AND PROPULSION CALCULATIONS

SHIP PARAMETERS

Length on waterline	L	66.60	m
Length between perpendiculars	L_{PP}	66.60	m
Breadth moulded	B_{RR}	12.50	m
Draught moulded on F.P.	T_F	3.40	m
Draught moulded on A.P.	T_A	3.40	m
Average moulded draft	T	3.40	m
Displacement volume moulded	V	1610	m^3
Longitudinal centre of buoyancy %LPP fwd of midships	LCB	-0.45	%
Transverse bulb area	A_{BT}	0.10	m^2
Centre of bulb area above keel line	C_{BB}	0.00	m
Midship section coefficient	C_M	0.918	
Waterplane area coefficient	C_{WP}	0.824	
Transom area	A_T	2.64	m^2
Wetted area appendages	S_{APP}	0.00	m^2
Propeller diameter	D	4.00	m
Number of propeller blades	Z	4	
Propeller Pitch	P	2.70	m
Clearance propeller with keel line		0.20	m
Revolutions per second	n	3.00	rps
Afterbody form		*Normal section shape*	
Screw vessel type		*Single-screw ship*	

SPEED RANGE

Cruising Speed	v_C	14	knots
Maximum Speed	v	18	knots

RESULTS

	CRUISING	MAXIMUM	
Resistance	91.89	196.28	kN
Effective Power	661.7	1817.4	kW
Propeller Thrust	104.4	223.0	kN
Blade Area Ratio	61.61%	61.61%	
Rotative Efficiency	1.000	1.003	
KT CORRECTED	0.118	0.057	
KQ CORRECTED	0.016	0.010	
Open Water Efficiency	57.77%	56.37%	
Shaft Power	1070.9	3006.5	kW
ACCURACY EVALUATION			
P/D Ratio CALC.	0.676	0.676	
P/D Ratio ACTUAL	0.676	0.676	
R^2	1.000	1.000	

Optimize for: Maximum Speed

Max. number of iterations: 100
Calculate Hull WSA: YES

Calculate

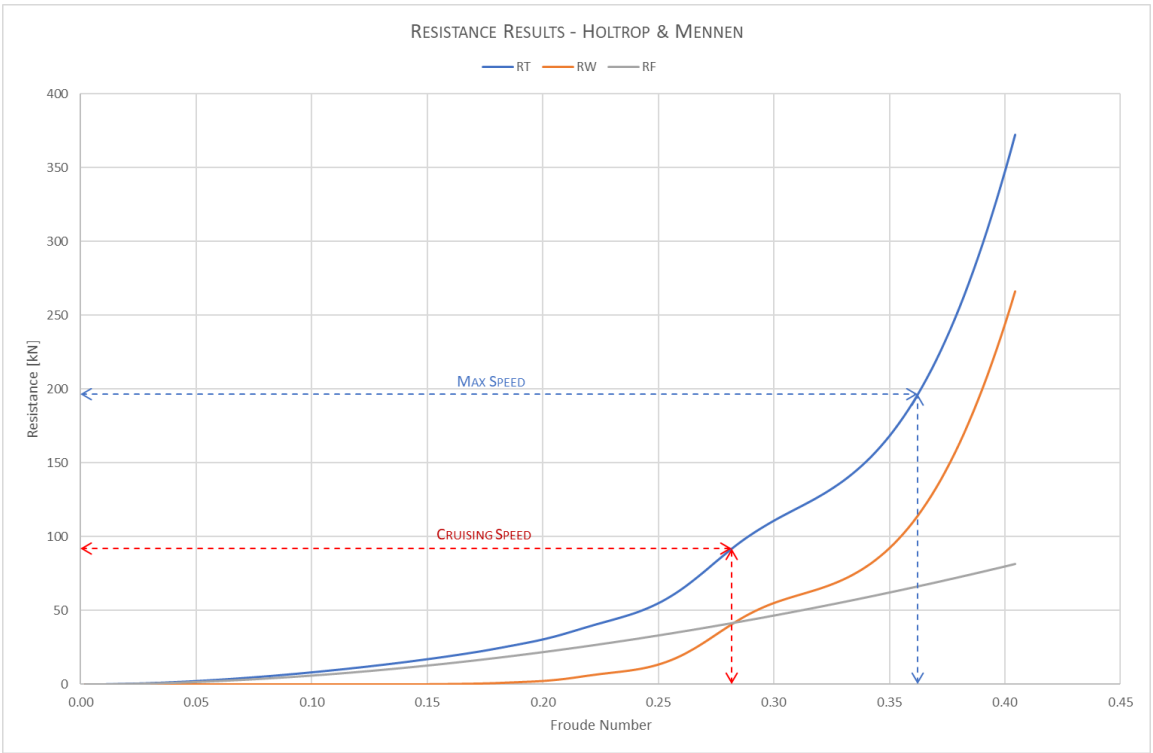

Appendix 2 GRID CONVERGENCE INDEX RESULTS

Item	Value	Unit
Cylinder Depth	0.10	m
Cylinder Diameter	1.00	m
Surface Area	0.314	m^2
Air Density (@25°C)	1.185	kg/m^3
Freestream Velocity	19.55	m/s
FoS	1.25	

225 RPM

Grid	Grid Size	Lift [N]	Drag [N]	CL	CD	Edge Cells	Cell Size	Refinement Factor		Variable Difference		
1	475600	17.15	1.721	2.41E-01	2.42E-02	689.64	1.45E-03	R2.1	1.141	E2.2	2.11E-03	-4.22E-05
2	365000	17.30	1.718	2.43E-01	2.42E-02	604.15	1.66E-03	R3.2	1.140	E3.3	1.97E-03	-9.84E-05
3	281000	17.44	1.71	2.45E-01	2.41E-02	530.09	1.89E-03					

	$P_{INITIAL}$	s	q	P_{ACTUAL}	R^2
CL	1	1	0.013	0.425	
	0.429	1	0.012	0.429	0.00
CD	1	1	0.013	6.499	
	6.479	0	0.010	6.479	0.00

Update

	CL	CD
Extrapolated Value (Fine Mesh)	2.41E-01	2.42E-02
Approximate Realtive Error	1.66%	0.58%
GCI	1.96%	0.31%

Item	Value	Unit
Cylinder Depth	0.10	m
Cylinder Diameter	1.00	m
Surface Area	0.314	m^2
Air Density (@25°C)	1.185	kg/m^3
Freestream Velocity	19.55	m/s
FoS	1.25	

450 RPM

Grid	Grid Size	Lift [N]	Drag [N]	CL	CD	Edge Cells	Cell Size	Refinement Factor		Variable Difference		
1	475600	45.63	2.884	6.42E-01	4.06E-02	689.64	1.45E-03	R2.1	1.141	E2.2	2.39E-03	1.97E-04
2	365000	45.80	2.898	6.44E-01	4.08E-02	604.15	1.66E-03	R3.2	1.140	E3.3	1.55E-03	1.41E-05
3	281000	45.91	2.899	6.46E-01	4.08E-02	530.09	1.89E-03					

	$P_{INITIAL}$	s	q	P_{ACTUAL}	R^2
CL	1	1	0.013	3.193	
	3.179	1	0.015	3.179	0.00
CD	1	1	0.013	19.845	
	19.708	0	0.031	19.708	0.00

Update

	CL	CD
Extrapolated Value (Fine Mesh)	6.42E-01	4.06E-02
Approximate Realtive Error	0.61%	0.52%
GCI	0.50%	0.43%

Appendix 3 Rotor results: 0 RPM

Item	Value	Unit
CFD Model		
Cylinder Depth	0.10	m
Cylinder Diameter	1.00	m
Rotation Speed	0	rpm
Surface Area	0.314	m^2
Circunferece	3.142	m
Full Size Model		
Rotor Height	8.00	m
Surface Area	25.133	m^2
General		
Air Density (@25°C)	1.185	kg/m^3
Rotational Speed	0.000	rad/s
Circunferece Velocity	0.000	m/s
Boat Speed	18.000	knots
	9.252	m/s

TWS [kts]	Ship Angle [degrees]	AWS [m/s]	AWA [degrees]	Lift [N]	Drag $_{CFD}$ [N]	CD	Drag [N]	Drive [N]	Thrust [N]
5.00	0.00	11.83	0.00	0.0	2.210	8.49E-02	176.80	-176.80	176.80
5.00	9.00	11.81	1.95	0.0	2.202	8.49E-02	176.06	-175.96	176.06
5.00	18.00	11.73	3.89	0.0	2.164	8.43E-02	172.72	-172.32	172.72
5.00	27.00	11.61	5.78	0.0	2.121	8.41E-02	168.82	-167.96	168.82
5.00	36.00	11.44	7.60	0.0	2.061	8.39E-02	163.43	-162.00	163.43
5.00	45.00	11.23	9.33	0.0	1.990	8.37E-02	157.09	-155.02	157.09
5.00	54.00	10.97	10.94	0.0	1.896	8.31E-02	148.88	-146.18	148.88
5.00	63.00	10.68	12.40	0.0	1.801	8.29E-02	140.72	-137.43	140.72
5.00	72.00	10.35	13.68	0.0	1.692	8.25E-02	131.52	-127.79	131.52
5.00	81.00	9.99	14.74	0.0	1.592	8.29E-02	123.17	-119.11	123.17
5.00	90.00	9.61	15.54	0.0	1.483	8.32E-02	114.31	-110.13	114.31
5.00	99.00	9.21	16.02	0.0	1.377	8.38E-02	105.88	-101.77	105.88
5.00	108.00	8.81	16.13	0.0	1.273	8.46E-02	97.81	-93.96	97.81
5.00	117.00	8.41	15.83	0.0	1.172	8.57E-02	90.22	-86.80	90.22
5.00	126.00	8.02	15.05	0.0	1.079	8.70E-02	83.37	-80.51	83.37
5.00	135.00	7.66	13.75	0.0	0.998	8.88E-02	77.58	-75.36	77.58
5.00	144.00	7.34	11.90	0.0	0.928	9.07E-02	72.65	-71.08	72.65
5.00	153.00	7.06	9.52	0.0	0.869	9.23E-02	68.55	-67.60	68.55
5.00	162.00	6.86	6.66	0.0	0.831	9.42E-02	66.00	-65.55	66.00
5.00	171.00	6.73	3.43	0.0	0.798	9.45E-02	63.72	-63.61	63.72
5.00	180.00	6.69	0.00	0.0	0.792	9.52E-02	63.34	-63.34	63.34
10.00	0.00	14.40	0.00	0.0	3.201	8.29E-02	256.08	-256.08	256.08
10.00	9.00	14.36	3.21	0.0	3.190	8.30E-02	254.80	-254.40	254.80
10.00	18.00	14.24	6.41	0.0	3.154	8.31E-02	250.74	-249.17	250.74
10.00	27.00	14.04	9.58	0.0	3.043	8.18E-02	240.04	-236.70	240.04
10.00	36.00	13.76	12.70	0.0	2.932	8.12E-02	228.82	-223.22	228.82
10.00	45.00	13.40	15.76	0.0	2.801	8.07E-02	215.66	-207.55	215.66
10.00	54.00	12.97	18.73	0.0	2.613	7.91E-02	197.97	-187.49	197.97
10.00	63.00	12.47	21.58	0.0	2.443	7.85E-02	181.74	-169.00	181.74
10.00	72.00	11.90	24.29	0.0	2.222	7.69E-02	162.03	-147.69	162.03
10.00	81.00	11.27	26.80	0.0	2.015	7.61E-02	143.88	-128.42	143.88
10.00	90.00	10.59	29.07	0.0	1.778	7.44E-02	124.32	-108.65	124.32
10.00	99.00	9.86	31.03	0.0	1.480	7.01E-02	101.48	-86.97	101.48
10.00	108.00	9.10	32.56	0.0	1.284	7.03E-02	86.56	-72.96	86.56
10.00	117.00	8.30	33.53	0.0	1.094	7.11E-02	72.93	-60.79	72.93
10.00	126.00	7.50	33.75	0.0	0.917	7.29E-02	61.00	-50.72	61.00
10.00	135.00	6.70	32.94	0.0	0.756	7.60E-02	50.74	-42.59	50.74
10.00	144.00	5.93	30.71	0.0	0.634	8.34E-02	43.60	-37.49	43.60
10.00	153.00	5.23	26.57	0.0	0.510	8.98E-02	36.51	-32.65	36.51
10.00	162.00	4.65	20.03	0.0	0.418	9.77E-02	31.42	-29.52	31.42
10.00	171.00	4.26	10.92	0.0	0.360	1.05E-01	28.30	-27.78	28.30
10.00	180.00	4.12	0.00	0.0	0.339	1.07E-01	27.09	-27.09	27.09
15.00	0.00	16.98	0.00	0.0	4.371	8.15E-02	349.68	-349.68	349.68
15.00	9.00	16.92	4.09	0.0	4.353	8.15E-02	347.35	-346.47	347.35
15.00	18.00	16.77	8.18	0.0	4.304	8.14E-02	340.82	-337.35	340.82
15.00	27.00	16.51	12.26	0.0	4.161	8.02E-02	325.29	-317.88	325.29
15.00	36.00	16.15	16.32	0.0	3.987	7.88E-02	306.12	-293.79	306.12
15.00	45.00	15.69	20.35	0.0	3.799	7.77E-02	284.95	-267.16	284.95
15.00	54.00	15.14	24.36	0.0	3.552	7.59E-02	258.86	-235.82	258.86
15.00	63.00	14.50	28.32	0.0	3.258	7.34E-02	229.43	-201.96	229.43
15.00	72.00	13.76	32.24	0.0	2.960	7.10E-02	200.30	-169.42	200.30
15.00	81.00	12.95	36.08	0.0	2.608	6.76E-02	168.62	-136.28	168.62
15.00	90.00	12.05	39.83	0.0	2.258	6.42E-02	138.73	-106.54	138.73
15.00	99.00	11.09	43.45	0.0	1.962	6.23E-02	113.97	-82.74	113.97
15.00	108.00	10.06	46.90	0.0	1.652	6.00E-02	90.33	-61.72	90.33
15.00	117.00	8.97	50.10	0.0	1.357	5.82E-02	69.65	-44.68	69.65
15.00	126.00	7.83	52.93	0.0	1.070	5.66E-02	51.61	-31.11	51.61
15.00	135.00	6.65	55.17	0.0	0.811	5.63E-02	37.04	-21.15	37.04
15.00	144.00	5.45	56.43	0.0	0.582	5.83E-02	25.73	-14.23	25.73
15.00	153.00	4.24	55.84	0.0	0.387	6.51E-02	17.40	-9.77	17.40
15.00	162.00	3.06	51.25	0.0	0.216	7.77E-02	10.84	-6.78	10.84
15.00	171.00	2.03	36.50	0.0	0.096	1.00E-01	6.18	-4.97	6.18
15.00	180.00	1.54	0.00	0.0	0.058	1.31E-01	4.66	-4.66	4.66
20.00	0.00	19.55	0.00	0.0	5.731	8.06E-02	458.48	-458.48	458.48
20.00	9.00	19.49	4.74	0.0	5.703	8.04E-02	454.68	-453.13	454.68
20.00	18.00	19.31	9.48	0.0	5.544	7.88E-02	437.46	-431.49	437.46
20.00	27.00	19.01	14.23	0.0	5.413	7.80E-02	419.75	-406.88	419.75
20.00	36.00	18.59	18.99	0.0	5.247	7.71E-02	396.92	-375.33	396.92
20.00	45.00	18.06	23.76	0.0	5.029	7.58E-02	368.23	-337.02	368.23
20.00	54.00	17.42	28.55	0.0	4.612	7.17E-02	324.10	-284.70	324.10
20.00	63.00	16.68	33.36	0.0	4.207	6.79E-02	281.10	-234.78	281.10
20.00	72.00	15.83	38.21	0.0	3.787	6.39E-02	238.06	-187.07	238.06
20.00	81.00	14.88	43.09	0.0	3.419	6.06E-02	199.74	-145.86	199.74
20.00	90.00	13.84	48.03	0.0	2.970	5.57E-02	158.88	-106.24	158.88
20.00	99.00	12.72	53.05	0.0	2.631	5.25E-02	126.49	-76.03	126.49
20.00	108.00	11.52	58.17	0.0	2.210	4.72E-02	93.24	-49.17	93.24
20.00	117.00	10.25	63.44	0.0	1.796	4.11E-02	64.25	-28.72	64.25
20.00	126.00	8.92	68.94	0.0	1.415	3.43E-02	40.67	-14.62	40.67
20.00	135.00	7.54	74.79	0.0	1.057	2.62E-02	22.17	-5.82	22.17
20.00	144.00	6.12	81.27	0.0	0.758	1.65E-02	9.20	-1.40	9.20
20.00	153.00	4.67	88.95	0.0	0.480	2.16E-03	0.70	-0.01	0.70
20.00	162.00	3.22	80.49	0.0	0.253	2.17E-02	3.35	-0.55	3.35
20.00	171.00	1.84	60.53	0.0	0.085	6.57E-02	3.33	-1.64	3.33
20.00	180.00	1.03	0.00	0.0	0.029	1.47E-01	2.32	-2.32	2.32

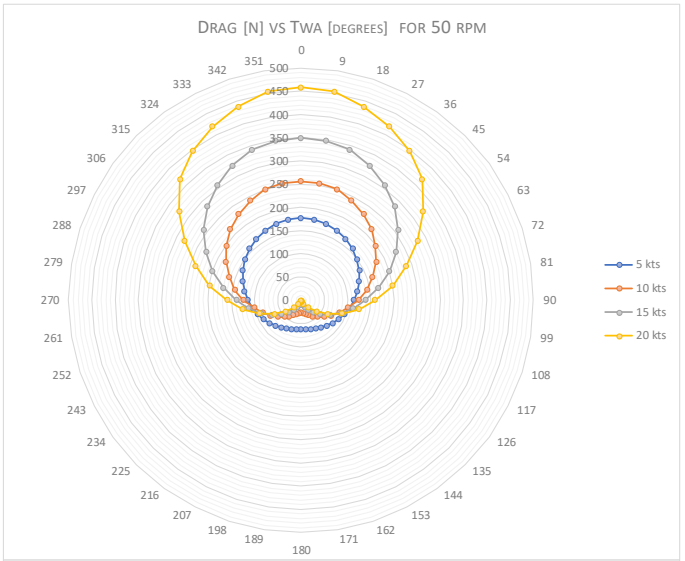

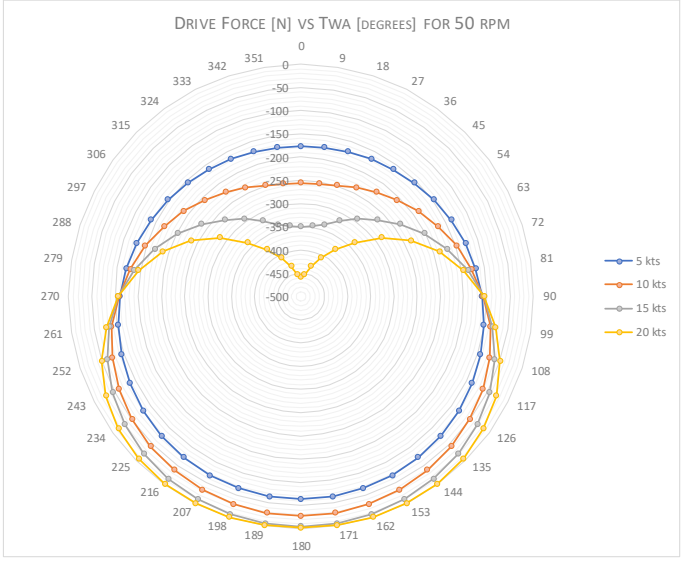

Appendix 4 Rotor results: 50 RPM

Item	Value	Unit
CFD Model		
Cylinder Depth	0.10	m
Cylinder Diameter	1.00	m
Rotation Speed	50	rpm
Surface Area	0.314	m^2
Circunferece	3.142	m
Full Size Model		
Rotor Height	8.00	m
Surface Area	25.133	m^2
General		
Air Density (@25°C)	1.185	kg/m^3
Rotational Speed	5.236	rad/s
Circunferece Velocity	2.618	m/s
Boat Speed	18.000	knots
	9.252	m/s

TWS [kts]	Ship Angle [degrees]	AWS [m/s]	AWA [degrees]	V_R	CL	Lift [N]	CD	Drag [N]	Drive [N]	Thrust [N]
5.00	0.00	11.83	0.00	0.221	1.75E-01	364.8	8.32E-02	173.28	-173.28	403.86
5.00	9.00	11.81	1.95	0.222	1.76E-01	365.8	8.29E-02	171.90	-159.33	404.14
5.00	18.00	11.73	3.89	0.223	1.77E-01	362.6	8.24E-02	168.73	-143.76	399.97
5.00	27.00	11.61	5.78	0.225	1.79E-01	359.8	8.27E-02	165.95	-128.90	396.26
5.00	36.00	11.44	7.60	0.229	1.80E-01	350.5	8.18E-02	159.39	-111.65	385.02
5.00	45.00	11.23	9.33	0.233	1.85E-01	347.7	8.18E-02	153.54	-95.15	380.07
5.00	54.00	10.97	10.94	0.239	1.88E-01	337.2	8.11E-02	145.31	-78.67	367.18
5.00	63.00	10.68	12.40	0.245	1.96E-01	332.4	8.03E-02	136.26	-61.68	359.25
5.00	72.00	10.35	13.68	0.253	2.01E-01	320.8	8.01E-02	127.63	-48.12	345.26
5.00	81.00	9.99	14.74	0.262	2.09E-01	311.0	8.11E-02	120.46	-37.37	333.48
5.00	90.00	9.61	15.54	0.272	2.18E-01	299.2	8.10E-02	111.30	-27.10	319.23
5.00	99.00	9.21	16.02	0.284	2.29E-01	289.4	8.23E-02	103.96	-20.06	307.55
5.00	108.00	8.81	16.13	0.297	2.42E-01	279.7	8.38E-02	96.83	-15.30	295.98
5.00	117.00	8.41	15.83	0.311	2.56E-01	269.9	8.54E-02	89.89	-12.87	284.51
5.00	126.00	8.02	15.05	0.326	2.72E-01	260.2	8.68E-02	83.12	-12.72	273.13
5.00	135.00	7.66	13.75	0.342	2.87E-01	250.4	8.75E-02	76.45	-14.75	261.84
5.00	144.00	7.34	11.90	0.357	3.00E-01	240.7	8.72E-02	69.81	-18.66	250.59
5.00	153.00	7.06	9.52	0.371	3.11E-01	230.9	8.49E-02	63.10	-24.03	239.38
5.00	162.00	6.86	6.66	0.382	3.16E-01	221.2	8.03E-02	56.24	-30.20	228.20
5.00	171.00	6.73	3.43	0.389	3.13E-01	211.4	7.29E-02	49.17	-36.43	217.05
5.00	180.00	6.69	0.00	0.391	3.03E-01	201.7	6.29E-02	41.89	-41.89	205.96
10.00	0.00	14.40	0.00	0.182	1.47E-01	452.6	8.24E-02	254.48	-254.48	519.27
10.00	9.00	14.36	3.21	0.182	1.46E-01	449.4	8.20E-02	251.68	-226.10	515.04
10.00	18.00	14.24	6.41	0.184	1.48E-01	446.2	8.13E-02	245.34	-193.97	509.16
10.00	27.00	14.04	9.58	0.186	1.50E-01	440.3	8.13E-02	238.47	-161.85	500.75
10.00	36.00	13.76	12.70	0.190	1.54E-01	434.4	8.06E-02	226.95	-125.87	490.11
10.00	45.00	13.40	15.76	0.195	1.58E-01	422.4	7.95E-02	212.58	-89.87	472.88
10.00	54.00	12.97	18.73	0.202	1.62E-01	406.7	7.76E-02	194.18	-53.32	450.70
10.00	63.00	12.47	21.58	0.210	1.67E-01	387.1	7.74E-02	178.99	-24.05	426.50
10.00	72.00	11.90	24.29	0.220	1.75E-01	368.5	7.59E-02	160.06	5.67	401.74
10.00	81.00	11.27	26.80	0.232	1.84E-01	348.3	7.47E-02	141.38	30.87	375.92
10.00	90.00	10.59	29.07	0.247	1.97E-01	328.2	7.32E-02	122.22	52.64	350.18
10.00	99.00	9.86	31.03	0.265	2.07E-01	299.2	7.36E-02	106.65	62.82	317.64
10.00	108.00	9.10	32.56	0.288	2.28E-01	280.4	7.31E-02	90.03	75.03	294.52
10.00	117.00	8.30	33.53	0.315	2.55E-01	261.7	7.36E-02	75.58	81.53	272.35
10.00	126.00	7.50	33.75	0.349	2.90E-01	242.9	7.56E-02	63.21	82.38	250.96
10.00	135.00	6.70	32.94	0.391	3.36E-01	224.1	7.91E-02	52.76	77.57	230.23
10.00	144.00	5.93	30.71	0.442	3.93E-01	205.3	8.42E-02	44.02	67.00	209.99
10.00	153.00	5.23	26.57	0.501	4.59E-01	186.6	9.03E-02	36.71	50.63	190.13
10.00	162.00	4.65	20.03	0.563	5.22E-01	167.8	9.46E-02	30.42	28.89	170.51
10.00	171.00	4.26	10.92	0.615	5.53E-01	149.0	9.19E-02	24.76	3.91	151.04
10.00	180.00	4.12	0.00	0.636	5.17E-01	130.2	7.16E-02	18.05	-18.05	131.47
15.00	0.00	16.98	0.00	0.154	1.26E-01	541.8	8.13E-02	348.80	-348.80	644.40
15.00	9.00	16.92	4.09	0.155	1.26E-01	535.2	8.16E-02	347.67	-308.60	638.21
15.00	18.00	16.77	8.18	0.156	1.26E-01	526.6	8.05E-02	336.94	-258.60	625.13
15.00	27.00	16.51	12.26	0.159	1.28E-01	519.2	7.91E-02	320.84	-203.33	610.30
15.00	36.00	16.15	16.32	0.162	1.32E-01	511.8	7.82E-02	303.51	-147.52	594.99
15.00	45.00	15.69	20.35	0.167	1.35E-01	495.3	7.61E-02	279.02	-89.34	568.47
15.00	54.00	15.14	24.36	0.173	1.41E-01	480.4	7.52E-02	256.53	-35.55	544.60
15.00	63.00	14.50	28.32	0.181	1.46E-01	457.3	7.28E-02	227.60	16.61	510.79
15.00	72.00	13.76	32.24	0.190	1.55E-01	435.8	6.95E-02	195.90	66.79	477.84
15.00	81.00	12.95	36.08	0.202	1.61E-01	402.4	6.68E-02	166.56	102.36	435.51
15.00	90.00	12.05	39.83	0.217	1.72E-01	373.0	6.40E-02	138.36	132.62	397.80
15.00	99.00	11.09	43.45	0.236	1.86E-01	340.8	5.98E-02	109.36	154.95	357.88
15.00	108.00	10.06	46.90	0.260	2.05E-01	308.6	5.62E-02	84.54	167.53	319.93
15.00	117.00	8.97	50.10	0.292	2.31E-01	276.4	5.33E-02	63.75	171.11	283.62
15.00	126.00	7.83	52.93	0.334	2.68E-01	244.2	5.13E-02	46.81	166.59	248.61
15.00	135.00	6.65	55.17	0.394	3.22E-01	212.0	5.07E-02	33.40	154.92	214.58
15.00	144.00	5.45	56.43	0.481	4.07E-01	179.8	5.25E-02	23.18	136.97	181.25
15.00	153.00	4.24	55.84	0.618	5.52E-01	147.6	5.87E-02	15.70	113.29	148.40
15.00	162.00	3.06	51.25	0.855	8.27E-01	115.4	7.43E-02	10.37	83.48	115.83
15.00	171.00	2.03	36.50	1.287	1.35E+00	83.2	1.01E-01	6.25	44.45	83.40
15.00	180.00	1.54	0.00	1.696	1.44E+00	51.0	4.45E-02	1.58	-1.58	50.99
20.00	0.00	19.55	0.00	0.134	1.11E-01	631.6	8.17E-02	464.90	-464.90	784.22
20.00	9.00	19.49	4.74	0.134	1.11E-01	627.1	8.10E-02	458.07	-404.69	776.56
20.00	18.00	19.31	9.48	0.136	1.12E-01	619.2	8.01E-02	444.28	-336.22	762.11
20.00	27.00	19.01	14.23	0.138	1.13E-01	608.0	7.88E-02	423.88	-261.43	741.15
20.00	36.00	18.59	18.99	0.141	1.15E-01	593.4	7.72E-02	397.35	-182.68	714.11
20.00	45.00	18.06	23.76	0.145	1.18E-01	575.4	7.52E-02	365.36	-102.60	681.56
20.00	54.00	17.42	28.55	0.150	1.23E-01	554.0	7.28E-02	328.73	-24.02	644.18
20.00	63.00	16.68	33.36	0.157	1.28E-01	529.2	6.97E-02	288.42	50.14	602.72
20.00	72.00	15.83	38.21	0.165	1.34E-01	501.1	6.59E-02	245.54	116.99	558.03
20.00	81.00	14.88	43.09	0.176	1.43E-01	469.6	6.11E-02	201.32	173.81	510.94
20.00	90.00	13.84	48.03	0.189	1.52E-01	434.7	5.51E-02	157.11	218.18	462.24
20.00	99.00	12.72	53.05	0.206	1.64E-01	396.1	4.99E-02	120.05	244.36	413.85
20.00	108.00	11.52	58.17	0.227	1.82E-01	359.4	4.40E-02	86.82	259.61	369.77
20.00	117.00	10.25	63.44	0.255	2.06E-01	321.6	3.79E-02	59.24	261.22	327.04
20.00	126.00	8.92	68.94	0.293	2.39E-01	282.7	3.13E-02	37.13	250.44	285.10
20.00	135.00	7.54	74.79	0.347	2.87E-01	242.5	2.39E-02	20.23	228.73	243.37
20.00	144.00	6.12	81.27	0.428	3.61E-01	201.2	1.47E-02	8.19	197.64	201.38
20.00	153.00	4.67	88.95	0.560	4.89E-01	158.7	1.89E-03	0.61	158.70	158.73
20.00	162.00	3.22	80.49	0.812	7.45E-01	115.1	1.75E-02	2.70	113.05	115.11
20.00	171.00	1.84	60.53	1.419	1.41E+00	71.4	8.47E-02	4.29	60.08	71.55
20.00	180.00	1.03	0.00	2.545	1.76E+00	27.8	6.82E-02	1.08	-1.08	27.79

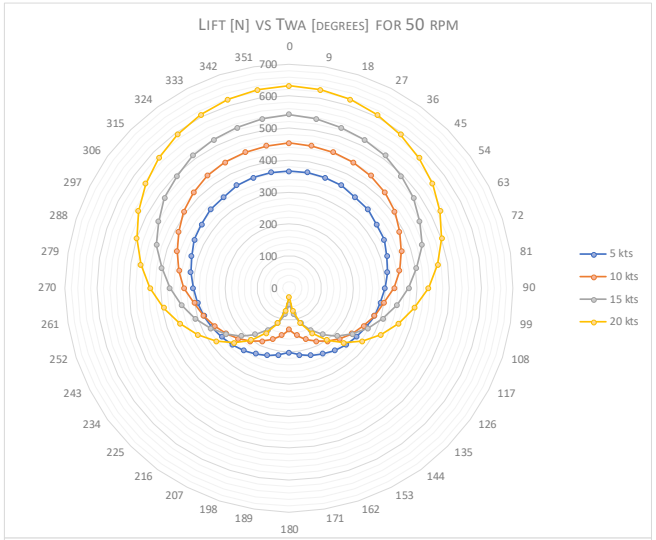

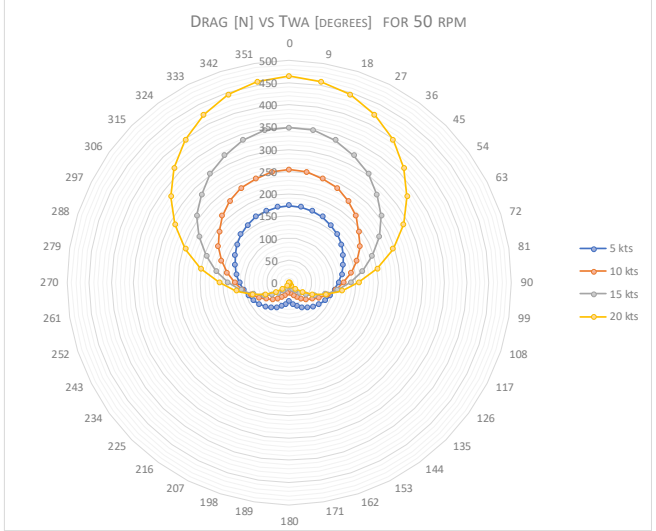

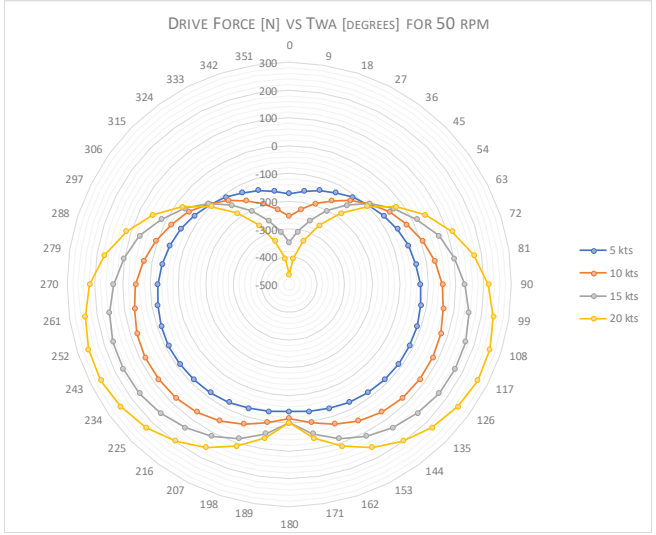

Appendix 5 ROTOR RESULTS: 100 RPM

Item	Value	Unit
CFD Model		
Cylinder Depth	0.10	m
Cylinder Diameter	1.00	m
Rotation Speed	100	rpm
Surface Area	0.314	m^2
Circunferece	3.142	m
Full Size Model		
Rotor Height	8.00	m
Surface Area	25.133	m^2
General		
Air Density (@25°C)	1.185	kg/m^3
Rotational Speed	10.472	rad/s
Circunferece Velocity	5.236	m/s
Boat Speed	18.000	knots
	9.252	m/s

TWS [kts]	Ship Angle [degrees]	AWS [m/s]	AWA [degrees]	V_R	CL	Lift [N]	CD	Drag [N]	Drive [N]	Thrust [N]
5.00	0.00	11.83	0.00	0.443	3.58E-01	745.8	7.98E-02	166.24	-166.24	764.14
5.00	9.00	11.81	1.95	0.443	3.59E-01	744.7	7.87E-02	163.19	-137.70	762.39
5.00	18.00	11.73	3.89	0.446	3.60E-01	737.2	7.82E-02	160.19	-109.85	754.40
5.00	27.00	11.61	5.78	0.451	3.67E-01	735.7	7.81E-02	156.64	-81.81	752.17
5.00	36.00	11.44	7.60	0.458	3.74E-01	728.2	7.79E-02	151.70	-54.08	743.79
5.00	45.00	11.23	9.33	0.466	3.75E-01	703.3	7.82E-02	146.75	-30.81	718.43
5.00	54.00	10.97	10.94	0.477	3.88E-01	695.3	7.64E-02	136.91	-2.45	708.63
5.00	63.00	10.68	12.40	0.490	3.96E-01	671.5	7.70E-02	130.56	16.73	684.09
5.00	72.00	10.35	13.68	0.506	4.12E-01	656.3	7.54E-02	120.09	38.58	667.22
5.00	81.00	9.99	14.74	0.524	4.25E-01	631.0	7.53E-02	111.87	52.37	640.80
5.00	90.00	9.61	15.54	0.545	4.43E-01	609.2	7.45E-02	102.44	64.47	617.75
5.00	99.00	9.21	16.02	0.568	4.67E-01	590.1	7.60E-02	95.99	70.55	597.85
5.00	108.00	8.81	16.13	0.594	4.94E-01	571.0	7.77E-02	89.74	72.44	577.99
5.00	117.00	8.41	15.83	0.623	5.24E-01	551.9	7.95E-02	83.67	70.01	558.18
5.00	126.00	8.02	15.05	0.653	5.56E-01	532.8	8.12E-02	77.75	63.23	538.41
5.00	135.00	7.66	13.75	0.684	5.88E-01	513.7	8.24E-02	71.94	52.20	518.67
5.00	144.00	7.34	11.90	0.714	6.17E-01	494.5	8.26E-02	66.15	37.28	498.95
5.00	153.00	7.06	9.52	0.741	6.40E-01	475.4	8.12E-02	60.31	19.18	479.25
5.00	162.00	6.86	6.66	0.763	6.52E-01	456.3	7.76E-02	54.33	-1.04	459.55
5.00	171.00	6.73	3.43	0.778	6.48E-01	437.2	7.14E-02	48.17	-21.92	439.87
5.00	180.00	6.69	0.00	0.783	6.28E-01	418.1	6.28E-02	41.80	-41.80	420.20
10.00	0.00	14.40	0.00	0.364	2.97E-01	916.9	7.90E-02	244.00	-244.00	948.79
10.00	9.00	14.36	3.21	0.365	2.97E-01	912.5	7.79E-02	239.30	-187.78	943.34
10.00	18.00	14.24	6.41	0.368	2.99E-01	902.7	7.90E-02	238.50	-136.19	933.69
10.00	27.00	14.04	9.58	0.373	3.03E-01	889.8	7.80E-02	228.92	-77.64	918.74
10.00	36.00	13.76	12.70	0.381	3.09E-01	871.0	7.81E-02	220.08	-23.17	898.33
10.00	45.00	13.40	15.76	0.391	3.18E-01	848.7	7.74E-02	206.73	31.55	873.53
10.00	54.00	12.97	18.73	0.404	3.26E-01	815.8	7.37E-02	184.56	87.12	836.38
10.00	63.00	12.47	21.58	0.420	3.42E-01	791.2	7.33E-02	169.61	133.30	809.18
10.00	72.00	11.90	24.29	0.440	3.57E-01	752.7	7.17E-02	151.24	171.75	767.76
10.00	81.00	11.27	26.80	0.464	3.78E-01	714.6	6.94E-02	131.24	205.11	726.59
10.00	90.00	10.59	29.07	0.494	3.97E-01	662.2	6.79E-02	113.41	222.68	671.88
10.00	99.00	9.86	31.03	0.531	4.31E-01	624.0	6.92E-02	100.15	235.80	631.99
10.00	108.00	9.10	32.56	0.576	4.76E-01	585.8	7.11E-02	87.63	241.36	592.29
10.00	117.00	8.30	33.53	0.631	5.34E-01	547.5	7.40E-02	75.92	239.16	552.77
10.00	126.00	7.50	33.75	0.698	6.09E-01	509.3	7.77E-02	65.01	228.89	513.43
10.00	135.00	6.70	32.94	0.782	7.06E-01	471.1	8.21E-02	54.80	210.13	474.24
10.00	144.00	5.93	30.71	0.883	8.28E-01	432.8	8.62E-02	45.05	182.30	435.16
10.00	153.00	5.23	26.57	1.002	9.70E-01	394.6	8.69E-02	35.33	144.93	396.17
10.00	162.00	4.65	20.03	1.127	1.11E+00	356.4	7.78E-02	25.00	98.58	357.23
10.00	171.00	4.26	10.92	1.230	1.18E+00	318.1	5.00E-02	13.47	47.03	318.40
10.00	180.00	4.12	0.00	1.272	1.11E+00	279.9	3.28E-03	0.83	-0.83	279.88
15.00	0.00	16.98	0.00	0.308	2.55E-01	1094.9	7.76E-02	332.96	-332.96	1144.39
15.00	9.00	16.92	4.09	0.309	2.55E-01	1086.8	7.88E-02	335.78	-257.38	1137.49
15.00	18.00	16.77	8.18	0.312	2.55E-01	1066.3	7.71E-02	322.84	-167.87	1114.12
15.00	27.00	16.51	12.26	0.317	2.64E-01	1069.2	7.79E-02	316.23	-82.07	1114.98
15.00	36.00	16.15	16.32	0.324	2.65E-01	1030.6	7.54E-02	292.91	8.39	1071.38
15.00	45.00	15.69	20.35	0.334	2.76E-01	1011.8	7.36E-02	269.95	98.79	1047.15
15.00	54.00	15.14	24.36	0.346	2.86E-01	975.3	7.20E-02	245.82	178.32	1005.78
15.00	63.00	14.50	28.32	0.361	2.94E-01	920.8	7.00E-02	218.94	244.17	946.47
15.00	72.00	13.76	32.24	0.380	3.08E-01	869.4	6.65E-02	187.58	305.08	889.37
15.00	81.00	12.95	36.08	0.404	3.27E-01	816.0	6.47E-02	161.45	350.06	831.82
15.00	90.00	12.05	39.83	0.434	3.52E-01	760.6	6.02E-02	130.25	387.15	771.71
15.00	99.00	11.09	43.45	0.472	3.90E-01	713.7	5.47E-02	100.01	418.20	720.64
15.00	108.00	10.06	46.90	0.521	4.43E-01	666.7	5.42E-02	81.62	431.00	671.66
15.00	117.00	8.97	50.10	0.584	4.99E-01	596.9	5.42E-02	64.88	416.30	600.44
15.00	126.00	7.83	52.93	0.669	5.78E-01	527.2	5.47E-02	49.94	390.50	529.53
15.00	135.00	6.65	55.17	0.787	6.95E-01	457.4	5.60E-02	36.86	354.43	458.90
15.00	144.00	5.45	56.43	0.961	8.78E-01	387.7	5.79E-02	25.56	308.87	388.50
15.00	153.00	4.24	55.84	1.236	1.19E+00	317.9	5.87E-02	15.68	254.25	318.29
15.00	162.00	3.06	51.25	1.710	1.78E+00	248.1	4.32E-02	6.02	189.75	248.22
15.00	171.00	2.03	36.50	2.573	2.89E+00	178.4	1.13E-01	6.98	100.51	178.52
15.00	180.00	1.54	0.00	3.393	3.06E+00	108.6	7.61E-02	2.70	-2.70	108.66
20.00	0.00	19.55	0.00	0.268	2.21E-01	1256.6	7.86E-02	447.28	-447.28	1333.79
20.00	9.00	19.49	4.74	0.269	2.22E-01	1253.8	7.88E-02	445.19	-340.08	1330.53
20.00	18.00	19.31	9.48	0.271	2.23E-01	1235.1	7.75E-02	430.12	-220.80	1307.87
20.00	27.00	19.01	14.23	0.275	2.27E-01	1223.0	7.63E-02	410.37	-97.15	1290.05
20.00	36.00	18.59	18.99	0.282	2.33E-01	1197.0	7.47E-02	384.52	25.86	1257.28
20.00	45.00	18.06	23.76	0.290	2.41E-01	1172.0	7.28E-02	353.58	148.55	1224.17
20.00	54.00	17.42	28.55	0.301	2.46E-01	1110.1	6.90E-02	311.87	256.53	1153.06
20.00	63.00	16.68	33.36	0.314	2.58E-01	1066.6	6.63E-02	274.35	357.37	1101.28
20.00	72.00	15.83	38.21	0.331	2.72E-01	1015.7	6.25E-02	232.97	445.12	1042.06
20.00	81.00	14.88	43.09	0.352	2.88E-01	948.6	5.81E-02	191.56	508.15	967.71
20.00	90.00	13.84	48.03	0.378	3.15E-01	897.3	5.30E-02	151.07	566.17	909.92
20.00	99.00	12.72	53.05	0.412	3.51E-01	846.0	5.01E-02	120.71	603.57	854.59
20.00	108.00	11.52	58.17	0.455	3.85E-01	760.1	4.69E-02	92.66	596.98	765.76
20.00	117.00	10.25	63.44	0.511	4.31E-01	674.2	4.30E-02	67.34	573.01	677.60
20.00	126.00	8.92	68.94	0.587	4.97E-01	588.4	3.81E-02	45.10	532.85	590.08
20.00	135.00	7.54	74.79	0.694	5.94E-01	502.5	3.11E-02	26.34	477.97	503.16
20.00	144.00	6.12	81.27	0.856	7.47E-01	416.6	2.05E-02	11.43	410.01	416.73
20.00	153.00	4.67	88.95	1.121	1.02E+00	330.7	2.82E-03	0.92	330.62	330.69
20.00	162.00	3.22	80.49	1.625	1.58E+00	244.8	2.68E-02	4.15	240.75	244.84
20.00	171.00	1.84	60.53	2.838	3.14E+00	158.9	1.84E-02	0.93	137.90	158.92
20.00	180.00	1.03	0.00	5.089	4.64E+00	73.0	6.86E-02	1.08	-1.08	73.03

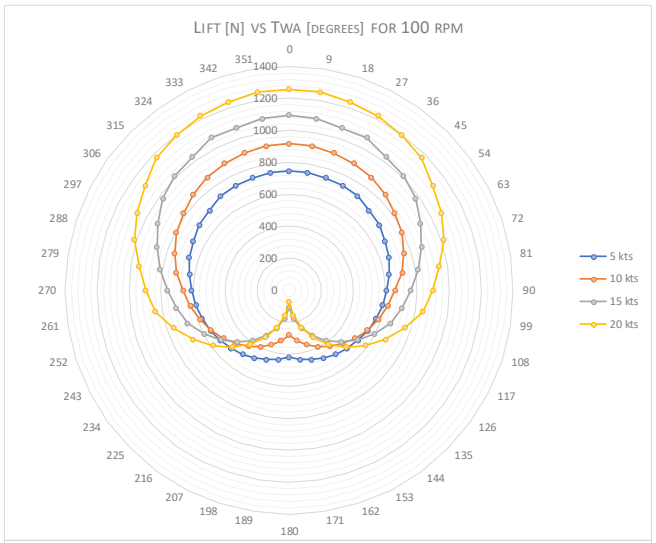

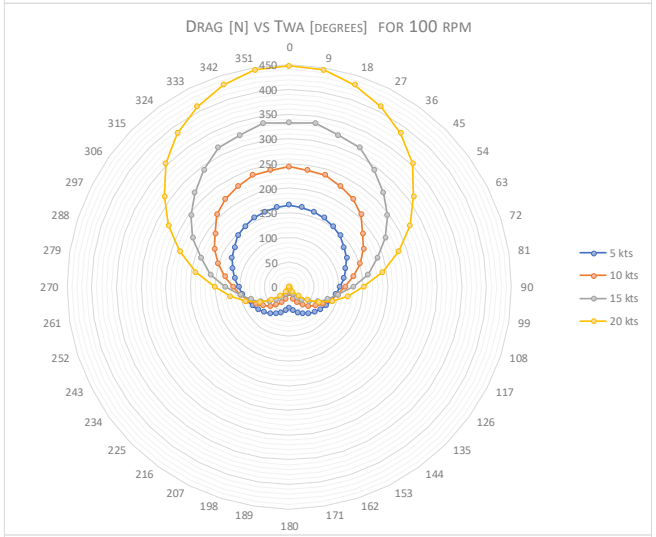

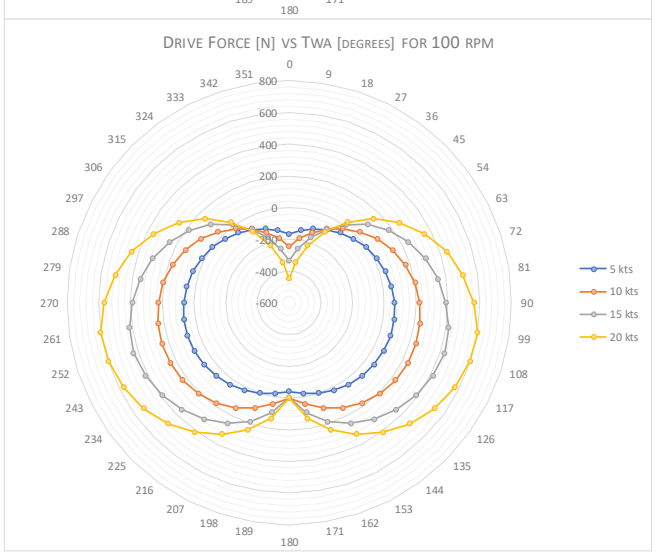

Appendix 6 ROTOR RESULTS: 150 RPM

Item	Value	Unit
CFD Model		
Cylinder Depth	0.10	m
Cylinder Diameter	1.00	m
Rotation Speed	150	rpm
Surface Area	0.314	m^2
Circunferece	3.142	m
Full Size Model		
Rotor Height	8.00	m
Surface Area	25.133	m^2
General		
Air Density (@25°C)	1.185	kg/m^3
Rotational Speed	15.708	rad/s
Circunferece Velocity	7.854	m/s
Boat Speed	18.000	knots
	9.252	m/s

TWS [kts]	Ship Angle [degrees]	AWS [m/s]	AWA [degrees]	V_R	CL	Lift [N]	Drag CFD [N]	CD	Drag [N]	Drive [N]	Thrust [N]
5.00	0.00	11.83	0.00	0.664	5.60E-01	1166.4	1.941	7.45E-02	155.28	-155.28	1176.69
5.00	9.00	11.81	1.95	0.665	5.62E-01	1167.0	1.924	7.41E-02	153.83	-113.95	1177.13
5.00	18.00	11.73	3.89	0.669	5.60E-01	1147.3	1.870	7.28E-02	149.26	-71.14	1156.95
5.00	27.00	11.61	5.78	0.676	5.71E-01	1145.6	1.841	7.30E-02	146.53	-30.50	1154.93
5.00	36.00	11.44	7.60	0.687	5.76E-01	1122.5	1.762	7.17E-02	139.72	9.93	1131.14
5.00	45.00	11.23	9.33	0.700	5.91E-01	1108.6	1.684	7.09E-02	132.94	48.54	1116.58
5.00	54.00	10.97	10.94	0.716	6.06E-01	1085.8	1.585	6.95E-02	124.50	83.85	1092.87
5.00	63.00	10.68	12.40	0.736	6.32E-01	1073.0	1.517	6.99E-02	118.53	114.71	1079.49
5.00	72.00	10.35	13.68	0.759	6.44E-01	1026.2	1.385	6.76E-02	107.66	138.15	1031.79
5.00	81.00	9.99	14.74	0.786	6.65E-01	987.6	1.272	6.62E-02	98.41	156.14	992.49
5.00	90.00	9.61	15.54	0.817	6.94E-01	954.3	1.176	6.59E-02	90.64	168.27	958.62
5.00	99.00	9.21	16.02	0.852	7.34E-01	927.6	1.098	6.68E-02	84.41	174.79	931.39
5.00	108.00	8.81	16.13	0.891	7.80E-01	900.8	1.020	6.78E-02	78.35	175.02	904.20
5.00	117.00	8.41	15.83	0.934	8.30E-01	874.0	0.941	6.88E-02	72.45	168.67	877.04
5.00	126.00	8.02	15.05	0.979	8.85E-01	847.3	0.863	6.96E-02	66.67	155.58	849.90
5.00	135.00	7.66	13.75	1.025	9.40E-01	820.5	0.785	6.98E-02	60.98	135.77	822.78
5.00	144.00	7.34	11.90	1.071	9.91E-01	793.8	0.707	6.90E-02	55.31	109.62	795.68
5.00	153.00	7.06	9.52	1.112	1.03E+00	767.0	0.628	6.67E-02	49.57	78.01	768.60
5.00	162.00	6.86	6.66	1.145	1.06E+00	740.2	0.550	6.24E-02	43.70	42.45	741.53
5.00	171.00	6.73	3.43	1.167	1.06E+00	713.5	0.472	5.59E-02	37.67	5.09	714.47
5.00	180.00	6.69	0.00	1.174	1.03E+00	686.7	0.394	4.73E-02	31.48	-31.48	687.44
10.00	0.00	14.40	0.00	0.545	4.52E-01	1396.3	2.901	7.51E-02	232.04	-232.04	1415.47
10.00	9.00	14.36	3.21	0.547	4.54E-01	1394.3	2.897	7.54E-02	231.43	-152.90	1413.40
10.00	18.00	14.24	6.41	0.552	4.54E-01	1371.8	2.823	7.43E-02	224.41	-69.81	1389.99
10.00	27.00	14.04	9.58	0.559	4.63E-01	1359.0	2.727	7.33E-02	215.12	14.07	1375.88
10.00	36.00	13.76	12.70	0.571	4.74E-01	1334.4	2.610	7.23E-02	203.69	94.72	1349.86
10.00	45.00	13.40	15.76	0.586	4.88E-01	1304.5	2.472	7.12E-02	190.31	171.13	1318.29
10.00	54.00	12.97	18.73	0.606	5.04E-01	1261.1	2.312	7.00E-02	175.20	238.98	1273.23
10.00	63.00	12.47	21.58	0.630	5.27E-01	1218.3	2.132	6.85E-02	158.59	300.65	1228.60
10.00	72.00	11.90	24.29	0.660	5.54E-01	1168.4	1.930	6.68E-02	140.73	352.30	1176.85
10.00	81.00	11.27	26.80	0.697	5.90E-01	1115.4	1.707	6.44E-02	121.89	394.15	1122.00
10.00	90.00	10.59	29.07	0.741	6.24E-01	1041.8	1.463	6.12E-02	102.28	416.83	1046.77
10.00	99.00	9.86	31.03	0.796	6.80E-01	984.1	1.309	6.20E-02	89.72	430.34	988.20
10.00	108.00	9.10	32.56	0.863	7.52E-01	926.5	1.155	6.32E-02	77.86	432.95	929.74
10.00	117.00	8.30	33.53	0.946	8.47E-01	868.8	1.001	6.50E-02	66.73	424.30	871.39
10.00	126.00	7.50	33.75	1.048	9.70E-01	811.2	0.847	6.73E-02	56.32	403.84	813.15
10.00	135.00	6.70	32.94	1.173	1.13E+00	753.6	0.693	6.97E-02	46.50	370.69	754.99
10.00	144.00	5.93	30.71	1.325	1.33E+00	695.9	0.539	7.08E-02	37.04	323.54	696.90
10.00	153.00	5.23	26.57	1.503	1.57E+00	638.3	0.384	6.77E-02	27.51	260.94	638.86
10.00	162.00	4.65	20.03	1.690	1.81E+00	580.6	0.230	5.39E-02	17.32	182.62	580.89
10.00	171.00	4.26	10.92	1.846	1.94E+00	523.0	0.076	2.23E-02	6.00	93.17	523.02
10.00	180.00	4.12	0.00	1.909	1.85E+00	465.3	-0.078	2.46E-02	6.21	-6.21	465.39
15.00	0.00	16.98	0.00	0.463	3.83E-01	1640.6	4.059	7.57E-02	324.69	-324.69	1672.46
15.00	9.00	16.92	4.09	0.464	3.85E-01	1640.0	4.040	7.56E-02	322.37	-204.52	1671.38
15.00	18.00	16.77	8.18	0.468	3.89E-01	1626.4	3.956	7.48E-02	313.25	-78.69	1656.29
15.00	27.00	16.51	12.26	0.476	3.94E-01	1597.4	3.835	7.39E-02	299.77	46.12	1625.24
15.00	36.00	16.15	16.32	0.486	4.03E-01	1564.1	3.676	7.27E-02	282.24	168.51	1589.34
15.00	45.00	15.69	20.35	0.500	4.13E-01	1515.9	3.480	7.12E-02	261.04	282.49	1538.23
15.00	54.00	15.14	24.36	0.519	4.31E-01	1469.6	3.247	6.94E-02	236.66	390.55	1488.53
15.00	63.00	14.50	28.32	0.542	4.50E-01	1409.0	2.977	6.70E-02	209.67	483.98	1424.55
15.00	72.00	13.76	32.24	0.571	4.75E-01	1338.2	2.670	6.41E-02	180.67	561.03	1350.38
15.00	81.00	12.95	36.08	0.607	5.07E-01	1265.0	2.326	6.03E-02	150.36	623.41	1273.86
15.00	90.00	12.05	39.83	0.652	5.47E-01	1183.6	1.944	5.52E-02	119.42	666.36	1189.61
15.00	99.00	11.09	43.45	0.708	5.90E-01	1079.7	1.728	5.49E-02	100.36	669.64	1084.31
15.00	108.00	10.06	46.90	0.781	6.48E-01	975.7	1.512	5.49E-02	82.67	655.91	979.21
15.00	117.00	8.97	50.10	0.876	7.28E-01	871.8	1.297	5.56E-02	66.54	626.08	874.30
15.00	126.00	7.83	52.93	1.003	8.42E-01	767.8	1.081	5.71E-02	52.12	581.19	769.59
15.00	135.00	6.65	55.17	1.181	1.01E+00	663.9	0.865	6.00E-02	39.52	522.38	665.05
15.00	144.00	5.45	56.43	1.442	1.27E+00	559.9	0.649	6.50E-02	28.72	450.67	560.66
15.00	153.00	4.24	55.84	1.854	1.71E+00	456.0	0.433	7.29E-02	19.47	366.38	456.40
15.00	162.00	3.06	51.25	2.565	2.52E+00	352.0	0.218	7.81E-02	10.90	267.73	352.21
15.00	171.00	2.03	36.50	3.860	4.03E+00	248.1	0.020	2.06E-02	1.27	146.57	248.10
15.00	180.00	1.54	0.00	5.089	4.07E+00	144.1	0.014	3.11E-02	1.10	-1.10	144.15
20.00	0.00	19.55	0.00	0.402	3.34E-01	1900.6	5.407	7.61E-02	432.58	-432.58	1949.17
20.00	9.00	19.49	4.74	0.403	3.37E-01	1907.2	5.367	7.57E-02	427.91	-268.88	1954.61
20.00	18.00	19.31	9.48	0.407	3.38E-01	1876.0	5.243	7.46E-02	413.69	-99.02	1921.07
20.00	27.00	19.01	14.23	0.413	3.43E-01	1842.5	5.074	7.32E-02	393.47	71.49	1884.02
20.00	36.00	18.59	18.99	0.422	3.51E-01	1806.5	4.861	7.15E-02	367.71	240.04	1843.52
20.00	45.00	18.06	23.76	0.435	3.61E-01	1753.1	4.603	6.94E-02	337.05	397.81	1785.23
20.00	54.00	17.42	28.55	0.451	3.74E-01	1689.8	4.301	6.69E-02	302.26	542.04	1716.66
20.00	63.00	16.68	33.36	0.471	3.89E-01	1609.2	3.955	6.38E-02	264.25	664.21	1630.75
20.00	72.00	15.83	38.21	0.496	4.10E-01	1527.6	3.564	6.01E-02	224.05	768.75	1543.94
20.00	81.00	14.88	43.09	0.528	4.36E-01	1437.3	3.129	5.55E-02	182.78	848.44	1448.86
20.00	90.00	13.84	48.03	0.567	4.72E-01	1344.8	2.649	4.97E-02	141.72	905.17	1352.25
20.00	99.00	12.72	53.05	0.618	5.07E-01	1220.6	2.354	4.70E-02	113.20	907.44	1225.84
20.00	108.00	11.52	58.17	0.682	5.55E-01	1096.4	2.059	4.40E-02	86.86	885.75	1099.84
20.00	117.00	10.25	63.44	0.766	6.22E-01	972.2	1.764	4.03E-02	63.08	841.44	974.25
20.00	126.00	8.92	68.94	0.880	7.16E-01	848.0	1.469	3.56E-02	42.22	776.19	849.06
20.00	135.00	7.54	74.79	1.042	8.55E-01	723.8	1.174	2.91E-02	24.63	692.01	724.23
20.00	144.00	6.12	81.27	1.284	1.08E+00	599.6	0.878	1.91E-02	10.67	591.04	599.70
20.00	153.00	4.67	88.95	1.681	1.46E+00	475.4	0.583	2.62E-03	0.85	475.32	475.41
20.00	162.00	3.22	80.49	2.437	2.27E+00	351.2	0.288	2.46E-02	3.81	345.76	351.23
20.00	171.00	1.84	60.53	4.257	4.48E+00	227.0	0.051	3.97E-02	2.01	196.66	227.02
20.00	180.00	1.03	0.00	7.634	6.53E+00	102.8	0.003	1.53E-02	0.24	-0.24	102.81

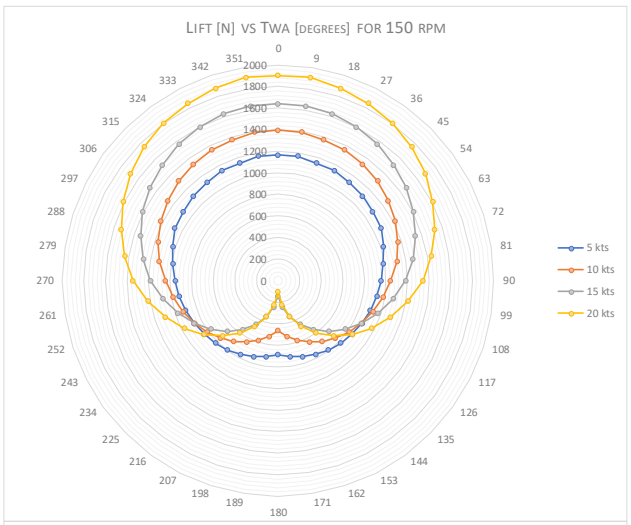

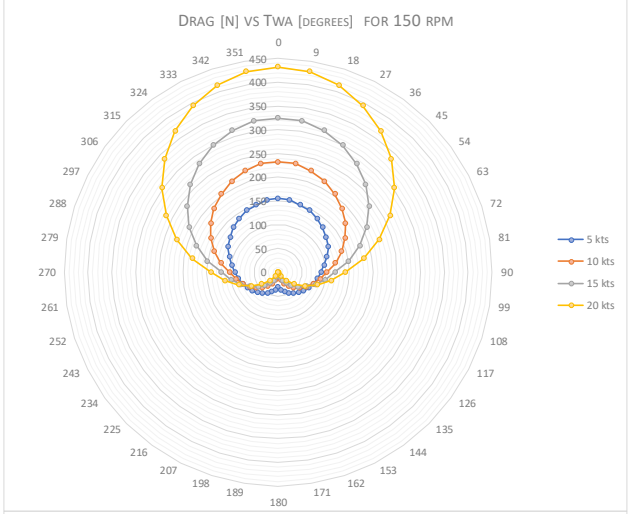

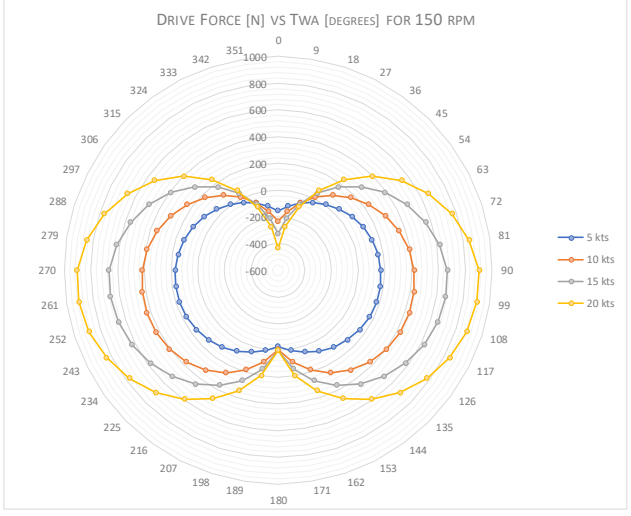

Appendix 7 Rotor results: 200 RPM

Item	Value	Unit
CFD Model		
Cylinder Depth	0.10	m
Cylinder Diameter	1.00	m
Rotation Speed	200	rpm
Surface Area	0.314	m^2
Circunferece	3.142	m
Full Size Model		
Rotor Height	8.00	m
Surface Area	25.133	m^2
General		
Air Density (@25°C)	1.185	kg/m^3
Rotational Speed	20.944	rad/s
Circunferece Velocity	10.472	m/s
Boat Speed	18.000	knots
	9.252	m/s

TWS [kts]	Ship Angle [degrees]	AWS [m/s]	AWA [degrees]	V_R	CL	Lift [N]	CD	Drag [N]	Drive [N]	Thrust [N]
5.00	0.00	11.83	0.00	0.885	7.69E-01	1602.0	6.51E-02	135.60	-135.60	1607.73
5.00	9.00	11.81	1.95	0.887	7.69E-01	1595.6	6.46E-02	134.08	-79.59	1601.22
5.00	18.00	11.73	3.89	0.893	7.76E-01	1589.8	6.46E-02	132.26	-24.19	1595.25
5.00	27.00	11.61	5.78	0.902	7.85E-01	1575.5	6.40E-02	128.46	30.75	1580.75
5.00	36.00	11.44	7.60	0.915	7.98E-01	1553.9	6.34E-02	123.47	83.09	1558.82
5.00	45.00	11.23	9.33	0.933	8.15E-01	1528.8	6.22E-02	116.60	132.77	1533.24
5.00	54.00	10.97	10.94	0.955	8.38E-01	1500.3	6.14E-02	110.04	176.72	1504.35
5.00	63.00	10.68	12.40	0.981	8.63E-01	1463.8	6.02E-02	102.20	214.61	1467.32
5.00	72.00	10.35	13.68	1.012	8.94E-01	1425.2	5.90E-02	94.05	245.77	1428.30
5.00	81.00	9.99	14.74	1.048	9.31E-01	1383.2	5.77E-02	85.64	269.15	1385.85
5.00	90.00	9.61	15.54	1.090	9.74E-01	1338.3	5.62E-02	77.23	284.04	1340.55
5.00	99.00	9.21	16.02	1.137	1.01E+00	1279.8	5.63E-02	71.13	284.73	1281.74
5.00	108.00	8.81	16.13	1.189	1.07E+00	1235.8	5.47E-02	63.25	282.59	1237.38
5.00	117.00	8.41	15.83	1.245	1.13E+00	1192.8	5.32E-02	55.96	271.47	1194.11
5.00	126.00	8.02	15.05	1.305	1.20E+00	1152.2	5.16E-02	49.44	251.36	1153.22
5.00	135.00	7.66	13.75	1.367	1.27E+00	1112.9	5.02E-02	43.83	221.91	1113.74
5.00	144.00	7.34	11.90	1.428	1.34E+00	1076.7	4.92E-02	39.37	183.58	1077.44
5.00	153.00	7.06	9.52	1.482	1.41E+00	1045.9	4.83E-02	35.90	137.64	1046.54
5.00	162.00	6.86	6.66	1.527	1.46E+00	1021.8	4.77E-02	33.37	85.37	1022.30
5.00	171.00	6.73	3.43	1.556	1.49E+00	1005.6	4.74E-02	31.94	28.29	1006.11
5.00	180.00	6.69	0.00	1.566	1.50E+00	1000.1	4.72E-02	31.44	-31.44	1000.57
10.00	0.00	14.40	0.00	0.727	6.23E-01	1922.5	6.93E-02	213.84	-213.84	1934.34
10.00	9.00	14.36	3.21	0.729	6.24E-01	1914.8	6.85E-02	210.47	-102.80	1926.33
10.00	18.00	14.24	6.41	0.735	6.31E-01	1904.5	6.87E-02	207.26	6.74	1915.72
10.00	27.00	14.04	9.58	0.746	6.40E-01	1877.3	6.77E-02	198.47	116.75	1887.74
10.00	36.00	13.76	12.70	0.761	6.54E-01	1842.5	6.65E-02	187.46	222.28	1851.99
10.00	45.00	13.40	15.76	0.782	6.74E-01	1800.4	6.53E-02	174.39	321.14	1808.83
10.00	54.00	12.97	18.73	0.807	6.93E-01	1734.4	6.26E-02	156.61	408.54	1741.46
10.00	63.00	12.47	21.58	0.840	7.25E-01	1677.9	6.21E-02	143.65	483.59	1684.06
10.00	72.00	11.90	24.29	0.880	7.62E-01	1606.6	5.91E-02	124.69	547.14	1611.39
10.00	81.00	11.27	26.80	0.929	8.11E-01	1533.9	5.62E-02	106.39	596.72	1537.61
10.00	90.00	10.59	29.07	0.989	8.71E-01	1454.2	5.38E-02	89.78	628.20	1457.01
10.00	99.00	9.86	31.03	1.062	9.38E-01	1358.6	5.25E-02	76.10	635.01	1360.69
10.00	108.00	9.10	32.56	1.151	1.03E+00	1266.9	4.90E-02	60.35	630.89	1268.32
10.00	117.00	8.30	33.53	1.261	1.15E+00	1181.8	4.57E-02	46.88	613.70	1182.69
10.00	126.00	7.50	33.75	1.397	1.31E+00	1095.0	4.24E-02	35.45	578.88	1095.61
10.00	135.00	6.70	32.94	1.564	1.50E+00	1001.2	3.97E-02	26.52	522.10	1001.55
10.00	144.00	5.93	30.71	1.767	1.70E+00	888.7	3.84E-02	20.08	436.58	888.95
10.00	153.00	5.23	26.57	2.004	1.87E+00	758.4	3.89E-02	15.81	325.14	758.56
10.00	162.00	4.65	20.03	2.253	1.99E+00	639.8	4.02E-02	12.93	207.00	639.89
10.00	171.00	4.26	10.92	2.461	2.09E+00	564.0	4.14E-02	11.15	95.88	564.11
10.00	180.00	4.12	0.00	2.545	2.13E+00	537.4	4.19E-02	10.56	-10.56	537.46
15.00	0.00	16.98	0.00	0.617	5.21E-01	2236.1	6.75E-02	289.36	-289.36	2254.72
15.00	9.00	16.92	4.09	0.619	5.26E-01	2240.6	6.96E-02	296.84	-136.20	2260.22
15.00	18.00	16.77	8.18	0.625	5.28E-01	2211.2	7.02E-02	293.94	23.61	2230.65
15.00	27.00	16.51	12.26	0.634	5.37E-01	2177.7	6.92E-02	280.58	188.06	2195.68
15.00	36.00	16.15	16.32	0.648	5.50E-01	2136.9	6.80E-02	264.19	346.74	2153.15
15.00	45.00	15.69	20.35	0.667	5.68E-01	2083.3	6.57E-02	240.77	498.82	2097.15
15.00	54.00	15.14	24.36	0.692	5.90E-01	2014.9	6.38E-02	217.69	632.74	2026.61
15.00	63.00	14.50	28.32	0.722	6.19E-01	1934.8	6.05E-02	189.15	751.50	1944.02
15.00	72.00	13.76	32.24	0.761	6.54E-01	1843.5	5.77E-02	162.74	845.72	1850.69
15.00	81.00	12.95	36.08	0.809	7.00E-01	1746.2	5.44E-02	135.71	918.63	1751.43
15.00	90.00	12.05	39.83	0.869	7.50E-01	1622.6	5.00E-02	108.07	956.27	1626.23
15.00	99.00	11.09	43.45	0.945	8.21E-01	1502.7	4.73E-02	86.54	970.63	1505.21
15.00	108.00	10.06	46.90	1.041	9.18E-01	1381.1	4.23E-02	63.74	964.85	1382.59
15.00	117.00	8.97	50.10	1.168	1.05E+00	1253.4	3.70E-02	44.24	933.11	1254.14
15.00	126.00	7.83	52.93	1.338	1.24E+00	1131.5	3.17E-02	28.89	885.37	1131.89
15.00	135.00	6.65	55.17	1.575	1.51E+00	995.4	2.69E-02	17.73	806.94	995.52
15.00	144.00	5.45	56.43	1.922	1.82E+00	802.1	2.41E-02	10.66	662.42	802.15
15.00	153.00	4.24	55.84	2.471	2.10E+00	560.6	2.37E-02	6.33	460.30	560.60
15.00	162.00	3.06	51.25	3.420	2.63E+00	366.7	2.44E-02	3.41	283.87	366.74
15.00	171.00	2.03	36.50	5.146	3.76E+00	231.8	3.03E-02	1.86	136.42	231.85
15.00	180.00	1.54	0.00	6.786	4.83E+00	171.4	4.06E-02	1.44	-1.44	171.37
20.00	0.00	19.55	0.00	0.536	4.52E-01	2571.4	7.22E-02	410.72	-410.72	2603.96
20.00	9.00	19.49	4.74	0.537	4.54E-01	2565.5	7.26E-02	410.11	-196.75	2598.09
20.00	18.00	19.31	9.48	0.542	4.58E-01	2539.2	7.13E-02	395.40	28.26	2569.80
20.00	27.00	19.01	14.23	0.551	4.64E-01	2493.0	7.00E-02	376.25	248.07	2521.19
20.00	36.00	18.59	18.99	0.563	4.74E-01	2437.4	6.77E-02	348.58	463.38	2462.16
20.00	45.00	18.06	23.76	0.580	4.90E-01	2379.4	6.43E-02	312.07	672.97	2399.74
20.00	54.00	17.42	28.55	0.601	5.08E-01	2293.2	6.20E-02	280.25	849.71	2310.26
20.00	63.00	16.68	33.36	0.628	5.31E-01	2199.1	5.93E-02	245.29	1004.45	2212.76
20.00	72.00	15.83	38.21	0.662	5.64E-01	2104.3	5.53E-02	206.25	1139.43	2114.40
20.00	81.00	14.88	43.09	0.704	6.01E-01	1979.9	5.07E-02	167.14	1230.59	1986.96
20.00	90.00	13.84	48.03	0.757	6.50E-01	1852.9	4.57E-02	130.20	1290.65	1857.45
20.00	99.00	12.72	53.05	0.823	7.12E-01	1714.8	4.18E-02	100.69	1309.91	1717.75
20.00	108.00	11.52	58.17	0.909	7.84E-01	1548.6	3.47E-02	68.60	1279.63	1550.16
20.00	117.00	10.25	63.44	1.022	8.98E-01	1404.3	2.80E-02	43.78	1236.60	1405.00
20.00	126.00	8.92	68.94	1.174	1.05E+00	1248.3	2.06E-02	24.43	1156.16	1248.56
20.00	135.00	7.54	74.79	1.389	1.30E+00	1099.8	1.34E-02	11.35	1058.36	1099.90
20.00	144.00	6.12	81.27	1.711	1.65E+00	919.7	6.86E-03	3.83	908.44	919.69
20.00	153.00	4.67	88.95	2.242	1.98E+00	644.5	7.83E-04	0.25	644.37	644.48
20.00	162.00	3.22	-80.49	3.250	2.53E+00	391.3	6.50E-03	1.00	-386.07	391.28
20.00	171.00	1.84	-60.53	5.676	4.14E+00	209.5	1.94E-02	0.98	-182.90	209.52
20.00	180.00	1.03	0.00	10.179	6.53E+00	102.8	1.52E-02	0.24	-0.24	102.80

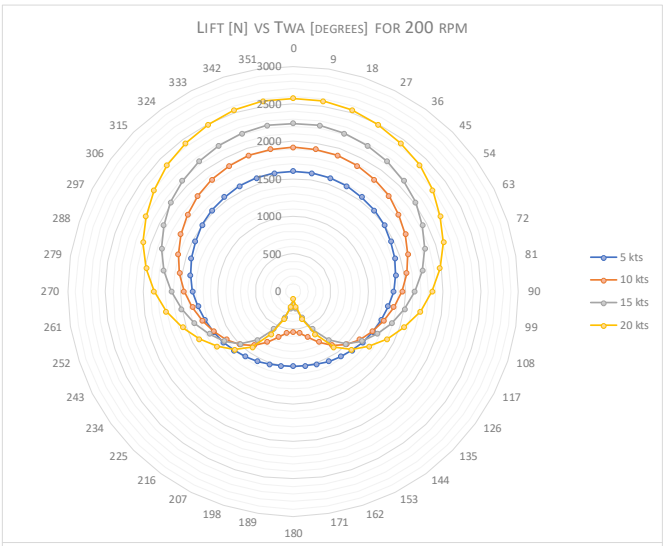

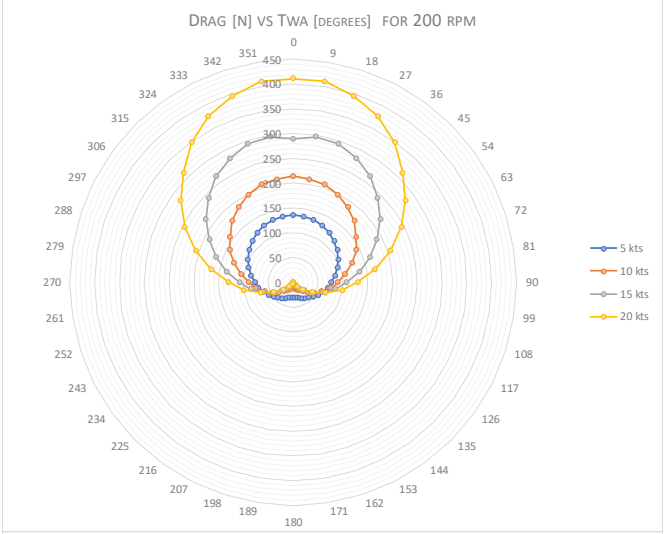

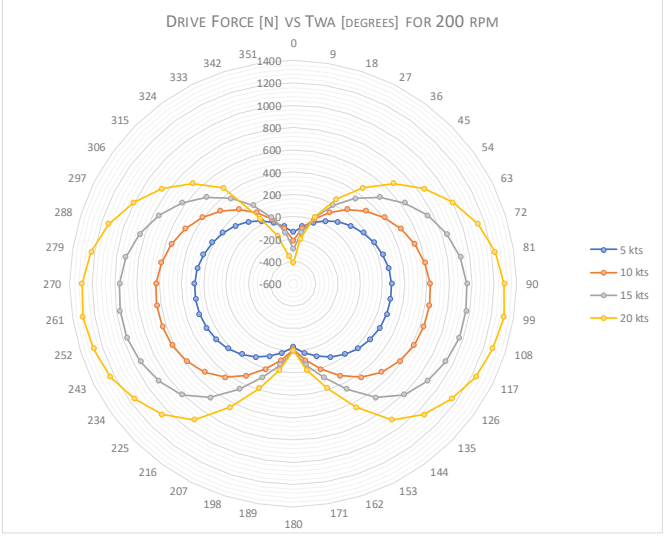

Appendix 8 ROTOR RESULTS: 250 RPM

Item	Value	Unit
CFD Model		
Cylinder Depth	0.10	m
Cylinder Diameter	1.00	m
Rotation Speed	250	rpm
Surface Area	0.314	m^2
Circunferece	3.142	m
Full Size Model		
Rotor Height	8.00	m
Surface Area	25.133	m^2
General		
Air Density (@25°C)	1.185	kg/m^3
Rotational Speed	26.180	rad/s
Circunferece Velocity	13.090	m/s
Boat Speed	18.000	knots
	9.252	m/s

TWS [kts]	Ship Angle [degrees]	AWS [m/s]	AWA [degrees]	V_R	Lift [N]	Drag [N]	L/D Ratio	Drive [N]	Thrust [N]
5.00	0.00	11.83	0.00	1.106	2073.0	118.40	17.51	-118.40	2076.42
5.00	9.00	11.81	1.95	1.109	2069.4	117.69	17.58	-47.06	2072.70
5.00	18.00	11.73	3.89	1.116	2058.4	115.65	17.80	24.14	2061.65
5.00	27.00	11.61	5.78	1.127	2040.4	112.23	18.18	93.68	2043.48
5.00	36.00	11.44	7.60	1.144	2015.8	107.61	18.73	159.89	2018.71
5.00	45.00	11.23	9.33	1.166	1984.5	101.91	19.47	221.13	1987.10
5.00	54.00	10.97	10.94	1.193	1947.0	95.28	20.43	275.99	1949.29
5.00	63.00	10.68	12.40	1.226	1904.4	87.98	21.65	323.15	1906.43
5.00	72.00	10.35	13.68	1.265	1858.1	80.29	23.14	361.54	1859.81
5.00	81.00	9.99	14.74	1.310	1808.6	72.57	24.92	390.04	1810.02
5.00	90.00	9.61	15.54	1.362	1755.6	64.67	27.15	407.91	1756.79
5.00	99.00	9.21	16.02	1.421	1683.3	60.36	27.89	406.42	1684.36
5.00	108.00	8.81	16.13	1.486	1625.7	53.33	30.48	400.46	1626.55
5.00	117.00	8.41	15.83	1.557	1567.0	47.03	33.32	382.10	1567.67
5.00	126.00	8.02	15.05	1.632	1507.2	41.64	36.19	351.07	1507.78
5.00	135.00	7.66	13.75	1.709	1446.1	37.07	39.01	307.66	1446.55
5.00	144.00	7.34	11.90	1.784	1385.6	33.58	41.26	252.96	1386.01
5.00	153.00	7.06	9.52	1.853	1331.0	30.85	43.14	189.78	1331.32
5.00	162.00	6.86	6.66	1.908	1286.5	29.00	44.36	120.41	1286.81
5.00	171.00	6.73	3.43	1.945	1257.4	27.95	44.99	47.34	1257.67
5.00	180.00	6.69	0.00	1.957	1247.3	27.60	45.19	-27.60	1247.59
10.00	0.00	14.40	0.00	0.909	2475.8	187.76	13.19	-187.76	2482.87
10.00	9.00	14.36	3.21	0.911	2452.6	188.58	13.01	-50.81	2459.80
10.00	18.00	14.24	6.41	0.919	2442.6	186.03	13.13	87.92	2449.63
10.00	27.00	14.04	9.58	0.932	2407.4	180.25	13.36	222.96	2414.18
10.00	36.00	13.76	12.70	0.952	2364.2	168.41	14.04	355.59	2370.23
10.00	45.00	13.40	15.76	0.977	2314.7	156.14	14.82	478.39	2319.98
10.00	54.00	12.97	18.73	1.009	2246.7	141.68	15.86	587.16	2251.18
10.00	63.00	12.47	21.58	1.050	2168.9	125.95	17.22	680.64	2172.53
10.00	72.00	11.90	24.29	1.100	2083.4	109.60	19.01	757.01	2086.24
10.00	81.00	11.27	26.80	1.161	1991.4	93.25	21.35	814.75	1993.62
10.00	90.00	10.59	29.07	1.236	1892.4	76.98	24.58	852.30	1893.97
10.00	99.00	9.86	31.03	1.327	1771.9	64.92	27.29	857.63	1773.11
10.00	108.00	9.10	32.56	1.439	1666.7	51.11	32.61	853.85	1667.50
10.00	117.00	8.30	33.53	1.576	1550.8	39.41	39.35	823.78	1551.30
10.00	126.00	7.50	33.75	1.746	1416.5	30.07	47.11	761.94	1416.80
10.00	135.00	6.70	32.94	1.955	1249.3	23.23	53.78	659.75	1249.50
10.00	144.00	5.93	30.71	2.209	1058.3	18.30	57.84	524.73	1058.48
10.00	153.00	5.23	26.57	2.504	879.1	14.74	59.65	380.11	879.24
10.00	162.00	4.65	20.03	2.817	740.7	12.10	61.21	242.36	740.82
10.00	171.00	4.26	10.92	3.076	658.1	10.45	62.99	114.39	658.16
10.00	180.00	4.12	0.00	3.181	629.4	9.92	63.45	-9.92	629.52
15.00	0.00	16.98	0.00	0.771	2870.6	280.41	10.24	-280.41	2884.22
15.00	9.00	16.92	4.09	0.773	2860.6	283.28	10.10	-78.43	2874.63
15.00	18.00	16.77	8.18	0.781	2837.7	275.17	10.31	131.31	2850.99
15.00	27.00	16.51	12.26	0.793	2794.6	261.81	10.67	337.33	2806.80
15.00	36.00	16.15	16.32	0.810	2739.8	243.46	11.25	536.00	2750.56
15.00	45.00	15.69	20.35	0.834	2669.0	222.69	11.99	719.47	2678.23
15.00	54.00	15.14	24.36	0.865	2588.4	198.96	13.01	886.35	2596.04
15.00	63.00	14.50	28.32	0.903	2501.2	175.49	14.25	1032.27	2507.35
15.00	72.00	13.76	32.24	0.951	2364.9	146.09	16.19	1137.91	2369.39
15.00	81.00	12.95	36.08	1.011	2243.3	120.39	18.63	1223.77	2246.51
15.00	90.00	12.05	39.83	1.086	2106.2	95.41	22.07	1275.73	2108.40
15.00	99.00	11.09	43.45	1.181	1936.2	74.98	25.82	1277.16	1937.69
15.00	108.00	10.06	46.90	1.302	1796.2	54.50	32.96	1274.20	1796.99
15.00	117.00	8.97	50.10	1.460	1648.0	37.36	44.11	1240.27	1648.42
15.00	126.00	7.83	52.93	1.672	1475.5	24.36	60.58	1162.57	1475.72
15.00	135.00	6.65	55.17	1.968	1238.8	15.58	79.51	1008.00	1238.90
15.00	144.00	5.45	56.43	2.403	934.8	9.91	94.34	773.43	934.85
15.00	153.00	4.24	55.84	3.089	654.4	5.93	110.37	538.17	654.43
15.00	162.00	3.06	51.25	4.275	467.5	3.91	119.70	362.17	467.54
15.00	171.00	2.03	36.50	6.433	290.0	1.67	173.45	171.17	290.00
15.00	180.00	1.54	0.00	8.482	207.1	1.28	161.81	-1.28	207.12
20.00	0.00	19.55	0.00	0.670	3263.6	388.80	8.39	-388.80	3286.68
20.00	9.00	19.49	4.74	0.672	3252.6	385.32	8.44	-115.28	3275.30
20.00	18.00	19.31	9.48	0.678	3227.0	371.97	8.68	164.67	3248.33
20.00	27.00	19.01	14.23	0.689	3174.5	354.07	8.97	437.09	3194.17
20.00	36.00	18.59	18.99	0.704	3113.6	328.76	9.47	702.14	3130.91
20.00	45.00	18.06	23.76	0.725	3040.5	299.69	10.15	950.64	3055.21
20.00	54.00	17.42	28.55	0.751	2939.9	265.92	11.06	1171.36	2951.92
20.00	63.00	16.68	33.36	0.785	2825.4	228.92	12.34	1362.54	2834.70
20.00	72.00	15.83	38.21	0.827	2689.6	190.54	14.12	1513.77	2696.34
20.00	81.00	14.88	43.09	0.880	2557.5	155.63	16.43	1633.60	2562.25
20.00	90.00	13.84	48.03	0.946	2377.8	118.01	20.15	1689.08	2380.69
20.00	99.00	12.72	53.05	1.029	2178.0	88.48	24.62	1687.44	2179.80
20.00	108.00	11.52	58.17	1.136	1994.5	60.03	33.22	1662.95	1995.38
20.00	117.00	10.25	63.44	1.277	1821.8	37.55	48.51	1612.86	1822.23
20.00	126.00	8.92	68.94	1.467	1641.7	20.67	79.43	1524.60	1641.81
20.00	135.00	7.54	74.79	1.736	1424.5	9.63	147.90	1372.08	1424.51
20.00	144.00	6.12	81.27	2.139	1107.7	3.46	320.00	1094.31	1107.69
20.00	153.00	4.67	88.95	2.802	745.9	0.24	3131.76	745.79	745.92
20.00	162.00	3.22	80.49	4.062	485.0	1.19	407.82	478.18	485.04
20.00	171.00	1.84	60.53	7.095	258.2	0.87	298.27	224.41	258.24
20.00	180.00	1.03	0.00	12.724	122.6	0.32	383.25	-0.32	122.64

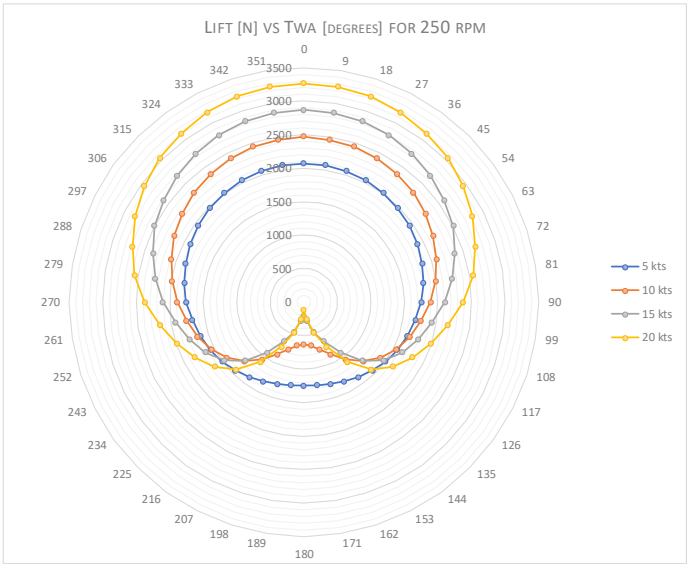

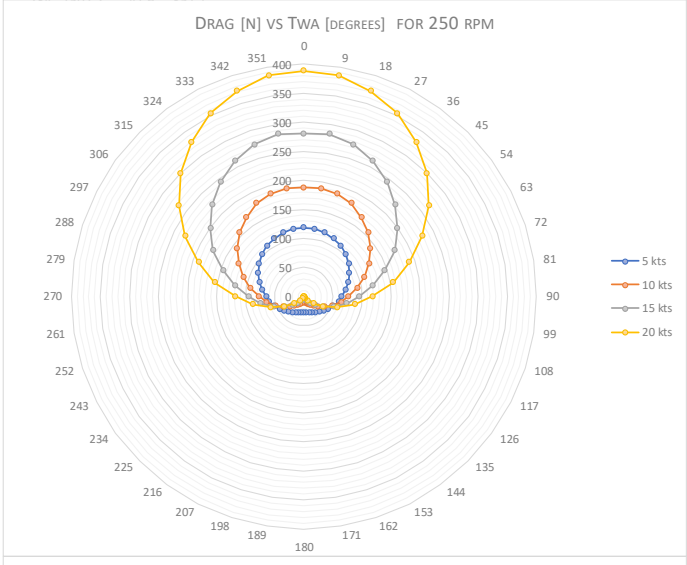

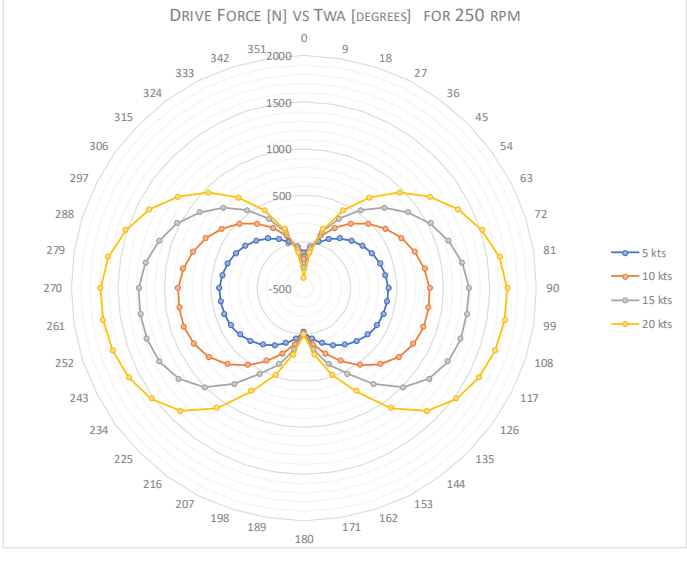

Appendix 9 Rotor results: 300 RPM

Item	Value	Unit
CFD Model		
Cylinder Depth	0.10	m
Cylinder Diameter	1.00	m
Rotation Speed	300	rpm
Surface Area	0.314	m^2
Circunferece	3.142	m
Full Size Model		
Rotor Height	8.00	m
Surface Area	25.133	m^2
General		
Air Density (@25°C)	1.185	kg/m^3
Rotational Speed	31.416	rad/s
Circunferece Velocity	15.708	m/s
Boat Speed	18.000	knots
	9.252	m/s

TWS [kts]	Ship Angle [degrees]	AWS [m/s]	AWA [degrees]	V_R	CL	Lift [N]	CD	Drag [N]	Drive [N]	Thrust [N]
5.00	0.00	11.83	0.00	1.328	1.24E+00	2585.6	4.93E-02	102.80	-102.80	2587.64
5.00	9.00	11.81	1.95	1.330	1.24E+00	2581.4	4.92E-02	102.10	-14.02	2583.38
5.00	18.00	11.73	3.89	1.339	1.25E+00	2568.8	4.89E-02	100.17	74.19	2570.75
5.00	27.00	11.61	5.78	1.353	1.27E+00	2548.1	4.83E-02	96.87	160.06	2549.92
5.00	36.00	11.44	7.60	1.373	1.29E+00	2519.4	4.74E-02	92.38	241.56	2521.05
5.00	45.00	11.23	9.33	1.399	1.32E+00	2483.0	4.63E-02	86.84	316.83	2484.56
5.00	54.00	10.97	10.94	1.432	1.36E+00	2439.2	4.51E-02	80.82	383.61	2440.54
5.00	63.00	10.68	12.40	1.471	1.41E+00	2388.8	4.38E-02	74.38	440.48	2389.96
5.00	72.00	10.35	13.68	1.518	1.46E+00	2330.6	4.23E-02	67.39	485.86	2331.61
5.00	81.00	9.99	14.74	1.572	1.53E+00	2268.8	4.06E-02	60.35	518.97	2269.60
5.00	90.00	9.61	15.54	1.635	1.60E+00	2201.1	3.89E-02	53.41	538.08	2201.77
5.00	99.00	9.21	16.02	1.705	1.65E+00	2087.0	4.15E-02	52.44	525.43	2087.70
5.00	108.00	8.81	16.13	1.783	1.73E+00	2002.5	4.04E-02	46.65	511.57	2003.02
5.00	117.00	8.41	15.83	1.868	1.82E+00	1911.0	3.94E-02	41.49	481.27	1911.49
5.00	126.00	8.02	15.05	1.958	1.89E+00	1813.9	3.89E-02	37.24	434.95	1814.30
5.00	135.00	7.66	13.75	2.051	1.96E+00	1715.6	3.85E-02	33.65	375.04	1715.93
5.00	144.00	7.34	11.90	2.141	2.02E+00	1621.9	3.85E-02	30.84	304.39	1622.21
5.00	153.00	7.06	9.52	2.223	2.07E+00	1541.4	3.87E-02	28.72	226.69	1541.63
5.00	162.00	6.86	6.66	2.290	2.11E+00	1479.2	3.88E-02	27.18	144.58	1479.45
5.00	171.00	6.73	3.43	2.334	2.14E+00	1440.2	3.90E-02	26.27	59.96	1440.48
5.00	180.00	6.69	0.00	2.349	2.14E+00	1426.9	3.91E-02	26.00	-26.00	1427.12
10.00	0.00	14.40	0.00	1.091	9.80E-01	3025.6	5.64E-02	174.24	-174.24	3030.61
10.00	9.00	14.36	3.21	1.094	9.70E-01	2978.2	5.62E-02	172.69	-5.47	2983.24
10.00	18.00	14.24	6.41	1.103	9.73E-01	2936.3	5.57E-02	168.22	160.75	2941.07
10.00	27.00	14.04	9.58	1.119	9.89E-01	2902.3	5.48E-02	160.84	324.46	2906.76
10.00	36.00	13.76	12.70	1.142	1.02E+00	2867.7	5.36E-02	151.01	483.28	2871.70
10.00	45.00	13.40	15.76	1.172	1.06E+00	2825.2	5.20E-02	138.90	633.64	2828.66
10.00	54.00	12.97	18.73	1.211	1.11E+00	2769.1	5.00E-02	125.09	770.59	2771.90
10.00	63.00	12.47	21.58	1.260	1.16E+00	2694.9	4.77E-02	110.32	888.63	2697.13
10.00	72.00	11.90	24.29	1.320	1.23E+00	2599.7	4.52E-02	95.31	982.41	2601.45
10.00	81.00	11.27	26.80	1.393	1.31E+00	2482.1	4.20E-02	79.55	1048.25	2483.39
10.00	90.00	10.59	29.07	1.483	1.40E+00	2342.1	3.89E-02	65.03	1081.26	2342.99
10.00	99.00	9.86	31.03	1.593	1.51E+00	2181.0	3.89E-02	56.28	1075.90	2181.77
10.00	108.00	9.10	32.56	1.727	1.63E+00	2001.8	3.61E-02	44.44	1039.82	2002.34
10.00	117.00	8.30	33.53	1.892	1.76E+00	1808.8	3.40E-02	34.88	970.08	1809.15
10.00	126.00	7.50	33.75	2.095	1.92E+00	1607.7	3.28E-02	27.47	870.33	1607.94
10.00	135.00	6.70	32.94	2.346	2.11E+00	1405.7	3.27E-02	21.82	745.99	1405.89
10.00	144.00	5.93	30.71	2.650	2.32E+00	1211.5	3.33E-02	17.40	603.73	1211.64
10.00	153.00	5.23	26.57	3.005	2.55E+00	1035.2	3.45E-02	14.02	450.56	1035.26
10.00	162.00	4.65	20.03	3.380	2.76E+00	888.2	3.62E-02	11.65	293.31	888.30
10.00	171.00	4.26	10.92	3.691	2.91E+00	783.7	4.52E-02	12.18	136.49	783.75
10.00	180.00	4.12	0.00	3.817	2.92E+00	735.9	4.79E-02	12.08	-12.08	736.01
15.00	0.00	16.98	0.00	0.925	8.26E-01	3544.2	6.16E-02	264.32	-264.32	3554.00
15.00	9.00	16.92	4.09	0.928	8.27E-01	3523.9	6.06E-02	258.46	-6.35	3533.39
15.00	18.00	16.77	8.18	0.937	8.38E-01	3508.1	6.08E-02	254.58	247.06	3517.31
15.00	27.00	16.51	12.26	0.951	8.53E-01	3461.8	5.97E-02	242.35	497.98	3470.23
15.00	36.00	16.15	16.32	0.973	8.74E-01	3395.1	5.82E-02	225.88	736.98	3402.63
15.00	45.00	15.69	20.35	1.001	8.95E-01	3282.2	5.52E-02	202.29	951.89	3288.47
15.00	54.00	15.14	24.36	1.037	9.30E-01	3174.3	5.27E-02	179.72	1145.55	3179.40
15.00	63.00	14.50	28.32	1.084	9.77E-01	3055.3	4.98E-02	155.91	1312.39	3059.26
15.00	72.00	13.76	32.24	1.141	1.04E+00	2923.5	4.65E-02	131.07	1448.61	2926.46
15.00	81.00	12.95	36.08	1.213	1.11E+00	2777.1	4.26E-02	106.30	1549.54	2779.15
15.00	90.00	12.05	39.83	1.303	1.21E+00	2623.4	3.85E-02	83.19	1616.37	2624.76
15.00	99.00	11.09	43.45	1.417	1.32E+00	2421.5	3.57E-02	65.40	1617.85	2422.40
15.00	108.00	10.06	46.90	1.562	1.49E+00	2244.1	3.14E-02	47.23	1606.21	2244.58
15.00	117.00	8.97	50.10	1.752	1.70E+00	2036.1	2.72E-02	32.59	1541.04	2036.34
15.00	126.00	7.83	52.93	2.007	1.93E+00	1762.4	2.41E-02	21.99	1392.88	1762.54
15.00	135.00	6.65	55.17	2.362	2.15E+00	1415.8	2.23E-02	14.67	1153.85	1415.92
15.00	144.00	5.45	56.43	2.884	2.40E+00	1060.4	2.13E-02	9.42	878.35	1060.44
15.00	153.00	4.24	55.84	3.707	2.89E+00	772.9	2.32E-02	6.20	636.06	772.90
15.00	162.00	3.06	51.25	5.130	4.00E+00	558.6	3.34E-02	4.66	432.70	558.58
15.00	171.00	2.03	36.50	7.719	5.66E+00	349.0	3.44E-02	2.12	205.88	348.97
15.00	180.00	1.54	0.00	10.179	6.75E+00	239.1	4.74E-02	1.68	-1.68	239.13
20.00	0.00	19.55	0.00	0.804	7.04E-01	4002.6	6.42E-02	365.28	-365.28	4019.19
20.00	9.00	19.49	4.74	0.806	7.06E-01	3991.6	6.36E-02	359.51	-28.50	4007.76
20.00	18.00	19.31	9.48	0.814	7.13E-01	3954.6	6.27E-02	348.15	308.01	3969.86
20.00	27.00	19.01	14.23	0.826	7.25E-01	3901.8	6.15E-02	330.66	638.56	3915.83
20.00	36.00	18.59	18.99	0.845	7.43E-01	3825.8	5.97E-02	307.17	954.29	3838.15
20.00	45.00	18.06	23.76	0.870	7.68E-01	3728.5	5.73E-02	278.39	1247.32	3738.86
20.00	54.00	17.42	28.55	0.902	8.02E-01	3622.7	5.43E-02	245.55	1515.56	3631.03
20.00	63.00	16.68	33.36	0.942	8.44E-01	3491.6	5.08E-02	210.16	1744.54	3497.92
20.00	72.00	15.83	38.21	0.993	8.88E-01	3310.2	4.67E-02	173.94	1910.62	3314.73
20.00	81.00	14.88	43.09	1.056	9.49E-01	3125.8	4.21E-02	138.59	2034.31	3128.91
20.00	90.00	13.84	48.03	1.135	1.03E+00	2937.5	3.71E-02	105.69	2113.53	2939.42
20.00	99.00	12.72	53.05	1.235	1.12E+00	2688.8	3.18E-02	76.52	2102.85	2689.89
20.00	108.00	11.52	58.17	1.364	1.26E+00	2493.0	2.63E-02	52.01	2090.79	2493.58
20.00	117.00	10.25	63.44	1.532	1.46E+00	2278.9	2.09E-02	32.63	2023.88	2279.11
20.00	126.00	8.92	68.94	1.761	1.71E+00	2026.5	1.55E-02	18.38	1884.53	2026.56
20.00	135.00	7.54	74.79	2.083	1.99E+00	1681.8	1.04E-02	8.81	1620.57	1681.78
20.00	144.00	6.12	81.27	2.567	2.25E+00	1255.4	5.58E-03	3.11	1240.34	1255.36
20.00	153.00	4.67	88.95	3.362	2.65E+00	860.0	6.54E-04	0.21	859.85	860.00
20.00	162.00	3.22	80.49	4.875	3.83E+00	592.2	6.70E-03	1.04	583.93	592.24
20.00	171.00	1.84	60.53	8.514	6.05E+00	306.6	3.10E-02	1.57	266.13	306.56
20.00	180.00	1.03	0.00	15.268	8.64E+00	136.2	3.38E-02	0.53	-0.53	136.16

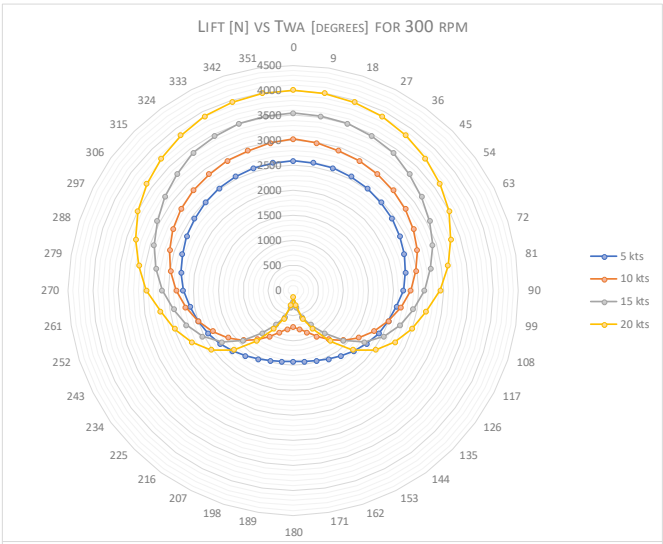

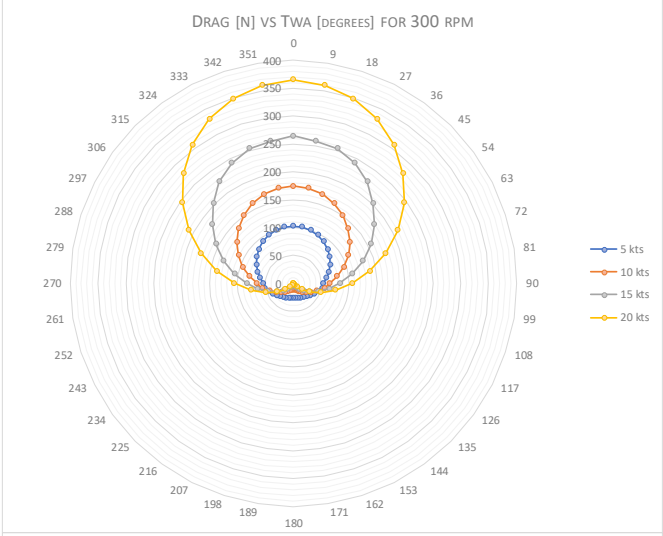

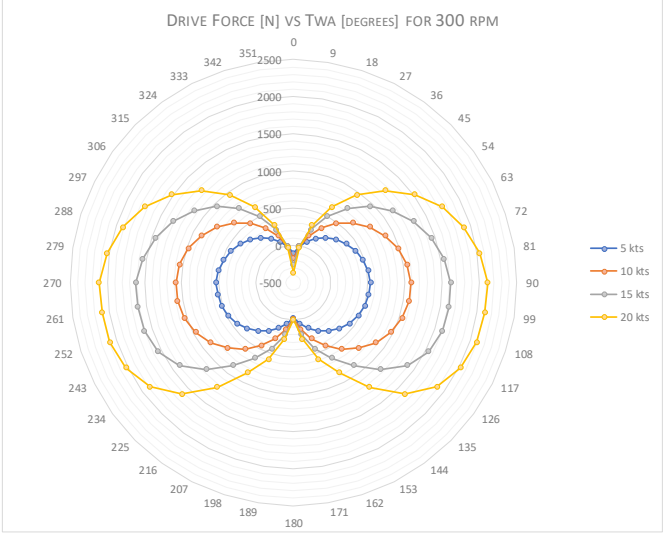

Appendix 10 ROTOR RESULTS: 350 RPM

Item	Value	Unit
CFD Model		
Cylinder Depth	0.10	m
Cylinder Diameter	1.00	m
Rotation Speed	350	rpm
Surface Area	0.314	m^2
Circunferece	3.142	m
Full Size Model		
Rotor Height	8.00	m
Surface Area	25.133	m^2
General		
Air Density (@25°C)	1.185	kg/m^3
Rotational Speed	36.652	rad/s
Circunferece Velocity	18.326	m/s
Boat Speed	18.000	knots
	9.252	m/s

TWS [kts]	Ship Angle [degrees]	AWS [m/s]	AWA [degrees]	V_R	CL	Lift [N]	CD	Drag [N]	Drive [N]	Thrust [N]
5.00	0.00	11.83	0.00	1.549	1.50E+00	3130.2	4.93E-02	102.80	-102.80	3131.85
5.00	9.00	11.81	1.95	1.552	1.51E+00	3125.1	4.92E-02	102.10	4.52	3126.79
5.00	18.00	11.73	3.89	1.562	1.52E+00	3110.2	4.89E-02	100.17	110.89	3111.85
5.00	27.00	11.61	5.78	1.578	1.54E+00	3085.4	4.83E-02	96.87	214.14	3086.96
5.00	36.00	11.44	7.60	1.602	1.57E+00	3049.9	4.74E-02	92.38	311.71	3051.32
5.00	45.00	11.23	9.33	1.632	1.60E+00	3003.7	4.63E-02	86.84	401.23	3004.93
5.00	54.00	10.97	10.94	1.671	1.65E+00	2949.0	4.51E-02	80.82	480.37	2950.15
5.00	63.00	10.68	12.40	1.717	1.70E+00	2889.6	4.38E-02	74.38	548.05	2890.56
5.00	72.00	10.35	13.68	1.771	1.77E+00	2821.0	4.23E-02	67.39	601.87	2821.84
5.00	81.00	9.99	14.74	1.834	1.85E+00	2751.8	4.06E-02	60.35	641.87	2752.42
5.00	90.00	9.61	15.54	1.907	1.95E+00	2677.9	3.89E-02	53.41	665.78	2678.45
5.00	99.00	9.21	16.02	1.989	2.03E+00	2559.3	3.82E-02	48.21	659.81	2559.78
5.00	108.00	8.81	16.13	2.080	2.10E+00	2431.8	3.74E-02	43.27	634.10	2432.18
5.00	117.00	8.41	15.83	2.179	2.18E+00	2295.5	3.71E-02	39.10	588.42	2295.83
5.00	126.00	8.02	15.05	2.284	2.26E+00	2160.7	3.69E-02	35.31	526.85	2161.00
5.00	135.00	7.66	13.75	2.393	2.33E+00	2030.7	3.68E-02	32.17	451.37	2030.98
5.00	144.00	7.34	11.90	2.498	2.39E+00	1913.6	3.70E-02	29.67	365.70	1913.80
5.00	153.00	7.06	9.52	2.594	2.44E+00	1815.2	3.73E-02	27.69	273.01	1815.43
5.00	162.00	6.86	6.66	2.672	2.49E+00	1741.2	3.74E-02	26.22	175.92	1741.36
5.00	171.00	6.73	3.43	2.723	2.51E+00	1695.9	3.75E-02	25.31	76.21	1696.06
5.00	180.00	6.69	0.00	2.740	2.52E+00	1680.0	3.76E-02	25.04	-25.04	1680.20
10.00	0.00	14.40	0.00	1.272	1.17E+00	3619.8	5.64E-02	174.24	-174.24	3623.97
10.00	9.00	14.36	3.21	1.276	1.17E+00	3582.9	5.62E-02	172.69	28.43	3587.08
10.00	18.00	14.24	6.41	1.287	1.17E+00	3536.2	5.57E-02	168.22	227.75	3540.16
10.00	27.00	14.04	9.58	1.305	1.19E+00	3500.2	5.48E-02	160.84	423.98	3503.94
10.00	36.00	13.76	12.70	1.332	1.23E+00	3463.8	5.36E-02	151.01	614.36	3467.14
10.00	45.00	13.40	15.76	1.368	1.28E+00	3417.6	5.20E-02	138.90	794.51	3420.39
10.00	54.00	12.97	18.73	1.413	1.34E+00	3353.9	5.00E-02	125.09	958.36	3356.25
10.00	63.00	12.47	21.58	1.470	1.41E+00	3267.3	4.77E-02	110.32	1099.20	3269.19
10.00	72.00	11.90	24.29	1.540	1.50E+00	3154.2	4.52E-02	95.31	1210.46	3155.59
10.00	81.00	11.27	26.80	1.626	1.59E+00	3012.6	4.20E-02	79.55	1287.48	3013.69
10.00	90.00	10.59	29.07	1.730	1.70E+00	2843.0	3.89E-02	65.03	1324.67	2843.73
10.00	99.00	9.86	31.03	1.858	1.83E+00	2647.3	3.67E-02	53.20	1318.85	2647.81
10.00	108.00	9.10	32.56	2.014	1.97E+00	2429.5	3.50E-02	43.15	1271.06	2429.92
10.00	117.00	8.30	33.53	2.207	2.14E+00	2195.7	3.37E-02	34.59	1184.02	2195.96
10.00	126.00	7.50	33.75	2.445	2.34E+00	1953.6	3.32E-02	27.77	1062.23	1953.77
10.00	135.00	6.70	32.94	2.737	2.57E+00	1713.0	3.33E-02	22.23	912.70	1713.11
10.00	144.00	5.93	30.71	3.092	2.84E+00	1485.5	3.43E-02	17.91	743.24	1485.65
10.00	153.00	5.23	26.57	3.506	3.16E+00	1284.9	3.19E-02	12.97	563.22	1284.97
10.00	162.00	4.65	20.03	3.943	3.50E+00	1126.6	5.37E-02	17.28	369.67	1126.69
10.00	171.00	4.26	10.92	4.307	3.81E+00	1027.9	4.55E-02	12.26	182.68	1028.01
10.00	180.00	4.12	0.00	4.453	4.00E+00	1008.4	5.49E-02	13.83	-13.83	1008.49
15.00	0.00	16.98	0.00	1.080	9.78E-01	4194.2	6.16E-02	264.32	-264.32	4202.48
15.00	9.00	16.92	4.09	1.083	9.81E-01	4182.8	6.06E-02	258.46	40.66	4190.78
15.00	18.00	16.77	8.18	1.093	9.92E-01	4149.8	6.08E-02	254.58	338.36	4157.64
15.00	27.00	16.51	12.26	1.110	1.01E+00	4095.7	5.97E-02	242.35	632.54	4102.84
15.00	36.00	16.15	16.32	1.135	1.04E+00	4019.5	5.82E-02	225.88	912.39	4025.86
15.00	45.00	15.69	20.35	1.168	1.07E+00	3921.4	5.52E-02	202.29	1174.20	3926.65
15.00	54.00	15.14	24.36	1.210	1.11E+00	3804.5	5.27E-02	179.72	1405.46	3808.72
15.00	63.00	14.50	28.32	1.264	1.17E+00	3672.6	4.98E-02	155.91	1605.31	3675.95
15.00	72.00	13.76	32.24	1.332	1.25E+00	3525.0	4.65E-02	131.07	1769.43	3527.40
15.00	81.00	12.95	36.08	1.415	1.35E+00	3360.6	4.26E-02	106.30	1893.17	3362.32
15.00	90.00	12.05	39.83	1.520	1.47E+00	3175.7	3.85E-02	83.19	1970.07	3176.77
15.00	99.00	11.09	43.45	1.653	1.68E+00	3074.5	3.34E-02	61.05	2070.08	3075.12
15.00	108.00	10.06	46.90	1.822	1.87E+00	2810.3	2.96E-02	44.49	2021.47	2810.61
15.00	117.00	8.97	50.10	2.044	2.07E+00	2482.7	2.65E-02	31.76	1884.22	2482.95
15.00	126.00	7.83	52.93	2.341	2.29E+00	2091.4	2.42E-02	22.07	1655.31	2091.49
15.00	135.00	6.65	55.17	2.755	2.53E+00	1667.0	2.27E-02	14.93	1359.89	1667.09
15.00	144.00	5.45	56.43	3.364	2.92E+00	1289.6	2.22E-02	9.79	1069.10	1289.61
15.00	153.00	4.24	55.84	4.325	3.79E+00	1013.0	2.52E-02	6.73	834.46	1013.02
15.00	162.00	3.06	51.25	5.985	4.89E+00	681.9	3.78E-02	5.28	528.47	681.88
15.00	171.00	2.03	36.50	9.006	6.99E+00	430.8	8.87E-02	5.47	251.91	430.88
15.00	180.00	1.54	0.00	11.875	8.06E+00	285.9	1.69E-01	6.00	-6.00	285.91
20.00	0.00	19.55	0.00	0.938	8.40E-01	4778.3	6.42E-02	365.28	-365.28	4792.26
20.00	9.00	19.49	4.74	0.940	8.45E-01	4775.1	6.40E-02	361.48	34.27	4788.78
20.00	18.00	19.31	9.48	0.949	8.54E-01	4738.4	6.29E-02	349.24	436.05	4751.25
20.00	27.00	19.01	14.23	0.964	8.70E-01	4676.5	6.17E-02	331.66	828.00	4688.23
20.00	36.00	18.59	18.99	0.986	8.92E-01	4591.4	5.96E-02	306.90	1203.63	4601.69
20.00	45.00	18.06	23.76	1.015	9.13E-01	4436.5	5.71E-02	277.51	1533.36	4445.15
20.00	54.00	17.42	28.55	1.052	9.50E-01	4290.3	5.46E-02	246.52	1833.74	4297.40
20.00	63.00	16.68	33.36	1.099	9.98E-01	4130.2	5.12E-02	212.08	2094.13	4135.68
20.00	72.00	15.83	38.21	1.158	1.06E+00	3949.4	4.67E-02	174.19	2305.81	3953.28
20.00	81.00	14.88	43.09	1.232	1.14E+00	3750.4	4.19E-02	138.10	2461.35	3752.94
20.00	90.00	13.84	48.03	1.324	1.24E+00	3540.5	3.69E-02	105.17	2562.21	3542.04
20.00	99.00	12.72	53.05	1.441	1.39E+00	3345.7	3.05E-02	73.41	2629.66	3346.46
20.00	108.00	11.52	58.17	1.591	1.61E+00	3172.2	2.48E-02	49.02	2669.41	3172.57
20.00	117.00	10.25	63.44	1.788	1.83E+00	2864.5	1.96E-02	30.58	2548.63	2864.66
20.00	126.00	8.92	68.94	2.054	2.08E+00	2468.2	1.48E-02	17.58	2296.98	2468.21
20.00	135.00	7.54	74.79	2.430	2.35E+00	1987.7	1.05E-02	8.87	1915.80	1987.73
20.00	144.00	6.12	81.27	2.995	2.66E+00	1482.9	6.02E-03	3.36	1465.20	1482.90
20.00	153.00	4.67	88.95	3.923	3.59E+00	1166.3	7.92E-04	0.26	1166.15	1166.34
20.00	162.00	3.22	80.49	5.687	4.67E+00	722.0	8.11E-03	1.25	711.88	722.01
20.00	171.00	1.84	60.53	9.933	7.28E+00	368.7	4.26E-02	2.16	319.92	368.69
20.00	180.00	1.03	0.00	17.813	1.07E+01	168.2	1.70E-01	2.67	-2.67	168.21

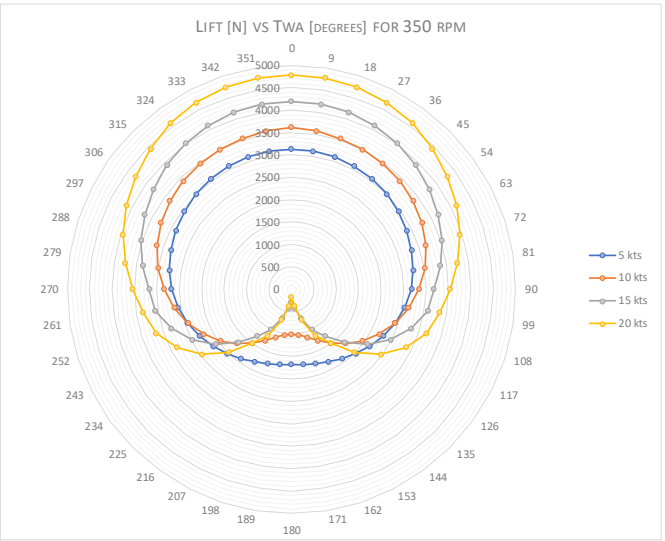

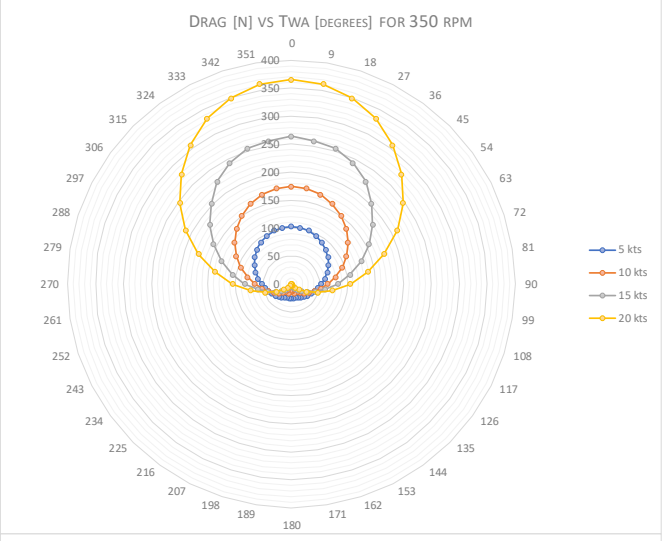

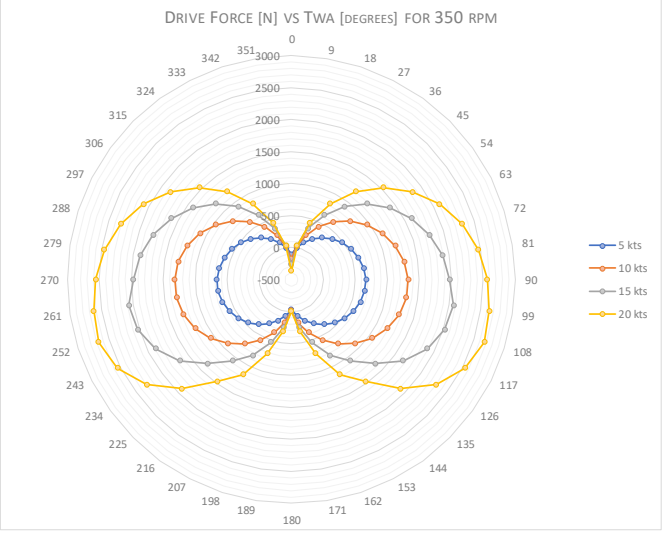

Appendix 11 ROTOR RESULTS: 400 RPM

Item	Value	Unit
CFD Model		
Cylinder Depth	0.10	m
Cylinder Diameter	1.00	m
Rotation Speed	400	rpm
Surface Area	0.314	m^2
Circunferece	3.142	m
Full Size Model		
Rotor Height	8.00	m
Surface Area	25.133	m^2
General		
Air Density (@25°C)	1.185	kg/m^3
Rotational Speed	41.888	rad/s
Circunferece Velocity	20.944	m/s
Boat Speed	18.000	knots
	9.252	m/s

TWS [kts]	Ship Angle [degrees]	AWS [m/s]	AWA [degrees]	V_R	CL	Lift [N]	CD	Drag [N]	Drive [N]	Thrust [N]
5.00	0.00	11.83	0.00	1.770	1.77E+00	3681.2	3.66E-02	76.16	-76.16	3681.96
5.00	9.00	11.81	1.95	1.774	1.76E+00	3659.7	3.65E-02	75.64	49.20	3660.47
5.00	18.00	11.73	3.89	1.785	1.77E+00	3636.6	3.62E-02	74.07	172.61	3637.33
5.00	27.00	11.61	5.78	1.804	1.80E+00	3615.2	3.57E-02	71.55	292.64	3615.91
5.00	36.00	11.44	7.60	1.831	1.84E+00	3589.5	3.51E-02	68.43	406.80	3590.17
5.00	45.00	11.23	9.33	1.866	1.89E+00	3554.6	3.44E-02	64.57	512.50	3555.16
5.00	54.00	10.97	10.94	1.909	1.96E+00	3506.6	3.35E-02	59.93	606.71	3507.12
5.00	63.00	10.68	12.40	1.962	2.03E+00	3443.0	3.26E-02	55.32	685.53	3443.41
5.00	72.00	10.35	13.68	2.024	2.11E+00	3362.1	3.18E-02	50.68	746.11	3362.52
5.00	81.00	9.99	14.74	2.097	2.20E+00	3263.8	3.11E-02	46.27	785.77	3264.08
5.00	90.00	9.61	15.54	2.179	2.29E+00	3148.6	3.07E-02	42.16	802.69	3148.88
5.00	99.00	9.21	16.02	2.273	2.39E+00	3018.6	3.07E-02	38.77	795.60	3018.83
5.00	108.00	8.81	16.13	2.377	2.49E+00	2876.8	3.04E-02	35.13	765.55	2876.97
5.00	117.00	8.41	15.83	2.490	2.59E+00	2727.3	3.02E-02	31.75	713.26	2727.50
5.00	126.00	8.02	15.05	2.611	2.69E+00	2575.6	3.01E-02	28.82	640.82	2575.76
5.00	135.00	7.66	13.75	2.734	2.78E+00	2428.1	3.03E-02	26.44	551.36	2428.22
5.00	144.00	7.34	11.90	2.855	2.86E+00	2292.4	3.04E-02	24.34	449.05	2292.48
5.00	153.00	7.06	9.52	2.965	2.93E+00	2177.2	3.10E-02	23.00	337.53	2177.32
5.00	162.00	6.86	6.66	3.053	2.99E+00	2092.5	3.11E-02	21.77	221.09	2092.61
5.00	171.00	6.73	3.43	3.112	3.04E+00	2049.3	3.17E-02	21.40	101.26	2049.39
5.00	180.00	6.69	0.00	3.132	3.09E+00	2059.7	3.16E-02	21.04	-21.04	2059.83
10.00	0.00	14.40	0.00	1.454	1.40E+00	4334.4	4.45E-02	137.28	-137.28	4336.56
10.00	9.00	14.36	3.21	1.458	1.40E+00	4284.7	4.49E-02	137.85	102.55	4286.87
10.00	18.00	14.24	6.41	1.471	1.41E+00	4245.6	4.45E-02	134.19	340.80	4247.74
10.00	27.00	14.04	9.58	1.492	1.43E+00	4205.9	4.34E-02	127.22	574.59	4207.82
10.00	36.00	13.76	12.70	1.522	1.48E+00	4155.9	4.18E-02	117.81	798.93	4157.57
10.00	45.00	13.40	15.76	1.563	1.53E+00	4087.8	4.00E-02	106.77	1007.47	4089.24
10.00	54.00	12.97	18.73	1.615	1.60E+00	3995.7	3.79E-02	94.86	1193.06	3996.87
10.00	63.00	12.47	21.58	1.680	1.67E+00	3875.4	3.57E-02	82.71	1348.54	3876.31
10.00	72.00	11.90	24.29	1.760	1.77E+00	3724.5	3.36E-02	70.86	1467.33	3725.18
10.00	81.00	11.27	26.80	1.858	1.87E+00	3542.4	3.16E-02	59.75	1544.02	3542.90
10.00	90.00	10.59	29.07	1.977	1.99E+00	3330.3	2.98E-02	49.68	1574.89	3330.70
10.00	99.00	9.86	31.03	2.123	2.13E+00	3091.3	2.82E-02	40.86	1558.29	3091.60
10.00	108.00	9.10	32.56	2.302	2.30E+00	2830.2	2.71E-02	33.38	1494.91	2830.40
10.00	117.00	8.30	33.53	2.522	2.49E+00	2553.6	2.66E-02	27.26	1387.83	2553.73
10.00	126.00	7.50	33.75	2.794	2.71E+00	2269.9	2.68E-02	22.43	1242.41	2270.01
10.00	135.00	6.70	32.94	3.128	2.98E+00	1989.4	2.81E-02	18.77	1065.89	1989.46
10.00	144.00	5.93	30.71	3.534	3.30E+00	1724.0	3.08E-02	16.10	866.58	1724.11
10.00	153.00	5.23	26.57	4.007	3.66E+00	1487.7	3.49E-02	14.18	652.87	1487.77
10.00	162.00	4.65	20.03	4.507	4.03E+00	1296.0	3.93E-02	12.64	432.07	1296.08
10.00	171.00	4.26	10.92	4.922	4.33E+00	1166.4	4.06E-02	10.96	210.18	1166.45
10.00	180.00	4.12	0.00	5.089	4.44E+00	1118.1	3.39E-02	8.54	-8.54	1118.12
15.00	0.00	16.98	0.00	1.234	1.15E+00	4913.2	5.07E-02	217.44	-217.44	4918.01
15.00	9.00	16.92	4.09	1.238	1.15E+00	4901.1	5.05E-02	215.13	135.14	4905.84
15.00	18.00	16.77	8.18	1.249	1.16E+00	4864.6	4.98E-02	208.34	485.82	4869.10
15.00	27.00	16.51	12.26	1.269	1.18E+00	4804.2	4.87E-02	197.40	826.85	4808.21
15.00	36.00	16.15	16.32	1.297	1.22E+00	4720.4	4.71E-02	182.73	1150.69	4723.94
15.00	45.00	15.69	20.35	1.335	1.26E+00	4614.5	4.49E-02	164.71	1450.47	4617.42
15.00	54.00	15.14	24.36	1.383	1.31E+00	4486.8	4.22E-02	144.15	1719.28	4489.12
15.00	63.00	14.50	28.32	1.445	1.39E+00	4334.8	3.94E-02	123.10	1948.38	4336.55
15.00	72.00	13.76	32.24	1.522	1.47E+00	4157.5	3.60E-02	101.43	2131.93	4158.76
15.00	81.00	12.95	36.08	1.618	1.59E+00	3961.5	3.25E-02	81.08	2267.41	3962.35
15.00	90.00	12.05	39.83	1.738	1.73E+00	3744.7	2.86E-02	61.93	2350.85	3745.23
15.00	99.00	11.09	43.45	1.889	1.89E+00	3455.3	2.58E-02	47.18	2342.05	3455.66
15.00	108.00	10.06	46.90	2.083	2.04E+00	3075.8	2.35E-02	35.33	2221.60	3075.99
15.00	117.00	8.97	50.10	2.336	2.24E+00	2676.1	2.17E-02	26.03	2036.26	2676.27
15.00	126.00	7.83	52.93	2.675	2.46E+00	2246.3	2.00E-02	18.27	1781.24	2246.41
15.00	135.00	6.65	55.17	3.149	2.79E+00	1838.6	2.01E-02	13.21	1501.70	1838.63
15.00	144.00	5.45	56.43	3.845	3.60E+00	1588.6	2.37E-02	10.48	1317.84	1588.59
15.00	153.00	4.24	55.84	4.943	4.09E+00	1092.3	3.09E-02	8.27	899.19	1092.30
15.00	162.00	3.06	51.25	6.840	5.55E+00	774.8	6.06E-02	8.46	598.93	774.81
15.00	171.00	2.03	36.50	10.293	7.50E+00	462.4	1.64E-01	10.09	266.98	462.54
15.00	180.00	1.54	0.00	13.572	8.24E+00	292.1	2.57E-01	9.12	-9.12	292.23
20.00	0.00	19.55	0.00	1.071	9.74E-01	5540.5	5.61E-02	318.80	-318.80	5549.64
20.00	9.00	19.49	4.74	1.075	9.78E-01	5525.6	5.61E-02	317.07	140.53	5534.69
20.00	18.00	19.31	9.48	1.085	9.88E-01	5482.2	5.56E-02	308.31	598.94	5490.82
20.00	27.00	19.01	14.23	1.102	1.01E+00	5409.7	5.40E-02	290.56	1048.06	5417.48
20.00	36.00	18.59	18.99	1.126	1.03E+00	5308.2	5.17E-02	265.98	1475.51	5314.82
20.00	45.00	18.06	23.76	1.159	1.07E+00	5176.7	4.87E-02	236.70	1868.94	5182.13
20.00	54.00	17.42	28.55	1.202	1.11E+00	5019.9	4.53E-02	204.73	2219.11	5024.09
20.00	63.00	16.68	33.36	1.256	1.17E+00	4843.0	4.15E-02	171.91	2519.61	4846.01
20.00	72.00	15.83	38.21	1.323	1.25E+00	4644.7	3.75E-02	139.84	2762.83	4646.82
20.00	81.00	14.88	43.09	1.408	1.34E+00	4424.8	3.33E-02	109.84	2942.73	4426.16
20.00	90.00	13.84	48.03	1.513	1.46E+00	4176.2	2.91E-02	82.90	3049.82	4177.06
20.00	99.00	12.72	53.05	1.647	1.62E+00	3905.1	2.48E-02	59.71	3084.99	3905.55
20.00	108.00	11.52	58.17	1.818	1.82E+00	3585.9	2.06E-02	40.63	3025.35	3586.14
20.00	117.00	10.25	63.44	2.043	2.01E+00	3145.2	1.64E-02	25.70	2801.93	3145.34
20.00	126.00	8.92	68.94	2.348	2.24E+00	2654.3	1.24E-02	14.73	2471.73	2654.35
20.00	135.00	7.54	74.79	2.778	2.52E+00	2131.0	8.59E-03	7.27	2054.48	2131.01
20.00	144.00	6.12	81.27	3.423	3.03E+00	1690.5	4.82E-03	2.68	1670.47	1690.48
20.00	153.00	4.67	88.95	4.483	3.86E+00	1253.8	6.06E-04	0.20	1253.59	1253.80
20.00	162.00	3.22	80.49	6.500	5.25E+00	811.4	7.25E-03	1.12	800.07	811.41
20.00	171.00	1.84	60.53	11.352	7.65E+00	387.4	5.19E-02	2.63	336.00	387.43
20.00	180.00	1.03	0.00	20.358	1.16E+01	183.2	3.80E-01	5.98	-5.98	183.29

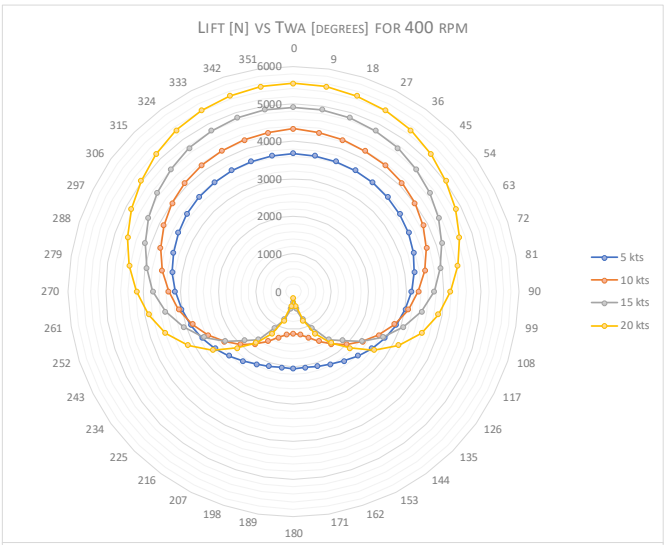

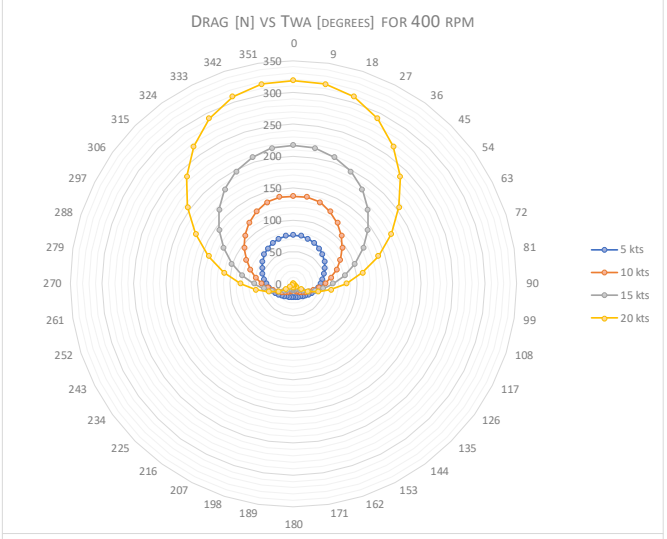

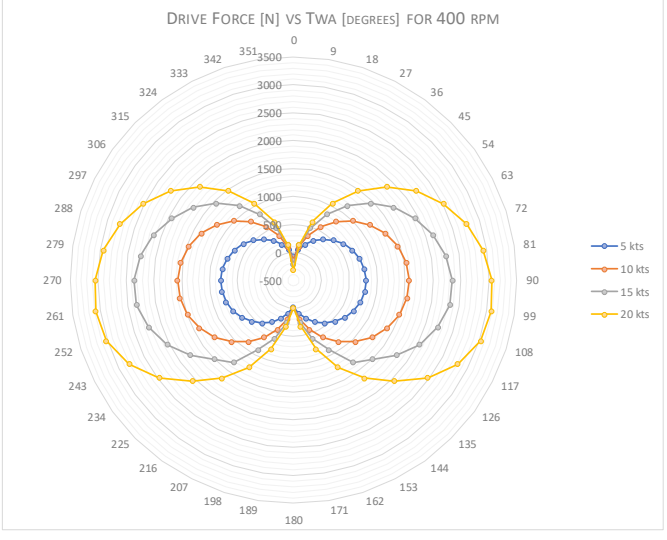

Appendix 12 ROTOR RESULTS: 450 RPM

Item	Value	Unit
CFD Model		
Cylinder Depth	0.10	m
Cylinder Diameter	1.00	m
Rotation Speed	450	rpm
Surface Area	0.314	m^2
Circunferece	3.142	m
Full Size Model		
Rotor Height	8.00	m
Surface Area	25.133	m^2
General		
Air Density (@25°C)	1.185	kg/m^3
Rotational Speed	47.124	rad/s
Circunferece Velocity	23.562	m/s
Boat Speed	18.000	knots
	9.252	m/s

TWS [kts]	Ship Angle [degrees]	AWS [m/s]	AWA [degrees]	V_R	CL	Lift [N]	C_D	Drag [N]	Drive [N]	Thrust [N]
5.00	0.00	11.83	0.00	1.992	2.07E+00	4304.6	8.70E-02	181.36	-181.36	4308.46
5.00	9.00	11.81	1.95	1.996	2.07E+00	4298.5	8.73E-02	181.07	-34.39	4302.29
5.00	18.00	11.73	3.89	2.008	2.09E+00	4279.8	8.80E-02	180.27	110.25	4283.64
5.00	27.00	11.61	5.78	2.029	2.12E+00	4249.3	8.92E-02	179.01	249.54	4253.05
5.00	36.00	11.44	7.60	2.060	2.16E+00	4207.6	9.11E-02	177.50	380.42	4211.34
5.00	45.00	11.23	9.33	2.099	2.22E+00	4155.4	9.38E-02	175.95	500.00	4159.16
5.00	54.00	10.97	10.94	2.148	2.29E+00	4099.0	9.76E-02	174.88	606.30	4102.77
5.00	63.00	10.68	12.40	2.207	2.38E+00	4030.4	1.02E-01	173.86	695.94	4034.15
5.00	72.00	10.35	13.68	2.277	2.48E+00	3955.2	1.09E-01	173.60	766.97	3959.01
5.00	81.00	9.99	14.74	2.359	2.60E+00	3862.2	1.17E-01	173.52	814.99	3866.06
5.00	90.00	9.61	15.54	2.452	2.74E+00	3765.0	1.27E-01	174.54	840.23	3769.00
5.00	99.00	9.21	16.02	2.557	2.86E+00	3617.1	1.36E-01	171.86	832.80	3621.13
5.00	108.00	8.81	16.13	2.674	2.96E+00	3422.9	1.43E-01	165.76	791.82	3426.94
5.00	117.00	8.41	15.83	2.802	3.09E+00	3252.3	1.53E-01	161.53	731.56	3256.28
5.00	126.00	8.02	15.05	2.937	3.24E+00	3105.1	1.66E-01	159.03	652.53	3109.15
5.00	135.00	7.66	13.75	3.076	3.41E+00	2981.4	1.81E-01	158.04	555.03	2985.55
5.00	144.00	7.34	11.90	3.212	3.60E+00	2881.1	1.98E-01	158.23	439.48	2885.44
5.00	153.00	7.06	9.52	3.335	3.77E+00	2804.3	2.14E-01	159.17	306.99	2808.82
5.00	162.00	6.86	6.66	3.435	3.93E+00	2751.0	2.29E-01	160.30	159.88	2755.65
5.00	171.00	6.73	3.43	3.501	4.04E+00	2721.1	2.39E-01	161.04	2.08	2725.88
5.00	180.00	6.69	0.00	3.523	4.08E+00	2714.7	2.42E-01	160.94	-160.94	2719.49
10.00	0.00	14.40	0.00	1.636	1.62E+00	5011.7	7.27E-02	224.46	-224.46	5016.76
10.00	9.00	14.36	3.21	1.641	1.61E+00	4950.6	7.20E-02	221.22	56.63	4955.52
10.00	18.00	14.24	6.41	1.655	1.62E+00	4904.8	7.20E-02	217.33	331.80	4909.57
10.00	27.00	14.04	9.58	1.678	1.66E+00	4860.6	7.25E-02	212.68	599.28	4865.25
10.00	36.00	13.76	12.70	1.713	1.71E+00	4806.5	7.35E-02	207.19	854.80	4810.96
10.00	45.00	13.40	15.76	1.758	1.77E+00	4733.0	7.49E-02	200.24	1092.72	4737.21
10.00	54.00	12.97	18.73	1.817	1.85E+00	4632.6	7.70E-02	192.67	1304.90	4636.64
10.00	63.00	12.47	21.58	1.890	1.94E+00	4500.1	7.98E-02	184.58	1483.60	4503.93
10.00	72.00	11.90	24.29	1.980	2.06E+00	4332.3	8.36E-02	176.34	1621.19	4335.90
10.00	81.00	11.27	26.80	2.090	2.18E+00	4128.0	8.90E-02	168.35	1711.15	4131.43
10.00	90.00	10.59	29.07	2.224	2.33E+00	3888.2	9.64E-02	161.01	1748.67	3891.52
10.00	99.00	9.86	31.03	2.389	2.50E+00	3615.9	1.06E-01	153.38	1732.25	3619.17
10.00	108.00	9.10	32.56	2.590	2.69E+00	3316.4	1.18E-01	145.86	1661.73	3319.58
10.00	117.00	8.30	33.53	2.838	2.92E+00	2996.8	1.35E-01	138.31	1540.07	2999.98
10.00	126.00	7.50	33.75	3.143	3.19E+00	2666.5	1.56E-01	130.73	1372.70	2669.70
10.00	135.00	6.70	32.94	3.519	3.50E+00	2336.9	1.85E-01	123.19	1167.23	2340.19
10.00	144.00	5.93	30.71	3.975	3.87E+00	2021.7	2.21E-01	115.81	932.85	2024.97
10.00	153.00	5.23	26.57	4.508	4.27E+00	1736.2	2.67E-01	108.68	679.54	1739.64
10.00	162.00	4.65	20.03	5.070	4.66E+00	1498.4	3.17E-01	101.84	417.60	1501.88
10.00	171.00	4.26	10.92	5.537	4.93E+00	1328.0	3.54E-01	95.33	157.95	1331.42
10.00	180.00	4.12	0.00	5.726	4.95E+00	1246.9	3.57E-01	89.97	-89.97	1250.11
15.00	0.00	16.98	0.00	1.388	1.33E+00	5684.0	6.80E-02	291.56	-291.56	5691.47
15.00	9.00	16.92	4.09	1.392	1.33E+00	5669.9	6.79E-02	289.41	115.90	5677.30
15.00	18.00	16.77	8.18	1.405	1.34E+00	5628.2	6.77E-02	283.46	520.09	5635.37
15.00	27.00	16.51	12.26	1.427	1.37E+00	5559.4	6.75E-02	273.86	912.44	5566.18
15.00	36.00	16.15	16.32	1.459	1.41E+00	5462.2	6.72E-02	261.01	1283.97	5468.47
15.00	45.00	15.69	20.35	1.501	1.46E+00	5335.8	6.69E-02	245.14	1625.93	5341.39
15.00	54.00	15.14	24.36	1.556	1.52E+00	5187.2	6.69E-02	228.42	1931.40	5192.23
15.00	63.00	14.50	28.32	1.625	1.60E+00	5007.2	6.74E-02	210.67	2190.32	5011.63
15.00	72.00	13.76	32.24	1.712	1.70E+00	4806.9	6.86E-02	193.52	2400.42	4810.77
15.00	81.00	12.95	36.08	1.820	1.84E+00	4589.8	7.15E-02	178.38	2558.79	4593.31
15.00	90.00	12.05	39.83	1.955	2.02E+00	4361.0	7.71E-02	166.75	2665.09	4364.23
15.00	99.00	11.09	43.45	2.125	2.16E+00	3950.7	8.23E-02	150.61	2607.66	3953.61
15.00	108.00	10.06	46.90	2.343	2.33E+00	3512.7	9.13E-02	137.43	2470.84	3515.38
15.00	117.00	8.97	50.10	2.628	2.57E+00	3079.4	1.06E-01	126.40	2281.21	3081.98
15.00	126.00	7.83	52.93	3.010	2.91E+00	2650.8	1.29E-01	117.43	2044.18	2653.41
15.00	135.00	6.65	55.17	3.543	3.38E+00	2227.0	1.68E-01	110.36	1765.04	2229.71
15.00	144.00	5.45	56.43	4.326	4.09E+00	1807.9	2.38E-01	104.97	1448.34	1810.93
15.00	153.00	4.24	55.84	5.561	5.21E+00	1393.5	3.77E-01	100.66	1096.60	1397.16
15.00	162.00	3.06	51.25	7.695	7.05E+00	983.9	6.81E-01	94.96	707.90	988.48
15.00	171.00	2.03	36.50	11.579	9.39E+00	579.0	##########	75.49	283.78	583.93
15.00	180.00	1.54	0.00	15.268	5.05E+00	178.9	4.91E-01	17.39	-17.39	179.73
20.00	0.00	19.55	0.00	1.205	1.12E+00	6367.9	6.68E-02	379.74	-379.74	6379.25
20.00	9.00	19.49	4.74	1.209	1.12E+00	6348.4	6.66E-02	376.36	149.42	6359.59
20.00	18.00	19.31	9.48	1.220	1.14E+00	6299.1	6.61E-02	366.82	675.79	6309.73
20.00	27.00	19.01	14.23	1.240	1.16E+00	6219.8	6.54E-02	351.65	1187.97	6229.69
20.00	36.00	18.59	18.99	1.267	1.19E+00	6110.6	6.45E-02	331.70	1674.43	6119.56
20.00	45.00	18.06	23.76	1.304	1.23E+00	5971.5	6.33E-02	307.60	2124.23	5979.37
20.00	54.00	17.42	28.55	1.352	1.28E+00	5802.4	6.20E-02	280.25	2526.74	5809.21
20.00	63.00	16.68	33.36	1.413	1.35E+00	5603.5	6.09E-02	251.97	2871.00	5609.20
20.00	72.00	15.83	38.21	1.489	1.44E+00	5374.7	6.02E-02	224.31	3147.95	5379.40
20.00	81.00	14.88	43.09	1.584	1.55E+00	5116.0	6.03E-02	198.74	3350.02	5119.86
20.00	90.00	13.84	48.03	1.702	1.69E+00	4827.4	6.16E-02	175.56	3472.02	4830.57
20.00	99.00	12.72	53.05	1.853	1.86E+00	4467.2	6.49E-02	156.19	3476.25	4469.96
20.00	108.00	11.52	58.17	2.045	2.01E+00	3972.0	6.94E-02	137.02	3302.56	3974.36
20.00	117.00	10.25	63.44	2.299	2.22E+00	3476.8	7.77E-02	121.55	3055.65	3478.89
20.00	126.00	8.92	68.94	2.641	2.52E+00	2981.5	9.24E-02	109.44	2743.07	2983.55
20.00	135.00	7.54	74.79	3.125	2.94E+00	2486.3	1.18E-01	100.21	2372.98	2488.33
20.00	144.00	6.12	81.27	3.851	3.57E+00	1991.1	1.67E-01	93.25	1953.84	1993.26
20.00	153.00	4.67	88.95	5.044	4.60E+00	1495.8	2.69E-01	87.50	1494.00	1498.40
20.00	162.00	3.22	80.49	7.312	6.47E+00	1000.6	5.42E-01	83.75	973.03	1004.11
20.00	171.00	1.84	60.53	12.771	9.97E+00	505.4	##########	67.92	406.59	509.93
20.00	180.00	1.03	0.00	22.902	6.45E-01	10.2	5.42E-01	8.54	-8.54	13.27

3476.25

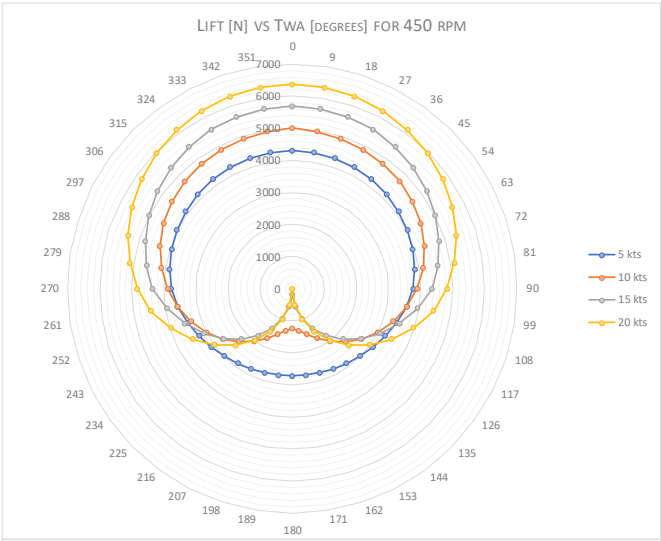

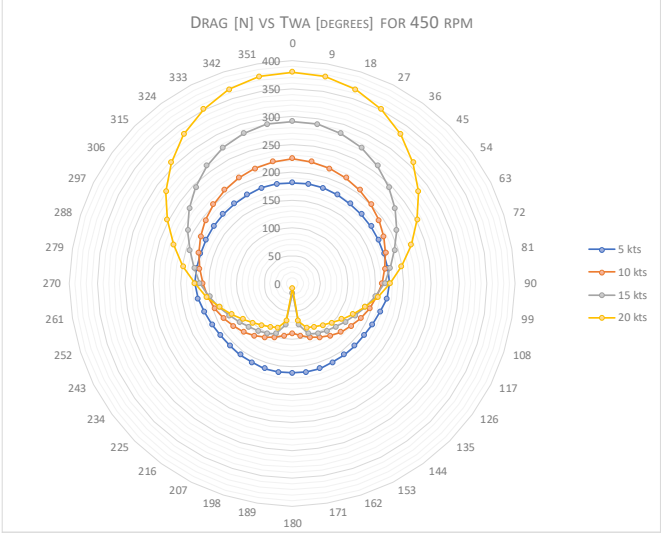

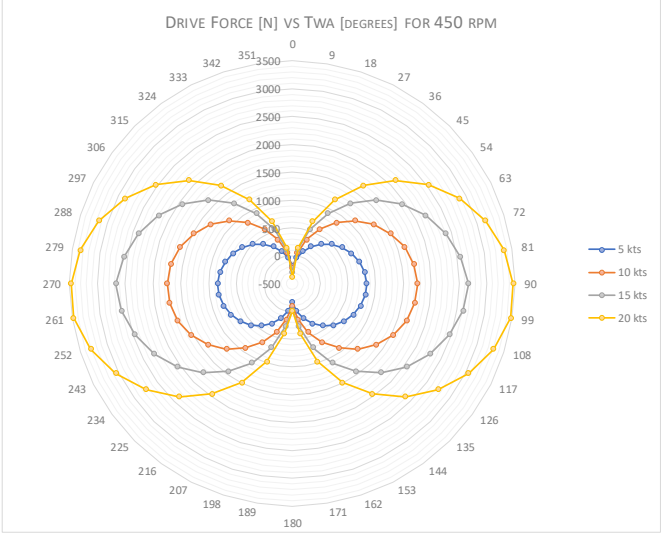

Appendix 13 AIRFOIL – GRID CONVERGENCE INDEX RESULTS

Item	Value	Unit
Cylinder Depth	1.00	m
Cylinder Diameter	1.00	m
Surface Area	3.142	m^2
Air Density (@25°C)	1.185	kg/m^3
Freestream Velocity	19.55	m/s
FoS	1.25	

AoA = 0°

Grid	Grid Size	Lift [N]	Drag [N]	CL	CD	Edge Cells	Cell Size	Refinement Factor		Variable Difference		
1	486280	0.02	0.458	2.74E-05	6.44E-04	697.34	1.43E-03	R2.1	1.191	E2.2	8.90E-06	1.42E-05
2	342780	0.03	0.468	3.63E-05	6.58E-04	585.47	1.71E-03	R3.2	1.152	E3.3	2.85E-05	7.87E-06
3	258424	0.01	0.47	7.80E-06	6.66E-04	508.35	1.97E-03					

	$P_{INITIAL}$	s	q	P_{ACTUAL}	R^2
CL	1	1	0.231	7.977	
	8.932	1	0.398	8.932	0.00
CD	1	1	0.231	2.054	
	2.829	0	0.095	2.829	0.00

	CL	CD
Extrapolated Value (Fine Mesh)	2.74E-05	6.44E-04
Approximate Realtive Error	71.54%	3.43%
GCI	18.76%	2.61%

Update

Item	Value	Unit
Cylinder Depth	1.00	m
Cylinder Diameter	1.00	m
Surface Area	3.142	m^2
Air Density (@25°C)	1.185	kg/m^3
Freestream Velocity	19.55	m/s
FoS	1.25	

AoA = 10°

Grid	Grid Size	Lift [N]	Drag [N]	CL	CD	Edge Cells	Cell Size	Refinement Factor		Variable Difference		
1	487046	29.54	0.984	4.15E-02	1.38E-03	697.89	1.43E-03	R2.1	1.196	E2.2	4.64E-04	5.15E-05
2	340426	29.21	1.021	4.11E-02	1.44E-03	583.46	1.71E-03	R3.2	1.153	E3.3	9.84E-05	4.22E-06
3	256022	29.28	1.024	4.12E-02	1.44E-03	505.99	1.98E-03					

	$P_{INITIAL}$	s	q	P_{ACTUAL}	R^2
CL	1	1	0.248	7.276	
	6.726	1	0.346	6.726	0.00
CD	1	1	0.248	12.586	
	11.761	0	0.395	11.761	0.00

	CL	CD
Extrapolated Value (Fine Mesh)	4.15E-02	1.38E-03
Approximate Realtive Error	0.88%	4.02%
GCI	0.33%	1.51%

Update

Item	Value	Unit
Cylinder Depth	1.00	m
Cylinder Diameter	1.00	m
Surface Area	3.142	m^2
Air Density (@25°C)	1.185	kg/m^3
Freestream Velocity	19.55	m/s
FoS	1.25	

AoA = 20°

Grid	Grid Size	Lift [N]	Drag [N]	CL	CD	Edge Cells	Cell Size	Refinement Factor		Variable Difference		
1	444986	30.48	5.202	4.29E-02	7.32E-03	667.07	1.50E-03	R2.1	1.188	E2.2	3.42E-04	5.60E-06
2	315284	30.24	5.206	4.25E-02	7.32E-03	561.50	1.78E-03	R3.2	1.158	E3.3	3.33E-04	7.06E-06
3	235302	30.00	5.211	4.22E-02	7.33E-03	485.08	2.06E-03					

	$P_{INITIAL}$	s	q	P_{ACTUAL}	R^2
CL	1	1	0.177	0.880	
	3.179	1	0.271	1.428	-1.75
CD	1	1	0.177	2.375	
	19.708	0	0.662	5.193	-14.51

	CL	CD
Extrapolated Value (Fine Mesh)	4.29E-02	7.32E-03
Approximate Realtive Error	1.57%	0.17%
GCI	1.14%	0.13%

Appendix 14 NACA0012H Re. STUDY RESULTS

C_L						
AoA	Re.					
[degrees]	6.4E+04	3.1E+05	5.5E+05	8.0E+05	1.0E+06	1.3E+06
0	0.00E+00	0.00E+00	0.00E+00	0.00E+00	0.00E+00	0.00E+00
2	3.27E-01	2.54E-01	1.98E-01	2.05E-01	2.11E-01	2.13E-01
4	4.51E-01	4.54E-01	3.97E-01	4.44E-01	4.08E-01	4.08E-01
6	6.99E-01	7.13E-01	7.26E-01	7.31E-01	7.27E-01	6.83E-01
8	8.64E-01	8.84E-01	9.05E-01	9.28E-01	9.43E-01	9.19E-01
10	9.74E-01	1.03E+00	1.08E+00	1.11E+00	1.12E+00	1.09E+00
12	1.15E+00	1.20E+00	1.25E+00	1.28E+00	1.30E+00	1.26E+00
14	1.36E+00	1.36E+00	1.37E+00	1.42E+00	1.46E+00	1.39E+00
16	1.72E+00	1.54E+00	1.41E+00	1.49E+00	1.54E+00	1.43E+00
18	1.99E+00	1.55E+00	1.24E+00	1.40E+00	1.51E+00	1.33E+00
20	2.09E+00	1.34E+00	1.33E-01	1.22E+00	1.21E+00	1.04E+00

C_D						
AoA	Re.					
[degrees]	6.4E+04	3.1E+05	5.5E+05	8.0E+05	1.0E+06	1.3E+06
0	1.54E-02	1.06E-02	6.91E-03	7.05E-03	6.63E-03	3.59E-03
2	1.46E-02	1.12E-02	8.46E-03	7.80E-03	6.71E-03	3.64E-03
4	1.85E-02	1.39E-02	1.01E-02	9.07E-03	7.63E-03	4.18E-03
6	2.33E-02	1.70E-02	1.18E-02	1.07E-02	9.13E-03	5.09E-03
8	3.08E-02	2.14E-02	1.38E-02	1.26E-02	1.08E-02	6.23E-03
10	4.66E-02	3.01E-02	1.69E-02	1.52E-02	1.30E-02	7.95E-03
12	7.59E-02	4.55E-02	2.12E-02	1.90E-02	1.62E-02	1.07E-02
14	9.31E-02	5.66E-02	2.74E-02	2.41E-02	2.04E-02	1.48E-02
16	1.18E-01	7.56E-02	4.13E-02	3.45E-02	2.83E-02	2.48E-02
18	1.55E-01	9.65E-02	5.35E-02	4.54E-02	3.60E-02	3.46E-02
20	1.64E-01	9.88E-02	6.35E-02	4.81E-02	4.16E-02	4.23E-02

Appendix 15 EPPLER 473 Re. STUDY RESULTS

C_L						
AoA	Re.					
[degrees]	6.4E+04	3.1E+05	5.5E+05	8.0E+05	1.0E+06	1.3E+06
0	0.00E+00	0.00E+00	0.00E+00	0.00E+00	0.00E+00	0.00E+00
2	2.16E-01	2.26E-01	2.32E-01	2.23E-01	2.24E-01	2.65E-01
4	5.87E-01	5.07E-01	4.45E-01	4.48E-01	4.57E-01	4.99E-01
6	7.50E-01	7.72E-01	7.90E-01	7.94E-01	8.00E-01	8.19E-01
8	8.96E-01	9.53E-01	1.01E+00	1.05E+00	1.08E+00	1.11E+00
10	1.04E+00	1.11E+00	1.18E+00	1.22E+00	1.25E+00	1.28E+00
12	1.47E+00	1.38E+00	1.32E+00	1.36E+00	1.39E+00	1.41E+00
14	1.88E+00	1.59E+00	1.38E+00	1.42E+00	1.45E+00	1.47E+00
16	2.36E+00	1.78E+00	1.35E+00	1.39E+00	1.43E+00	1.45E+00
18	3.05E+00	1.99E+00	1.17E+00	1.19E+00	1.21E+00	1.23E+00
20	3.47E+00	2.13E+00	1.08E+00	1.07E+00	1.07E+00	1.09E+00

C_D						
AoA	Re.					
[degrees]	6.4E+04	3.1E+05	5.5E+05	8.0E+05	1.0E+06	1.3E+06
0	1.64E-02	1.06E-02	3.55E-03	6.09E-03	1.78E-03	3.48E-03
2	1.88E-02	1.21E-02	3.86E-03	6.79E-03	1.75E-03	3.88E-03
4	2.77E-02	1.73E-02	4.76E-03	1.06E-02	1.92E-03	6.05E-03
6	3.78E-02	2.38E-02	6.41E-03	1.33E-02	3.29E-03	7.60E-03
8	5.16E-02	3.14E-02	7.61E-03	1.77E-02	5.36E-03	1.01E-02
10	7.71E-02	4.67E-02	9.51E-03	2.51E-02	8.98E-03	1.51E-02
12	1.07E-01	6.46E-02	1.25E-02	3.19E-02	1.51E-02	1.89E-02
14	1.25E-01	7.78E-02	1.78E-02	4.72E-02	2.72E-02	2.45E-02
16	1.51E-01	1.06E-01	3.90E-02	5.81E-02	3.93E-02	3.76E-02
18	1.89E-01	1.34E-01	8.70E-02	7.02E-02	6.60E-02	4.68E-02
20	2.15E-01	1.46E-01	1.27E-01	7.69E-02	8.82E-02	5.69E-02

Appendix 16
NACA0012H Polar plot

Item	Value	Unit
Boat Speed	18.00	knots
	9.252	m/s
Air Density (@25°C)	1.185	kg/m^3
Air Vicosity (@25°C)	1.84E-05	kg/m.s
Airfoil C.Length	1.78	m
Wing Height	8.90	m
Surface Area	63.74	m^2
Aspect Ratio	5.00	

TWS [kts]	Ship Angle [degrees]	AWS [m/s]	AWA [degrees]	AoA [degrees]	$C_{L\cdot 2D}$	$C_{D\cdot 2D}$	C_{di}	C_D	C_L / C_D	Lift [N]	Drag [N]	Drive [N]	$C_{D\cdot @0°}$	Drag - 0° [N]	Drive [N]
5.00	0.00	11.83	0.00	0.00	0.901	0.0131	0.0041	0.0171	52.669	4762.2	90.4	-90.4	0.0056	29.7	-29.69
5.00	9.00	11.81	1.12	8.00	0.901	0.0131	0.0041	0.0171	68.985	4741.9	90.1	2.8	0.0056	29.6	2.81
5.00	18.00	11.73	2.23	8.00	0.901	0.0131	0.0041	0.0171	68.847	4681.3	89.1	92.8	0.0056	29.2	92.85
5.00	27.00	11.61	3.29	8.00	0.901	0.0131	0.0040	0.0172	68.621	4582.1	87.4	176.0	0.0056	28.7	176.00
5.00	36.00	11.44	4.31	8.00	0.900	0.0132	0.0040	0.0172	68.310	4446.7	85.1	249.0	0.0057	27.9	248.99
5.00	45.00	11.23	5.24	8.00	0.899	0.0132	0.0040	0.0173	67.920	4278.6	82.2	309.1	0.0057	27.0	309.12
5.00	54.00	10.97	6.09	6.00	0.729	0.0108	0.0027	0.0134	67.622	3310.9	61.0	290.4	0.0057	25.9	290.43
5.00	63.00	10.68	6.82	6.00	0.729	0.0108	0.0027	0.0135	67.162	3134.7	58.1	314.5	0.0057	24.6	314.46
5.00	72.00	10.35	7.42	6.00	0.728	0.0109	0.0026	0.0136	66.655	2943.8	54.9	325.5	0.0058	23.3	325.51
5.00	81.00	9.99	7.86	6.00	0.728	0.0110	0.0026	0.0137	66.113	2743.0	51.5	324.1	0.0058	21.8	324.12
5.00	90.00	9.61	8.13	6.00	0.728	0.0111	0.0026	0.0137	65.544	2537.2	47.9	311.4	0.0058	20.4	311.45
5.00	99.00	9.21	8.21	6.00	0.727	0.0112	0.0026	0.0139	64.753	2329.2	44.4	288.8	0.0059	18.9	288.82
5.00	108.00	8.81	8.09	6.00	0.725	0.0114	0.0026	0.0140	63.883	2125.9	41.0	258.7	0.0060	17.5	258.66
5.00	117.00	8.41	7.75	6.00	0.724	0.0115	0.0026	0.0141	63.038	1933.2	37.7	223.5	0.0060	16.1	223.48
5.00	126.00	8.02	7.19	6.00	0.723	0.0116	0.0026	0.0142	62.239	1755.9	34.5	185.6	0.0061	14.9	185.57
5.00	135.00	7.66	6.41	6.00	0.721	0.0118	0.0026	0.0144	61.309	1597.6	31.8	146.8	0.0062	13.8	146.82
5.00	144.00	7.34	5.42	6.00	0.720	0.0119	0.0026	0.0145	60.487	1462.7	29.4	109.0	0.0063	12.8	108.98
5.00	153.00	7.06	4.25	6.00	0.719	0.0120	0.0026	0.0146	59.813	1354.5	27.5	73.0	0.0064	12.0	72.98
5.00	162.00	6.86	2.93	6.00	0.718	0.0121	0.0026	0.0147	59.311	1275.4	26.1	39.0	0.0065	11.5	39.04
5.00	171.00	6.73	1.49	6.00	0.718	0.0122	0.0026	0.0147	59.001	1227.2	25.2	6.7	0.0065	11.1	6.74
5.00	180.00	6.69	0.00	0.00	0.717	0.0122	0.0026	0.0147	58.896	1211.0	24.9	-24.9	0.0065	11.0	-10.98
10.00	0.00	14.40	0.00	0.00	0.908	0.0124	0.0041	0.0165	73.023	7109.9	129.6	-129.6	0.0055	42.8	-42.77
10.00	9.00	14.36	2.00	8.00	0.908	0.0124	0.0041	0.0166	72.950	7068.8	128.9	117.4	0.0055	42.5	117.44
10.00	18.00	14.24	3.97	8.00	0.907	0.0125	0.0041	0.0166	72.731	6946.6	127.0	354.5	0.0055	41.9	354.51
10.00	27.00	14.04	5.90	8.00	0.907	0.0125	0.0041	0.0166	72.372	6746.3	123.8	570.8	0.0055	40.8	570.82
10.00	36.00	13.76	7.77	8.00	0.906	0.0126	0.0041	0.0167	71.973	6474.2	119.3	757.0	0.0055	39.2	757.03
10.00	45.00	13.40	9.54	8.00	0.905	0.0127	0.0041	0.0168	71.489	6136.6	113.6	905.3	0.0055	37.4	905.32
10.00	54.00	12.97	11.20	8.00	0.904	0.0128	0.0041	0.0168	70.913	5742.0	106.9	1010.1	0.0055	35.1	1010.11
10.00	63.00	12.47	12.70	8.00	0.903	0.0129	0.0041	0.0169	70.233	5300.0	99.4	1068.4	0.0056	32.6	1068.39
10.00	72.00	11.90	14.02	8.00	0.901	0.0130	0.0041	0.0171	69.161	4819.6	91.4	1079.1	0.0056	30.0	1079.11
10.00	81.00	11.27	15.12	8.00	0.899	0.0132	0.0040	0.0173	68.006	4315.6	82.8	1045.7	0.0057	27.2	1045.65
10.00	90.00	10.59	15.95	6.00	0.729	0.0109	0.0027	0.0135	67.032	3085.5	57.3	792.8	0.0057	24.3	792.78
10.00	99.00	9.86	16.46	6.00	0.728	0.0110	0.0026	0.0137	65.923	2673.7	50.3	709.4	0.0058	21.3	709.41
10.00	108.00	9.10	16.60	6.00	0.726	0.0113	0.0026	0.0139	64.498	2269.3	43.4	606.7	0.0059	18.5	606.71
10.00	117.00	8.30	16.31	6.00	0.724	0.0115	0.0026	0.0141	62.817	1883.7	36.8	493.7	0.0061	15.8	493.66
10.00	126.00	7.50	15.53	6.00	0.721	0.0118	0.0026	0.0144	60.893	1529.0	30.6	379.9	0.0063	13.3	379.87
10.00	135.00	6.70	14.21	6.00	0.717	0.0122	0.0026	0.0147	58.917	1214.3	25.0	273.9	0.0065	11.0	273.91
10.00	144.00	5.93	12.32	6.00	0.714	0.0126	0.0025	0.0151	56.637	946.6	20.1	182.4	0.0069	9.1	182.44
10.00	153.00	5.23	9.87	6.00	0.710	0.0130	0.0025	0.0155	54.552	732.7	16.0	109.9	0.0073	7.5	109.85
10.00	162.00	4.65	6.91	6.00	0.707	0.0135	0.0025	0.0160	52.413	576.6	13.0	56.5	0.0078	6.4	56.48
10.00	171.00	4.26	3.56	6.00	0.705	0.0139	0.0025	0.0163	50.839	481.8	11.2	18.8	0.0083	5.7	18.80
10.00	180.00	4.12	0.00	0.00	0.704	0.0140	0.0025	0.0165	50.297	450.1	10.5	-10.5	0.0085	5.4	-5.44
15.00	0.00	16.98	0.00	0.00	0.915	0.0118	0.0042	0.0160	77.218	9949.7	174.3	-174.3	0.0054	58.4	-58.42
15.00	9.00	16.92	2.70	8.00	0.915	0.0119	0.0042	0.0160	77.139	9887.6	173.3	292.2	0.0054	58.1	292.16
15.00	18.00	16.77	5.38	8.00	0.914	0.0119	0.0042	0.0161	76.905	9702.8	170.5	739.3	0.0054	57.1	739.32
15.00	27.00	16.51	8.02	8.00	0.913	0.0119	0.0042	0.0161	76.520	9400.1	165.7	1146.7	0.0054	55.4	1146.72
15.00	36.00	16.15	10.60	8.00	0.913	0.0120	0.0042	0.0162	75.989	8987.4	159.2	1496.2	0.0054	53.1	1496.21
15.00	45.00	15.69	13.09	8.00	0.911	0.0121	0.0041	0.0162	75.322	8475.3	151.1	1773.0	0.0054	50.3	1772.97
15.00	54.00	15.14	15.48	8.00	0.910	0.0122	0.0041	0.0164	74.370	7875.5	141.7	1965.8	0.0054	47.0	1965.84
15.00	63.00	14.50	17.73	8.00	0.908	0.0124	0.0041	0.0165	73.190	7204.1	131.1	2069.1	0.0055	43.3	2069.05
15.00	72.00	13.76	19.80	8.00	0.906	0.0126	0.0041	0.0167	71.981	6480.0	119.3	2082.6	0.0055	39.3	2082.59
15.00	81.00	12.95	21.64	8.00	0.904	0.0128	0.0041	0.0168	70.884	5722.4	106.6	2011.4	0.0055	35.0	2011.43
15.00	90.00	12.05	23.20	8.00	0.902	0.0130	0.0041	0.0170	69.445	4946.1	93.5	1862.8	0.0056	30.7	1862.79
15.00	99.00	11.09	24.41	6.00	0.728	0.0107	0.0026	0.0134	67.735	3378.2	62.2	1339.5	0.0057	26.4	1339.45
15.00	108.00	10.06	25.17	6.00	0.728	0.0110	0.0026	0.0136	66.212	2779.3	52.1	1135.0	0.0058	22.1	1134.95
15.00	117.00	8.97	25.37	6.00	0.726	0.0113	0.0026	0.0139	64.217	2203.3	42.3	905.9	0.0059	18.0	905.88
15.00	126.00	7.83	24.87	6.00	0.722	0.0117	0.0026	0.0143	61.745	1670.3	33.1	672.5	0.0062	14.3	672.55
15.00	135.00	6.65	23.51	6.00	0.717	0.0122	0.0026	0.0148	58.809	1197.6	24.7	455.1	0.0065	10.9	455.07
15.00	144.00	5.45	21.09	6.00	0.712	0.0129	0.0025	0.0154	55.194	797.0	17.3	270.7	0.0071	8.0	270.72
15.00	153.00	4.24	17.48	6.00	0.705	0.0139	0.0025	0.0164	50.769	477.7	11.1	132.9	0.0084	5.7	132.90
15.00	162.00	3.06	12.61	6.00	0.697	0.0155	0.0024	0.0179	44.931	246.6	6.3	47.6	0.0109	3.8	47.63
15.00	171.00	2.03	6.63	4.00	0.535	0.0136	0.0014	0.0151	39.230	83.7	2.4	7.3	0.0146	2.3	7.33
15.00	180.00	1.54	0.00	0.00	0.687	0.0240	0.0024	0.0264	28.656	61.8	2.4	-2.4	0.0177	1.6	-1.59
20.00	0.00	19.55	0.00	0.00	0.920	0.0115	0.0042	0.0157	80.169	13265.4	226.4	-226.4	0.0053	76.4	-76.38
20.00	9.00	19.49	3.27	8.00	0.920	0.0115	0.0042	0.0157	80.113	13182.5	225.1	527.4	0.0053	75.9	527.43
20.00	18.00	19.31	6.53	8.00	0.919	0.0115	0.0042	0.0157	79.945	12936.0	221.2	1250.8	0.0053	74.6	1250.82
20.00	27.00	19.01	9.76	8.00	0.919	0.0115	0.0042	0.0157	79.667	12532.2	214.8	1911.8	0.0053	72.5	1911.76
20.00	36.00	18.59	12.94	8.00	0.918	0.0116	0.0042	0.0158	79.283	11981.4	206.1	2481.8	0.0053	69.5	2481.76
20.00	45.00	18.06	16.06	8.00	0.917	0.0117	0.0042	0.0159	78.624	11295.1	195.4	2936.4	0.0053	65.8	2936.44
20.00	54.00	17.42	19.09	8.00	0.916	0.0118	0.0042	0.0160	77.794	10492.5	182.8	3259.1	0.0054	61.4	3259.12
20.00	63.00	16.68	22.02	8.00	0.914	0.0119	0.0042	0.0161	76.767	9593.6	168.8	3439.8	0.0054	56.5	3439.78
20.00	72.00	15.83	24.80	8.00	0.912	0.0121	0.0042	0.0162	75.512	8620.9	153.4	3476.3	0.0054	51.1	3476.25
20.00	81.00	14.88	27.39	8.00	0.909	0.0123	0.0041	0.0164	73.886	7598.6	137.3	3374.1	0.0054	45.5	3374.08
20.00	90.00	13.84	29.75	8.00	0.906	0.0126	0.0041	0.0167	72.087	6554.8	120.6	3148.0	0.0055	39.7	3147.95
20.00	99.00	12.72	31.80	8.00	0.904	0.0128	0.0041	0.0169	70.583	5519.6	103.1	2820.7	0.0055	33.9	2820.67
20.00	108.00	11.52	33.43	8.00	0.900	0.0132	0.0040	0.0172	68.455	4509.9	86.2	2412.8	0.0056	28.3	2412.80
20.00	117.00	10.25	34.52	6.00	0.728	0.0109	0.0026	0.0136	66.508	2889.0	53.9	1592.6	0.0058	22.9	1592.57
20.00	126.00	8.92	34.85	6.00	0.726	0.0113	0.0026	0.0139	64.120	2180.7	41.9	1211.8	0.0060	17.9	1211.76
20.00	135.00	7.54	34.15	6.00	0.721	0.0118	0.0026	0.0144	61.004	1547.3	30.9	842.9	0.0063	13.4	842.94
20.00	144.00	6.12	32.00	6.00	0.715	0.0125	0.0026	0.0150	57.234	1010.4	21.3	517.4	0.0068	9.6	517.41
20.00	153.00	4.67	27.87	6.00	0.707	0.0135	0.0025	0.0160	52.514	582.8	13.2	260.8	0.0078	6.4	260.79
20.00	162.00	3.22	21.15	6.00	0.698	0.0152	0.0024	0.0176	46.022	273.6	6.9	92.3	0.0103	4.0	92.32
20.00	171.00	1.84	11.60	6.00	0.688	0.0199	0.0024	0.0222	34.622	88.4	2.9	15.0	0.0157	2.0	14.98
20.00	180.00	1.03	0.00	0.00	0.686	0.0310	0.0024	0.0334	22.139	27.4	1.3	-1.3	0.0210	0.8	-0.84

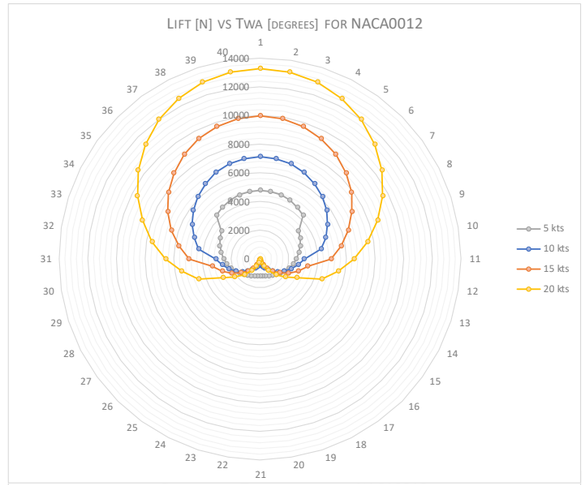

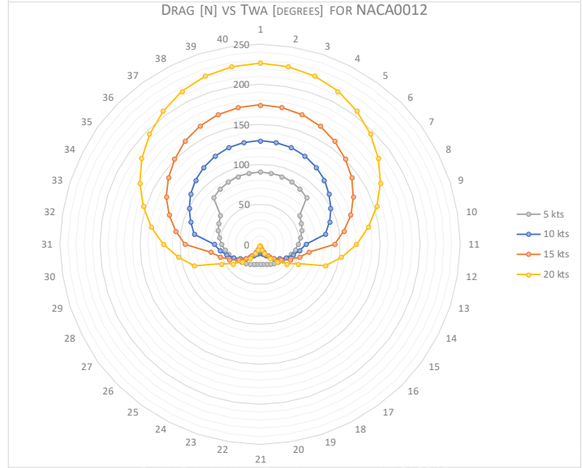

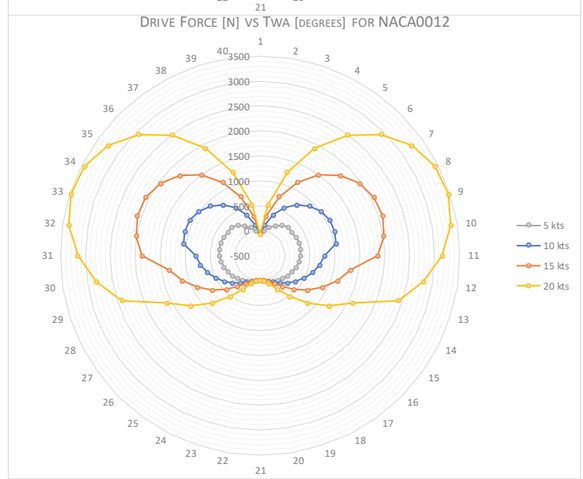

Appendix 17
EPPLER 473 POLAR PLOT

Item	Value	Unit
Boat Speed	18.00	knots
	9.252	m/s
Air Density (@25°C)	1.185	kg/m^3
Air Vicosity (@25°C)	1.84E-05	kg/m.s
Airfoil C.Length	1.73	m
Wing Height	8.66	m
Surface Area	60.31	m^2
Aspect Ratio	5.00	

TWS [kts]	Ship Angle [degrees]	AWS [m/s]	AWA [degrees]	AoA [degrees]	$C_{L\text{-}2D}$	$C_{D\text{-}2D}$	C_{di}	C_D	C_L / C_D	Lift [N]	Drag [N]	Drive [N]	$C_{D\text{-}@0°}$	Drag - 0° [N]	Drive [N]
5.00	0.00	11.83	0.00	0.00	0.997	0.0119	0.0052	0.0171	58.314	4984.5	85.5	-85.5	0.0097	48.6	-48.63
5.00	9.00	11.81	1.12	8.00	0.997	0.0119	0.0052	0.0171	58.308	4964.4	85.1	12.1	0.0097	48.5	12.10
5.00	18.00	11.73	2.23	8.00	0.998	0.0119	0.0053	0.0171	58.288	4904.5	84.1	106.4	0.0097	47.9	106.43
5.00	27.00	11.61	3.29	8.00	0.998	0.0119	0.0053	0.0171	58.256	4806.4	82.5	193.8	0.0098	47.1	193.75
5.00	36.00	11.44	4.31	8.00	0.999	0.0119	0.0053	0.0172	58.211	4672.1	80.3	270.7	0.0098	45.9	270.71
5.00	45.00	11.23	5.24	8.00	1.001	0.0119	0.0053	0.0172	58.154	4505.0	77.5	334.5	0.0099	44.4	334.53
5.00	54.00	10.97	6.09	8.00	1.002	0.0120	0.0053	0.0173	58.073	4307.5	74.2	383.0	0.0099	42.7	383.02
5.00	63.00	10.68	6.82	8.00	1.001	0.0120	0.0053	0.0173	57.858	4075.1	70.4	413.8	0.0100	40.7	413.84
5.00	72.00	10.35	7.42	8.00	1.000	0.0121	0.0053	0.0174	57.620	3823.7	66.4	427.7	0.0101	38.6	427.68
5.00	81.00	9.99	7.86	8.00	0.999	0.0121	0.0053	0.0174	57.362	3559.6	62.1	425.3	0.0102	36.3	425.29
5.00	90.00	9.61	8.13	8.00	0.997	0.0122	0.0052	0.0175	57.090	3289.3	57.6	408.2	0.0103	33.9	408.24
5.00	99.00	9.21	8.21	8.00	0.995	0.0123	0.0052	0.0176	56.667	3018.1	53.3	378.5	0.0104	31.6	378.50
5.00	108.00	8.81	8.09	8.00	0.993	0.0125	0.0052	0.0177	56.187	2753.8	49.0	339.1	0.0105	29.2	339.09
5.00	117.00	8.41	7.75	8.00	0.991	0.0126	0.0052	0.0178	55.715	2503.4	44.9	293.2	0.0107	26.9	293.20
5.00	126.00	8.02	7.19	8.00	0.989	0.0127	0.0052	0.0179	55.265	2273.1	41.1	243.8	0.0108	24.8	243.80
5.00	135.00	7.66	6.41	8.00	0.986	0.0129	0.0051	0.0181	54.640	2067.0	37.8	193.3	0.0109	22.9	193.27
5.00	144.00	7.34	5.42	8.00	0.984	0.0131	0.0051	0.0182	54.079	1891.5	35.0	144.0	0.0111	21.3	144.00
5.00	153.00	7.06	4.25	8.00	0.982	0.0132	0.0051	0.0183	53.616	1750.7	32.7	97.2	0.0112	20.0	97.22
5.00	162.00	6.86	2.93	8.00	0.981	0.0133	0.0051	0.0184	53.269	1647.9	30.9	53.2	0.0113	19.0	53.20
5.00	171.00	6.73	1.49	8.00	0.980	0.0134	0.0051	0.0185	53.054	1585.3	29.9	11.4	0.0114	18.4	11.37
5.00	180.00	6.69	0.00	0.00	0.979	0.0134	0.0051	0.0185	52.981	1564.3	29.5	-29.5	0.0114	18.2	-18.19
10.00	0.00	14.40	0.00	0.00	0.975	0.0116	0.0050	0.0166	58.820	7222.2	122.8	-122.8	0.0093	68.8	-68.85
10.00	9.00	14.36	2.00	8.00	0.975	0.0116	0.0050	0.0166	58.824	7184.1	122.1	128.3	0.0093	68.5	128.26
10.00	18.00	14.24	3.97	8.00	0.976	0.0116	0.0050	0.0166	58.835	7070.5	120.2	369.9	0.0093	67.4	369.89
10.00	27.00	14.04	5.90	8.00	0.978	0.0116	0.0050	0.0166	58.855	6883.9	117.0	591.7	0.0093	65.7	591.74
10.00	36.00	13.76	7.77	8.00	0.981	0.0116	0.0051	0.0167	58.799	6629.1	112.7	784.4	0.0094	63.4	784.42
10.00	45.00	13.40	9.54	8.00	0.984	0.0117	0.0051	0.0168	58.711	6311.1	107.5	940.2	0.0094	60.5	940.25
10.00	54.00	12.97	11.20	8.00	0.988	0.0117	0.0052	0.0169	58.607	5936.5	101.3	1053.4	0.0095	57.1	1053.38
10.00	63.00	12.47	12.70	8.00	0.993	0.0118	0.0052	0.0170	58.485	5512.7	94.3	1120.1	0.0096	53.2	1120.14
10.00	72.00	11.90	14.02	8.00	0.996	0.0118	0.0052	0.0171	58.333	5041.1	86.4	1137.6	0.0097	49.1	1137.59
10.00	81.00	11.27	15.12	8.00	1.000	0.0119	0.0053	0.0172	58.167	4541.8	78.1	1109.2	0.0099	44.7	1109.25
10.00	90.00	10.59	15.95	8.00	1.001	0.0120	0.0053	0.0173	57.797	4010.3	69.4	1035.2	0.0100	40.2	1035.23
10.00	99.00	9.86	16.46	8.00	0.998	0.0122	0.0053	0.0174	57.272	3468.6	60.6	924.8	0.0102	35.5	924.76
10.00	108.00	9.10	16.60	8.00	0.995	0.0124	0.0052	0.0176	56.527	2940.2	52.0	790.1	0.0104	30.9	790.13
10.00	117.00	8.30	16.31	8.00	0.990	0.0126	0.0052	0.0178	55.591	2439.1	43.9	642.8	0.0107	26.3	642.83
10.00	126.00	7.50	15.53	8.00	0.985	0.0130	0.0051	0.0181	54.357	1977.7	36.4	494.4	0.0110	22.1	494.44
10.00	135.00	6.70	14.21	8.00	0.979	0.0134	0.0051	0.0185	52.996	1568.5	29.6	356.4	0.0114	18.2	356.37
10.00	144.00	5.93	12.32	10.00	1.126	0.0162	0.0067	0.0229	49.217	1413.4	28.7	273.6	0.0118	14.9	273.64
10.00	153.00	5.23	9.87	10.00	1.120	0.0167	0.0066	0.0234	47.940	1092.8	22.8	164.9	0.0123	12.0	164.94
10.00	162.00	4.65	6.91	10.00	1.113	0.0175	0.0065	0.0241	46.268	858.4	18.6	84.9	0.0128	9.9	84.93
10.00	171.00	4.26	3.56	10.00	1.107	0.0182	0.0065	0.0246	44.921	716.0	15.9	28.6	0.0132	8.6	28.60
10.00	180.00	4.12	0.00	0.00	1.105	0.0184	0.0064	0.0249	44.455	668.4	15.0	-15.0	0.0134	8.1	-8.08
15.00	0.00	16.98	0.00	0.00	0.953	0.0115	0.0048	0.0163	58.335	9803.8	168.1	-168.1	0.0089	91.9	-91.85
15.00	9.00	16.92	2.70	8.00	0.953	0.0115	0.0048	0.0163	58.349	9748.3	167.1	291.9	0.0089	91.4	291.87
15.00	18.00	16.77	5.38	8.00	0.954	0.0115	0.0048	0.0163	58.389	9583.2	164.1	734.4	0.0090	90.0	734.42
15.00	27.00	16.51	8.02	8.00	0.956	0.0115	0.0048	0.0164	58.455	9311.6	159.3	1140.7	0.0090	87.6	1140.75
15.00	36.00	16.15	10.60	8.00	0.959	0.0115	0.0049	0.0164	58.547	8939.3	152.7	1493.8	0.0091	84.4	1493.79
15.00	45.00	15.69	13.09	8.00	0.963	0.0115	0.0049	0.0164	58.663	8473.8	144.4	1779.1	0.0091	80.3	1779.12
15.00	54.00	15.14	15.48	8.00	0.968	0.0115	0.0049	0.0165	58.748	7926.9	134.9	1986.1	0.0092	75.4	1986.07
15.00	63.00	14.50	17.73	8.00	0.974	0.0116	0.0050	0.0166	58.811	7309.5	124.3	2107.6	0.0093	69.7	2107.62
15.00	72.00	13.76	19.80	8.00	0.981	0.0116	0.0051	0.0167	58.800	6634.5	112.8	2141.1	0.0094	63.4	2141.08
15.00	81.00	12.95	21.64	8.00	0.988	0.0117	0.0052	0.0169	58.601	5917.8	101.0	2088.7	0.0095	56.9	2088.69
15.00	90.00	12.05	23.20	8.00	0.996	0.0118	0.0052	0.0171	58.374	5165.6	88.5	1953.9	0.0097	50.2	1953.89
15.00	99.00	11.09	24.41	8.00	1.002	0.0119	0.0053	0.0172	58.118	4397.7	75.7	1748.5	0.0099	43.5	1748.46
15.00	108.00	10.06	25.17	8.00	0.999	0.0121	0.0053	0.0174	57.409	3607.3	62.8	1477.4	0.0102	36.7	1477.38
15.00	117.00	8.97	25.37	8.00	0.994	0.0124	0.0052	0.0176	56.372	2854.4	50.6	1177.3	0.0105	30.1	1177.34
15.00	126.00	7.83	24.87	8.00	0.988	0.0128	0.0051	0.0180	54.936	2161.7	39.3	873.5	0.0109	23.8	873.52
15.00	135.00	6.65	23.51	8.00	0.979	0.0134	0.0051	0.0185	52.921	1546.9	29.2	590.2	0.0114	18.0	590.18
15.00	144.00	5.45	21.09	10.00	1.122	0.0166	0.0066	0.0232	48.337	1189.1	24.6	405.0	0.0122	12.9	405.01
15.00	153.00	4.24	17.48	10.00	1.107	0.0182	0.0065	0.0247	44.861	709.8	15.8	198.1	0.0132	8.5	198.10
15.00	162.00	3.06	12.61	10.00	1.086	0.0223	0.0062	0.0285	38.038	363.5	9.6	70.0	0.0149	5.0	70.01
15.00	171.00	2.03	6.63	12.00	1.149	0.0307	0.0070	0.0376	30.519	169.9	5.6	14.1	0.0172	2.5	14.10
15.00	180.00	1.54	0.00	0.00	0.518	0.0332	0.0014	0.0346	14.937	44.0	2.9	-2.9	0.0238	2.0	-2.02
20.00	0.00	19.55	0.00	0.00	0.933	0.0116	0.0046	0.0161	57.775	12730.6	220.3	-220.3	0.0086	117.7	-117.68
20.00	9.00	19.49	3.27	8.00	0.933	0.0115	0.0046	0.0161	57.801	12658.9	219.0	503.6	0.0086	117.0	503.62
20.00	18.00	19.31	6.53	8.00	0.935	0.0115	0.0046	0.0161	57.878	12445.3	215.0	1201.2	0.0086	115.1	1201.15
20.00	27.00	19.01	9.76	8.00	0.937	0.0115	0.0046	0.0162	58.005	12093.9	208.5	1843.7	0.0087	111.9	1843.70
20.00	36.00	18.59	12.94	8.00	0.940	0.0115	0.0047	0.0162	58.181	11611.7	199.6	2405.3	0.0087	107.6	2405.30
20.00	45.00	18.06	16.06	8.00	0.944	0.0115	0.0047	0.0162	58.253	11006.2	188.9	2862.7	0.0088	102.3	2862.71
20.00	54.00	17.42	19.09	8.00	0.949	0.0115	0.0048	0.0163	58.299	10291.3	176.5	3199.3	0.0089	96.1	3199.26
20.00	63.00	16.68	22.02	8.00	0.955	0.0115	0.0048	0.0163	58.413	9485.3	162.4	3405.1	0.0090	89.1	3405.10
20.00	72.00	15.83	24.80	8.00	0.962	0.0115	0.0049	0.0164	58.629	8606.5	146.8	3476.3	0.0091	81.5	3476.25
20.00	81.00	14.88	27.39	8.00	0.970	0.0115	0.0050	0.0165	58.774	7673.2	130.6	3414.4	0.0092	73.0	3414.42
20.00	90.00	13.84	29.75	8.00	0.980	0.0116	0.0051	0.0167	58.819	6704.8	114.0	3228.1	0.0094	64.1	3228.09
20.00	99.00	12.72	31.80	8.00	0.991	0.0117	0.0052	0.0169	58.546	5724.0	97.8	2932.9	0.0095	55.1	2932.90
20.00	108.00	11.52	33.43	8.00	0.999	0.0119	0.0053	0.0172	58.232	4734.8	81.3	2540.8	0.0098	46.4	2540.77
20.00	117.00	10.25	34.52	8.00	1.000	0.0121	0.0053	0.0174	57.550	3751.5	65.2	2072.1	0.0101	38.0	2072.08
20.00	126.00	8.92	34.85	8.00	0.994	0.0124	0.0052	0.0176	56.318	2825.1	50.2	1573.2	0.0105	29.9	1573.19
20.00	135.00	7.54	34.15	8.00	0.985	0.0130	0.0051	0.0181	54.433	2001.5	36.8	1093.1	0.0110	22.3	1093.07
20.00	144.00	6.12	32.00	8.00	0.975	0.0138	0.0050	0.0189	51.679	1303.4	25.2	669.3	0.0117	15.7	669.33
20.00	153.00	4.67	27.87	10.00	1.113	0.0175	0.0065	0.0240	46.354	867.7	18.7	389.0	0.0128	10.0	389.04
20.00	162.00	3.22	21.15	10.00	1.089	0.0213	0.0063	0.0275	39.568	404.0	10.2	136.3	0.0146	5.4	136.29
20.00	171.00	1.84	11.60	10.00	0.987	0.0386	0.0051	0.0438	22.553	120.0	5.3	18.9	0.0195	2.4	18.92
20.00	180.00	1.03	0.00	0.00	0.402	0.0315	0.0009	0.0323	12.432	15.2	1.2	-1.2	0.0311	1.2	-1.18

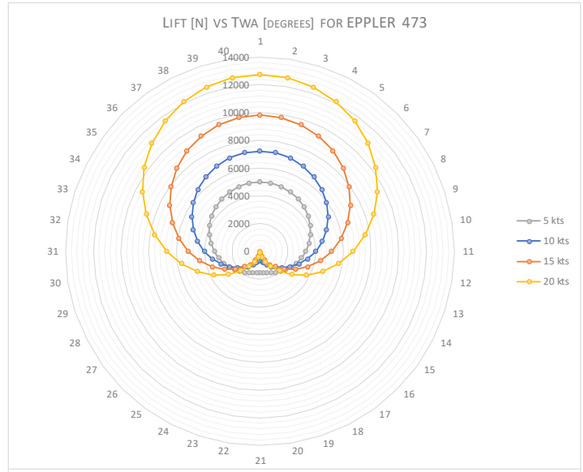

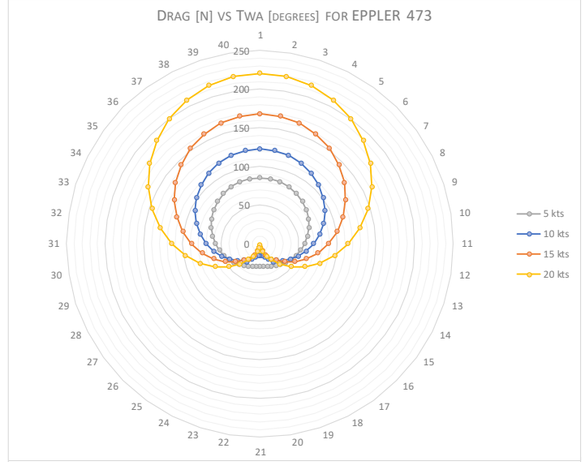

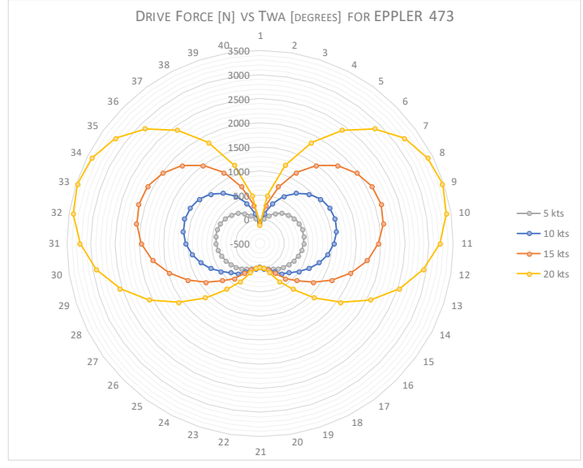

Appendix 18 VPP RESULTS – MAX SPEED

Item	Value	Unit
Boat Speed	18.00	knots
	9.252	m/s
Boat Resistance	196.28	kN

TWS [kts]	Ship Angle [degrees]	AWS [m/s]	AWA [degrees]	Drive [N] F.Rotor	Drive [N] NACA 0012	Drive [N] EPPLER 473	Best Section	F.Rotor Resistance [N]		NACA 0012 Resistance [N]		EPPLER 473 Resistance [N]	
5.00	0.00	11.83	0.00	-76.16	-29.69	-48.63	NACA 0012	197.04	0.39%	196.58	0.15%	196.77	0.25%
5.00	9.00	11.81	1.12	49.20	2.81	12.10	F.Rotor	195.79	-0.25%	196.25	-0.01%	196.16	-0.06%
5.00	18.00	11.73	2.23	172.61	92.85	106.43	F.Rotor	194.55	-0.88%	195.35	-0.47%	195.22	-0.54%
5.00	27.00	11.61	3.29	292.64	176.00	193.75	F.Rotor	193.35	-1.49%	194.52	-0.90%	194.34	-0.99%
5.00	36.00	11.44	4.31	406.80	248.99	270.71	F.Rotor	192.21	-2.07%	193.79	-1.27%	193.57	-1.38%
5.00	45.00	11.23	5.24	512.50	309.12	334.53	F.Rotor	191.16	-2.61%	193.19	-1.57%	192.94	-1.70%
5.00	54.00	10.97	6.09	606.71	290.43	383.02	F.Rotor	190.21	-3.09%	193.38	-1.48%	192.45	-1.95%
5.00	63.00	10.68	6.82	695.94	314.46	413.84	F.Rotor	189.32	-3.55%	193.14	-1.60%	192.14	-2.11%
5.00	72.00	10.35	7.42	766.97	325.51	427.68	F.Rotor	188.61	-3.91%	193.03	-1.66%	192.00	-2.18%
5.00	81.00	9.99	7.86	814.99	324.12	425.29	F.Rotor	188.13	-4.15%	193.04	-1.65%	192.03	-2.17%
5.00	90.00	9.61	8.13	840.23	311.45	408.24	F.Rotor	187.88	-4.28%	193.17	-1.59%	192.20	-2.08%
5.00	99.00	9.21	8.21	832.80	288.82	378.50	F.Rotor	187.95	-4.24%	193.39	-1.47%	192.50	-1.93%
5.00	108.00	8.81	8.09	791.82	258.66	339.09	F.Rotor	188.36	-4.03%	193.69	-1.32%	192.89	-1.73%
5.00	117.00	8.41	7.75	731.56	223.48	293.20	F.Rotor	188.97	-3.73%	194.05	-1.14%	193.35	-1.49%
5.00	126.00	8.02	7.19	652.53	185.57	243.80	F.Rotor	189.76	-3.32%	194.43	-0.95%	193.84	-1.24%
5.00	135.00	7.66	6.41	555.03	146.82	193.27	F.Rotor	190.73	-2.83%	194.81	-0.75%	194.35	-0.98%
5.00	144.00	7.34	5.42	449.05	108.98	144.00	F.Rotor	191.79	-2.29%	195.19	-0.56%	194.84	-0.73%
5.00	153.00	7.06	4.25	337.53	72.98	97.22	F.Rotor	192.91	-1.72%	195.55	-0.37%	195.31	-0.50%
5.00	162.00	6.86	2.93	221.09	39.04	53.20	F.Rotor	194.07	-1.13%	195.89	-0.20%	195.75	-0.27%
5.00	171.00	6.73	1.49	101.26	6.74	11.37	F.Rotor	195.27	-0.52%	196.21	-0.03%	196.17	-0.06%
5.00	180.00	6.69	0.00	-21.04	-10.98	-18.19	NACA 0012	196.49	0.11%	196.39	0.06%	196.46	0.09%
10.00	0.00	14.40	0.00	-137.28	-42.77	-68.85	NACA 0012	197.65	0.70%	196.71	0.22%	196.97	0.35%
10.00	9.00	14.36	2.00	102.55	117.44	128.26	EPPLER 473	195.26	-0.52%	195.11	-0.60%	195.00	-0.65%
10.00	18.00	14.24	3.97	340.80	354.51	369.89	EPPLER 473	192.87	-1.74%	192.74	-1.81%	192.58	-1.88%
10.00	27.00	14.04	5.90	599.28	570.82	591.74	F.Rotor	190.29	-3.05%	190.57	-2.91%	190.36	-3.01%
10.00	36.00	13.76	7.77	854.80	757.03	784.42	F.Rotor	187.73	-4.35%	188.71	-3.86%	188.44	-4.00%
10.00	45.00	13.40	9.54	1092.72	905.32	940.25	F.Rotor	185.35	-5.57%	187.23	-4.61%	186.88	-4.79%
10.00	54.00	12.97	11.20	1304.90	1010.11	1053.38	F.Rotor	183.23	-6.65%	186.18	-5.15%	185.75	-5.37%
10.00	63.00	12.47	12.70	1483.60	1068.39	1120.14	F.Rotor	181.45	-7.56%	185.60	-5.44%	185.08	-5.71%
10.00	72.00	11.90	14.02	1621.19	1079.11	1137.59	F.Rotor	180.07	-8.26%	185.49	-5.50%	184.91	-5.80%
10.00	81.00	11.27	15.12	1711.15	1045.65	1109.25	F.Rotor	179.17	-8.72%	185.82	-5.33%	185.19	-5.65%
10.00	90.00	10.59	15.95	1748.67	792.78	1035.23	F.Rotor	178.79	-8.91%	188.35	-4.04%	185.93	-5.27%
10.00	99.00	9.86	16.46	1732.25	709.41	924.76	F.Rotor	178.96	-8.83%	189.19	-3.61%	187.03	-4.71%
10.00	108.00	9.10	16.60	1661.73	606.71	790.13	F.Rotor	179.66	-8.47%	190.21	-3.09%	188.38	-4.03%
10.00	117.00	8.30	16.31	1540.07	493.66	642.83	F.Rotor	180.88	-7.85%	191.34	-2.52%	189.85	-3.28%
10.00	126.00	7.50	15.53	1372.70	379.87	494.44	F.Rotor	182.55	-6.99%	192.48	-1.94%	191.34	-2.52%
10.00	135.00	6.70	14.21	1167.23	273.91	356.37	F.Rotor	184.61	-5.95%	193.54	-1.40%	192.72	-1.82%
10.00	144.00	5.93	12.32	932.85	182.44	273.64	F.Rotor	186.95	-4.75%	194.46	-0.93%	193.54	-1.39%
10.00	153.00	5.23	9.87	679.54	109.85	164.94	F.Rotor	189.49	-3.46%	195.18	-0.56%	194.63	-0.84%
10.00	162.00	4.65	6.91	432.07	56.48	84.93	F.Rotor	191.96	-2.20%	195.72	-0.29%	195.43	-0.43%
10.00	171.00	4.26	3.56	210.18	18.80	28.60	F.Rotor	194.18	-1.07%	196.09	-0.10%	195.99	-0.15%
10.00	180.00	4.12	0.00	6.21	-5.44	-8.08	F.Rotor	196.22	-0.03%	196.34	0.03%	196.36	0.04%
15.00	0.00	16.98	0.00	-217.44	-58.42	-91.85	NACA 0012	198.46	1.11%	196.87	0.30%	197.20	0.47%
15.00	9.00	16.92	2.70	135.14	292.16	291.87	NACA 0012	194.93	-0.69%	193.36	-1.49%	193.36	-1.49%
15.00	18.00	16.77	5.38	520.09	739.32	734.42	NACA 0012	191.08	-2.65%	188.89	-3.77%	188.94	-3.74%
15.00	27.00	16.51	8.02	912.44	1146.72	1140.75	NACA 0012	187.16	-4.65%	184.81	-5.84%	184.87	-5.81%
15.00	36.00	16.15	10.60	1283.97	1496.21	1493.79	NACA 0012	183.44	-6.54%	181.32	-7.62%	181.34	-7.61%
15.00	45.00	15.69	13.09	1625.93	1772.97	1779.12	EPPLER 473	180.02	-8.28%	178.55	-9.03%	178.49	-9.06%
15.00	54.00	15.14	15.48	1931.40	1965.84	1986.07	EPPLER 473	176.97	-9.84%	176.62	-10.02%	176.42	-10.12%
15.00	63.00	14.50	17.73	2190.32	2069.05	2107.62	F.Rotor	174.38	-11.16%	175.59	-10.54%	175.20	-10.74%
15.00	72.00	13.76	19.80	2400.42	2082.59	2141.08	F.Rotor	172.28	-12.23%	175.46	-10.61%	174.87	-10.91%
15.00	81.00	12.95	21.64	2558.79	2011.43	2088.69	F.Rotor	170.69	-13.04%	176.17	-10.25%	175.39	-10.64%
15.00	90.00	12.05	23.20	2665.09	1862.79	1953.89	F.Rotor	169.63	-13.58%	177.65	-9.49%	176.74	-9.95%
15.00	99.00	11.09	24.41	2607.66	1339.45	1748.46	F.Rotor	170.20	-13.29%	182.89	-6.82%	178.80	-8.91%
15.00	108.00	10.06	25.17	2470.84	1134.95	1477.38	F.Rotor	171.57	-12.59%	184.93	-5.78%	181.51	-7.53%
15.00	117.00	8.97	25.37	2281.21	905.88	1177.34	F.Rotor	173.47	-11.62%	187.22	-4.62%	184.51	-6.00%
15.00	126.00	7.83	24.87	2044.18	672.55	873.52	F.Rotor	175.84	-10.41%	189.56	-3.43%	187.55	-4.45%
15.00	135.00	6.65	23.51	1765.04	455.07	590.18	F.Rotor	178.63	-8.99%	191.73	-2.32%	190.38	-3.01%
15.00	144.00	5.45	21.09	1448.34	270.72	405.01	F.Rotor	181.80	-7.38%	193.57	-1.38%	192.23	-2.06%
15.00	153.00	4.24	17.48	1096.60	132.90	198.10	F.Rotor	185.32	-5.59%	194.95	-0.68%	194.30	-1.01%
15.00	162.00	3.06	12.61	707.90	47.63	70.01	F.Rotor	189.20	-3.61%	195.80	-0.24%	195.58	-0.36%
15.00	171.00	2.03	6.63	283.78	7.33	14.10	F.Rotor	193.44	-1.45%	196.21	-0.04%	196.14	-0.07%
15.00	180.00	1.54	0.00	-1.10	-1.59	-2.02	F.Rotor	196.29	0.01%	196.30	0.01%	196.30	0.01%
20.00	0.00	19.55	0.00	-318.80	-76.38	-117.68	NACA 0012	199.47	1.62%	197.04	0.39%	197.46	0.60%
20.00	9.00	19.49	3.27	149.42	527.43	503.62	NACA 0012	194.79	-0.76%	191.01	-2.69%	191.24	-2.57%
20.00	18.00	19.31	6.53	675.79	1250.82	1201.15	NACA 0012	189.52	-3.44%	183.77	-6.37%	184.27	-6.12%
20.00	27.00	19.01	9.76	1187.97	1911.76	1843.70	NACA 0012	184.40	-6.05%	177.16	-9.74%	177.84	-9.39%
20.00	36.00	18.59	12.94	1674.43	2481.76	2405.30	NACA 0012	179.54	-8.53%	171.46	-12.64%	172.23	-12.25%
20.00	45.00	18.06	16.06	2124.23	2936.44	2862.71	NACA 0012	175.04	-10.82%	166.92	-14.96%	167.65	-14.58%
20.00	54.00	17.42	19.09	2526.74	3259.12	3199.26	NACA 0012	171.01	-12.87%	163.69	-16.60%	164.29	-16.30%
20.00	63.00	16.68	22.02	2871.00	3439.78	3405.10	NACA 0012	167.57	-14.63%	161.88	-17.52%	162.23	-17.35%
20.00	72.00	15.83	24.80	3147.95	3476.25	3476.25	EPPLER 473	164.80	-16.04%	161.52	-17.71%	161.52	-17.71%
20.00	81.00	14.88	27.39	3350.02	3374.08	3414.42	EPPLER 473	162.78	-17.07%	162.54	-17.19%	162.14	-17.40%
20.00	90.00	13.84	29.75	3472.02	3147.95	3228.09	F.Rotor	161.56	-17.69%	164.80	-16.04%	164.00	-16.45%
20.00	99.00	12.72	31.80	3476.25	2820.67	2932.90	F.Rotor	161.52	-17.71%	168.07	-14.37%	166.95	-14.94%
20.00	108.00	11.52	33.43	3302.56	2412.80	2540.77	F.Rotor	163.26	-16.83%	172.15	-12.29%	170.87	-12.94%
20.00	117.00	10.25	34.52	3055.65	1592.57	2072.08	F.Rotor	165.72	-15.57%	180.36	-8.11%	175.56	-10.56%
20.00	126.00	8.92	34.85	2743.07	1211.76	1573.19	F.Rotor	168.85	-13.98%	184.16	-6.17%	180.55	-8.01%
20.00	135.00	7.54	34.15	2372.98	842.94	1093.07	F.Rotor	172.55	-12.09%	187.85	-4.29%	185.35	-5.57%
20.00	144.00	6.12	32.00	1953.84	517.41	669.33	F.Rotor	176.74	-9.95%	191.11	-2.64%	189.59	-3.41%
20.00	153.00	4.67	27.87	1494.00	260.79	389.04	F.Rotor	181.34	-7.61%	193.67	-1.33%	192.39	-1.98%
20.00	162.00	3.22	21.15	973.03	92.32	136.29	F.Rotor	186.55	-4.96%	195.36	-0.47%	194.92	-0.69%
20.00	171.00	1.84	11.60	406.59	14.98	18.92	F.Rotor	192.22	-2.07%	196.13	-0.08%	196.09	-0.10%
20.00	180.00	1.03	0.00	-0.24	-0.84	-1.18	F.Rotor	196.28	0.00%	196.29	0.00%	196.29	0.01%

Appendix 19 VPP RESULTS – CRUISING SPEED

Item	Value	Unit
Boat Speed	14.00	knots
	7.196	m/s
Boat Resistance	196.28	kN

TWS [kts]	Ship Angle [degrees]	AWS [m/s]	AWA [degrees]	Drive [N] F.Rotor	Drive [N] NACA 0012	Drive [N] EPPLER 473	Best Section	F.Rotor Resistance [N]		NACA 0012 Resistance [N]		EPPLER 473 Resistance [N]	
5.00	0.00	9.77	0.00	-76.16	-20.99	-34.96	NACA 0012	197.04	0.39%	196.49	0.11%	196.63	0.18%
5.00	9.00	9.75	1.39	49.20	13.88	23.17	F.Rotor	195.79	-0.25%	196.14	-0.07%	196.05	-0.12%
5.00	18.00	9.68	2.77	172.61	89.28	102.80	F.Rotor	194.55	-0.88%	195.39	-0.45%	195.25	-0.52%
5.00	27.00	9.56	4.10	292.64	158.58	175.96	F.Rotor	193.35	-1.49%	194.70	-0.81%	194.52	-0.90%
5.00	36.00	9.40	5.37	406.80	218.90	239.53	F.Rotor	192.21	-2.07%	194.09	-1.12%	193.89	-1.22%
5.00	45.00	9.20	6.56	512.50	267.93	291.00	F.Rotor	191.16	-2.61%	193.60	-1.37%	193.37	-1.48%
5.00	54.00	8.96	7.64	606.71	250.53	328.69	F.Rotor	190.21	-3.09%	193.78	-1.28%	192.99	-1.67%
5.00	63.00	8.68	8.59	695.94	268.44	351.64	F.Rotor	189.32	-3.55%	193.60	-1.37%	192.76	-1.79%
5.00	72.00	8.36	9.39	766.97	274.95	359.78	F.Rotor	188.61	-3.91%	193.53	-1.40%	192.68	-1.83%
5.00	81.00	8.02	10.00	814.99	270.63	353.89	F.Rotor	188.13	-4.15%	193.57	-1.38%	192.74	-1.80%
5.00	90.00	7.65	10.41	840.23	256.51	335.14	F.Rotor	187.88	-4.28%	193.72	-1.31%	192.93	-1.71%
5.00	99.00	7.26	10.58	832.80	234.47	306.14	F.Rotor	187.95	-4.24%	193.94	-1.19%	193.22	-1.56%
5.00	108.00	6.86	10.49	791.82	206.58	269.62	F.Rotor	188.36	-4.03%	194.22	-1.05%	193.58	-1.37%
5.00	117.00	6.45	10.13	731.56	175.08	228.49	F.Rotor	188.97	-3.73%	194.53	-0.89%	194.00	-1.16%
5.00	126.00	6.06	9.46	652.53	142.11	185.41	F.Rotor	189.76	-3.32%	194.86	-0.72%	194.43	-0.94%
5.00	135.00	5.68	8.49	555.03	109.83	143.37	F.Rotor	190.73	-2.83%	195.18	-0.56%	194.85	-0.73%
5.00	144.00	5.34	7.23	449.05	79.76	104.30	F.Rotor	191.79	-2.29%	195.48	-0.41%	195.24	-0.53%
5.00	153.00	5.05	5.70	337.53	52.74	69.29	F.Rotor	192.91	-1.72%	195.75	-0.27%	195.59	-0.35%
5.00	162.00	4.82	3.94	221.09	28.80	38.26	F.Rotor	194.07	-1.13%	195.99	-0.15%	195.90	-0.19%
5.00	171.00	4.68	2.01	101.26	7.33	10.53	F.Rotor	195.27	-0.52%	196.21	-0.04%	196.18	-0.05%
5.00	180.00	4.63	0.00	-21.04	-6.37	-9.83	NACA 0012	196.49	0.11%	196.34	0.03%	196.38	0.05%
10.00	0.00	12.35	0.00	-137.28	-32.07	-52.30	NACA 0012	197.65	0.70%	196.60	0.16%	196.80	0.27%
10.00	9.00	12.31	2.41	102.55	120.53	134.68	EPPLER 473	195.26	-0.52%	195.08	-0.61%	194.93	-0.69%
10.00	18.00	12.20	4.81	340.80	329.75	353.01	EPPLER 473	192.87	-1.74%	192.98	-1.68%	192.75	-1.80%
10.00	27.00	12.01	7.16	599.28	520.45	552.84	F.Rotor	190.29	-3.05%	191.08	-2.65%	190.75	-2.82%
10.00	36.00	11.76	9.45	854.80	684.09	725.56	F.Rotor	187.73	-4.35%	189.44	-3.49%	189.03	-3.70%
10.00	45.00	11.43	11.65	1092.72	813.74	864.00	F.Rotor	185.35	-5.57%	188.14	-4.15%	187.64	-4.40%
10.00	54.00	11.04	13.74	1304.90	904.44	962.82	F.Rotor	183.23	-6.65%	187.24	-4.61%	186.65	-4.91%
10.00	63.00	10.58	15.67	1483.60	952.73	1014.40	F.Rotor	181.45	-7.56%	186.75	-4.85%	186.14	-5.17%
10.00	72.00	10.06	17.42	1621.19	958.94	1021.22	F.Rotor	180.07	-8.26%	186.69	-4.89%	186.07	-5.20%
10.00	81.00	9.48	18.94	1711.15	925.36	985.92	F.Rotor	179.17	-8.72%	187.03	-4.71%	186.42	-5.02%
10.00	90.00	8.85	20.17	1748.67	701.10	912.04	F.Rotor	178.79	-8.91%	189.27	-3.57%	187.16	-4.65%
10.00	99.00	8.17	21.06	1732.25	621.39	807.95	F.Rotor	178.96	-8.83%	190.07	-3.17%	188.20	-4.12%
10.00	108.00	7.45	21.51	1661.73	524.74	681.62	F.Rotor	179.66	-8.47%	191.03	-2.67%	189.46	-3.47%
10.00	117.00	6.68	21.45	1540.07	419.41	544.21	F.Rotor	180.88	-7.85%	192.09	-2.14%	190.84	-2.77%
10.00	126.00	5.90	20.76	1372.70	313.54	406.13	F.Rotor	182.55	-6.99%	193.15	-1.60%	192.22	-2.07%
10.00	135.00	5.09	19.34	1167.23	215.74	278.94	F.Rotor	184.61	-5.95%	194.12	-1.10%	193.49	-1.42%
10.00	144.00	4.29	17.08	932.85	132.92	198.20	F.Rotor	186.95	-4.75%	194.95	-0.68%	194.30	-1.01%
10.00	153.00	3.51	13.93	679.54	70.66	105.01	F.Rotor	189.49	-3.46%	195.57	-0.36%	195.23	-0.54%
10.00	162.00	2.80	9.90	432.07	30.05	43.76	F.Rotor	191.96	-2.20%	195.98	-0.15%	195.84	-0.22%
10.00	171.00	2.27	5.16	210.18	8.27	11.48	F.Rotor	194.18	-1.07%	196.20	-0.04%	196.17	-0.06%
10.00	180.00	2.06	0.00	6.21	-2.32	-2.59	F.Rotor	196.22	-0.03%	196.30	0.01%	196.31	0.01%
15.00	0.00	14.92	0.00	-217.44	-45.68	-73.36	NACA 0012	198.46	1.11%	196.74	0.23%	197.01	0.37%
15.00	9.00	14.87	3.20	135.14	286.13	297.09	EPPLER 473	194.93	-0.69%	193.42	-1.46%	193.31	-1.51%
15.00	18.00	14.73	6.38	520.09	692.99	709.37	EPPLER 473	191.08	-2.65%	189.35	-3.53%	189.19	-3.61%
15.00	27.00	14.51	9.53	912.44	1064.43	1088.46	EPPLER 473	187.16	-4.65%	185.64	-5.42%	185.40	-5.55%
15.00	36.00	14.19	12.63	1283.97	1384.31	1418.84	EPPLER 473	183.44	-6.54%	182.44	-7.05%	182.09	-7.23%
15.00	45.00	13.78	15.67	1625.93	1639.71	1687.42	EPPLER 473	180.02	-8.28%	179.88	-8.35%	179.41	-8.60%
15.00	54.00	13.29	18.61	1931.40	1821.18	1884.21	F.Rotor	176.97	-9.84%	178.07	-9.28%	177.44	-9.60%
15.00	63.00	12.72	21.44	2190.32	1922.96	2002.62	F.Rotor	174.38	-11.16%	177.05	-9.80%	176.25	-10.20%
15.00	72.00	12.07	24.13	2400.42	1942.91	2037.11	F.Rotor	172.28	-12.23%	176.85	-9.90%	175.91	-10.38%
15.00	81.00	11.35	26.62	2558.79	1884.80	1990.28	F.Rotor	170.69	-13.04%	177.43	-9.60%	176.38	-10.14%
15.00	90.00	10.55	28.86	2665.09	1755.74	1861.42	F.Rotor	169.63	-13.58%	178.72	-8.95%	177.67	-9.48%
15.00	99.00	9.70	30.78	2607.66	1280.21	1663.98	F.Rotor	170.20	-13.29%	183.48	-6.52%	179.64	-8.48%
15.00	108.00	8.78	32.28	2470.84	1092.49	1418.54	F.Rotor	171.57	-12.59%	185.36	-5.57%	182.10	-7.23%
15.00	117.00	7.81	33.22	2281.21	882.50	1144.93	F.Rotor	173.47	-11.62%	187.46	-4.50%	184.83	-5.83%
15.00	126.00	6.79	33.41	2044.18	666.04	862.74	F.Rotor	175.84	-10.41%	189.62	-3.39%	187.65	-4.40%
15.00	135.00	5.73	32.56	1765.04	459.38	593.60	F.Rotor	178.63	-8.99%	191.69	-2.34%	190.35	-3.02%
15.00	144.00	4.64	30.31	1448.34	278.35	415.08	F.Rotor	181.80	-7.38%	193.50	-1.42%	192.13	-2.11%
15.00	153.00	3.52	26.18	1096.60	137.26	203.64	F.Rotor	185.32	-5.59%	194.91	-0.70%	194.24	-1.04%
15.00	162.00	2.39	19.69	707.90	46.26	67.13	F.Rotor	189.20	-3.61%	195.82	-0.24%	195.61	-0.34%
15.00	171.00	1.28	10.71	283.78	4.08	3.67	F.Rotor	193.44	-1.45%	196.24	-0.02%	196.24	-0.02%
15.00	180.00	0.51	0.00	-1.10	-0.24	-0.36	NACA 0012	196.29	0.01%	196.28	0.00%	196.28	0.00%
20.00	0.00	17.49	0.00	-318.80	-61.86	-96.75	NACA 0012	199.47	1.62%	196.90	0.32%	197.25	0.49%
20.00	9.00	17.44	3.81	149.42	515.82	508.64	NACA 0012	194.79	-0.76%	191.12	-2.63%	191.19	-2.59%
20.00	18.00	17.28	7.61	675.79	1188.59	1170.54	NACA 0012	189.52	-3.44%	184.40	-6.06%	184.58	-5.96%
20.00	27.00	17.02	11.40	1187.97	1805.69	1781.81	NACA 0012	184.40	-6.05%	178.22	-9.20%	178.46	-9.08%
20.00	36.00	16.66	15.16	1674.43	2341.33	2319.63	NACA 0012	179.54	-8.53%	172.87	-11.93%	173.08	-11.82%
20.00	45.00	16.20	18.88	2124.23	2774.78	2763.62	NACA 0012	175.04	-10.82%	168.53	-14.14%	168.64	-14.08%
20.00	54.00	15.65	22.55	2526.74	3090.78	3098.14	EPPLER 473	171.01	-12.87%	165.37	-15.75%	165.30	-15.78%
20.00	63.00	15.00	26.15	2871.00	3279.50	3313.86	EPPLER 473	167.57	-14.63%	163.49	-16.71%	163.14	-16.88%
20.00	72.00	14.27	29.66	3147.95	3339.49	3405.89	EPPLER 473	164.80	-16.04%	162.89	-17.01%	162.22	-17.35%
20.00	81.00	13.45	33.06	3350.02	3277.39	3376.34	EPPLER 473	162.78	-17.07%	163.51	-16.70%	162.52	-17.20%
20.00	90.00	12.56	36.31	3472.02	3103.89	3232.49	F.Rotor	161.56	-17.69%	165.24	-15.81%	163.96	-16.47%
20.00	99.00	11.60	39.35	3476.25	2832.42	2978.45	F.Rotor	161.52	-17.71%	167.96	-14.43%	166.50	-15.17%
20.00	108.00	10.58	42.12	3302.56	2486.41	2631.58	F.Rotor	163.26	-16.83%	171.42	-12.67%	169.97	-13.41%
20.00	117.00	9.51	44.50	3055.65	1707.66	2216.45	F.Rotor	165.72	-15.57%	179.20	-8.70%	174.12	-11.29%
20.00	126.00	8.40	46.30	2743.07	1369.40	1775.94	F.Rotor	168.85	-13.98%	182.59	-6.98%	178.52	-9.05%
20.00	135.00	7.28	47.25	2372.98	1036.30	1341.98	F.Rotor	172.55	-12.09%	185.92	-5.28%	182.86	-6.84%
20.00	144.00	6.15	46.81	1953.84	729.62	942.81	F.Rotor	176.74	-9.95%	188.98	-3.72%	186.85	-4.80%
20.00	153.00	5.07	44.02	1494.00	467.16	697.37	F.Rotor	181.34	-7.61%	191.61	-2.38%	189.31	-3.55%
20.00	162.00	4.10	37.02	973.03	260.12	386.75	F.Rotor	186.55	-4.96%	193.68	-1.33%	192.41	-1.97%
20.00	171.00	3.37	22.75	406.59	109.01	161.37	F.Rotor	192.22	-2.07%	195.19	-0.56%	194.67	-0.82%
20.00	180.00	3.09	0.00	-0.24	-3.88	-5.07	F.Rotor	196.28	0.00%	196.32	0.02%	196.33	0.03%